

VIBRATIONAL SPECTROSCOPIC STUDIES OF SOLID  
STATE REACTIONS

by

DANITA DE WAAL

Submitted in partial fulfilment of the  
requirements for the degree

**Master of Science**

in the

Faculty of Mathematics and Sciences

University of Pretoria

July 1988

**C O N T E N T S**

	<b>Page</b>
<b>Acknowledgements</b>	(viii)
<b>Summary</b>	(ix)
<b>Opsomming</b>	(x)
<b>Abbreviations</b>	(xi)
<b>General introduction</b>	(xii)
 <b>CHAPTER I</b>	
<b>METHODS OF VIBRATIONAL ANALYSIS</b>	1
 1. The Correlation method	
1.1 Introduction	1
1.2 (a) Use of the correlation method	1
(b) Example: $\text{Cr}_2\text{O}_3$	2
1.3 Molecular Crystals: intramolecular vibration	8
1.4 Chain Structures	
(a) Use of the correlation method	9
(b) Example: $\text{CrO}_3$	9
 2. Factor Group Analysis	
2.1 Introduction	12
2.2 The Method of analysis	12
2.3 Layer Structures	13

	Page
<b>CHAPTER II</b>	
<b>REACTION KINETICS THEORY</b>	16
1. Introduction	16
2. The ln.ln-method	16
3. The Mampel intermediate law	20
4. The Arrhenius equation	22
<b>CHAPTER III</b>	
<b>THE DECOMPOSITION OF THE SOLID <math>(\text{NH}_4)_2\text{CrO}_4</math></b>	23
1. Introduction	23
2. Crystallographic properties	23
3. Infrared and Raman Spectra	
3.1 Previous Studies	24
3.2 Experimental	25
3.3 Results and Discussion	
3.3.1 Vibrational Analysis	26
3.3.2 Description of the Spectra	28
4. Thermal decomposition	
4.1 Literature on the products, mechanism and kinetics of the decomposition of $(\text{NH}_4)_2\text{CrO}_4$	34

	<b>Page</b>
4.2 Experimental work	
4.2.1 Decomposition products	37
4.2.2 Reaction kinetics	37
4.3 Results and Discussion	
4.3.1 Decomposition products	38
4.3.2 Reaction kinetics	41
4.4 Conclusions	
4.4.1 Decomposition products	48
4.4.2 Reaction kinetics	48
<b>CHAPTER IV</b>	
<b>THE DECOMPOSITION OF THE SOLID <math>(\text{NH}_4)_2\text{Cr}_2\text{O}_7</math></b>	<b>50</b>
1. Introduction	50
2. Crystallographic properties	50
3. Infrared and Raman spectra	
3.1 Previous Studies	51
3.2 Vibrational Analysis	52
3.3 Description of the spectra	55
4. The Thermal Decomposition of $(\text{NH}_4)_2\text{Cr}_2\text{O}_7$	
4.1 Literature on the products and mechanism of the reaction	59
4.2 Experimental work	63
4.3 Results and Discussion	
4.3.1 Raman Spectroscopy results	65

	<b>Page</b>
4.3.2 FT-IR	65
(a) Rapid heating up to 498 K	65
(b) Rapid heating up to 503 K	68
(c) Gradual heating up to 518 K	68
(d) Gradual heating up to 613 K	70
(e) Product after 3 hours at 693 K	70
4.3.3 Percentages N and H in products at various decomposition stages	71
4.3.4 X-Ray Powder Diffraction	72
4.3.5 Diffuse Reflectance Electronic Spectra	74
4.4 Conclusions	76
<b>CHAPTER V</b>	
<b>FURTHER STUDY ON THE PRODUCTS OF THE DECOMPOSITION</b>	
<b>REACTION OF <math>(\text{NH}_4)_2\text{Cr}_2\text{O}_7</math></b>	
	79
1. $\text{CrO}_3$	
1.1 Introduction	79
1.2 Structure	79
1.3 Crystallographic properties	79
1.4 Preparation of single crystals of $\text{CrO}_3$	81
1.5 Vibrational Analysis	81
1.6 Infrared and Raman Spectra	
1.6.1 Previous Studies	82
1.6.2 Description of the spectra	82
2. $\text{Cr}_2\text{O}_3$	
2.1 Introduction	83
2.2 The Corundum Structure	84

	<b>Page</b>
2.3 Crystallographic properties of $\text{Cr}_2\text{O}_3$	87
2.4 Vibrational Analysis	87
2.5 Infrared Spectra	
2.5.1 Previous Studies	88
2.5.2 Description of the spectra	88
3. Comparison between the chromium compounds	90
 <b>CHAPTER VI</b>	
<b>A COMPARISON BETWEEN <math>\text{K}_2\text{Cr}_2\text{O}_7</math> AND <math>(\text{NH}_4)_2\text{Cr}_2\text{O}_7</math></b>	93
1. Introduction	93
2. Crystallographic Properties of $\text{K}_2\text{Cr}_2\text{O}_7$	93
3. Vibrational Analysis and Infrared Spectra	
3.1 Previous Studies on $\text{K}_2\text{Cr}_2\text{O}_7$	94
3.2 Vibrational Analysis of triclinic and monoclinic $\text{K}_2\text{Cr}_2\text{O}_7$	95
3.3 Description of the Infrared spectra of $\text{K}_2\text{Cr}_2\text{O}_7$ and comparison with $(\text{NH}_4)_2\text{Cr}_2\text{O}_7$	97
4. Thermal behaviour of the Raman modes of $\text{K}_2\text{Cr}_2\text{O}_7$	
4.1 Introduction	99
4.2 Experimental	101
4.3 Results, Discussion and Comparison with $(\text{NH}_4)_2\text{Cr}_2\text{O}_7$	101
4.4 Conclusions	108

	<b>Page</b>
<b>CHAPTER VII</b>	
<b>THE PHOTOCHEMICAL CONVERSION OF <math>[\text{Co}(\text{NH}_3)_5\text{NO}_2]\text{Cl}_2</math></b>	
<b>TO <math>[\text{Co}(\text{NH}_3)_5\text{ONO}]\text{Cl}_2</math></b>	<b>111</b>
1. Introduction	111
2. Crystal Structures	
2.1 $[\text{Co}(\text{NH}_3)_5\text{NO}_2]\text{Cl}_2$	112
2.2 $[\text{Co}(\text{NH}_3)_5\text{ONO}]\text{Cl}_2$	113
3. An Infrared kinetic study of the reaction	
$[\text{Co}(\text{NH}_3)_5\text{NO}_2]\text{Cl}_2 \xrightarrow{h\nu} [\text{Co}(\text{NH}_3)_5\text{ONO}]\text{Cl}_2$	
3.1 Introduction	113
3.2 Experimental	114
3.3 Co-NH <sub>3</sub> and Co-NO <sub>2</sub> vibrations	115
3.4 The Infrared spectra	117
3.5 The Rates of isomerization	129
<b>CHAPTER VIII</b>	
<b>EXPERIMENTAL DETAIL</b>	<b>134</b>
1. Introduction	134
2. Raman Spectrometer and oven	134

	<b>Page</b>
3. FT-IR spectroscopy	
3.1 Introduction	134
3.2 FT-IR spectrometer	136
3.3 Sample form	137
3.4 IR Diffuse reflectance spectroscopy	137
4. Electronic Diffuse reflectance spectra	138
APPENDIX A	140
LITERATURE	151



**ACKNOWLEDGEMENTS**

I wish to express my sincere thanks to the following persons:

Prof. A.M. Heyns, my promotor, for leading, motivating and encouraging me throughout this study.

Prof. K.-J. Range of the University of Regensburg, Federal Republic of Germany, for his interest in the Raman Kinetic study.

Mrs. A. Kok for her neat and correct typing of the work.

**SUMMARY**

A vibrational spectroscopy study on the following solid state reactions are presented:

The thermal decomposition reactions of  $(\text{NH}_4)_2\text{CrO}_4$  to  $(\text{NH}_4)_2\text{Cr}_2\text{O}_7$  and  $(\text{NH}_4)_2\text{Cr}_2\text{O}_7$  to  $\text{Cr}_2\text{O}_3$ , and the photoisomerization of  $[\text{Co}(\text{NH}_3)_5\text{NO}_2]\text{Cl}_2$  to  $[\text{Co}(\text{NH}_3)_5\text{ONO}]\text{Cl}_2$ .

A literature survey on the above reactions, as well as vibrational mode determination and assignment of these to infrared and Raman bands of the reagents, products and intermediates involved, are included.

The reaction kinetics of the decomposition of  $(\text{NH}_4)_2\text{CrO}_4$  and photoisomerization of  $[\text{Co}(\text{NH}_3)_5\text{NO}_2]\text{Cl}_2$  are determined by Raman and infrared methods respectively. Results obtained for the former reaction can be interpreted in terms of either the contracting cylinder or contracting area equations. Kinetics of the photochemical reaction  $[\text{Co}(\text{NH}_3)_5\text{NO}_2]\text{Cl}_2 \xrightarrow{h\nu} [\text{Co}(\text{NH}_3)_5\text{ONO}]\text{Cl}_2$  are reported for the first time, and it is a first order reaction. In addition these measurements provide direct evidence of structural changes during the course of the different reactions.

OPSOMMING

'n Infrarooi en Raman spektroskopiese studie van die volgende vastetoestand reaksies word aangebied:

Die termiese ontbindingsreaksies van  $(\text{NH}_4)_2\text{CrO}_4$  na  $(\text{NH}_4)_2\text{Cr}_2\text{O}_7$  en  $(\text{NH}_4)_2\text{Cr}_2\text{O}_7$  na  $\text{Cr}_2\text{O}_3$  en die fotochemiese isomerisasie van  $[\text{Co}(\text{NH}_3)_5\text{NO}_2]\text{Cl}_2$  na  $[\text{Co}(\text{NH}_3)_5\text{ONO}]\text{Cl}_2$ .

Verslag word gelewer oor die literatuur van bogenoemde reaksies. Vibrasie modes van die reagense, produkte en tussen-produkte is bepaal en toegeken aan bepaalde infrarooi en Raman bande.

Die reaksie kinetika van die ontbinding van  $(\text{NH}_4)_2\text{CrO}_4$  en die foto-isomerisasie van  $[\text{Co}(\text{NH}_3)_5\text{NO}_2]\text{Cl}_2$  word bepaal deur respektiewelik Raman en infrarooi spektroskopie te gebruik. Resultate verkry vir die eerste reaksie kan geïnterpreteer word volgens die inkrimpde silinder of die inkrimpde area vergelykings. Die kinetika van die fotochemiese reaksie  $[\text{Co}(\text{NH}_3)_5\text{NO}_2]\text{Cl}_2 \xrightarrow{h\nu} [\text{Co}(\text{NH}_3)_5\text{ONO}]\text{Cl}_2$  word vir die eerste keer gerapporteer. Dit is 'n eerste orde reaksie. Die metings verskaf ook direkte inligting van struktuurveranderinge gedurende die reaksies.

ABBREVIATIONS

1. Description of vibrational modes

$\nu$  - stretching

$\delta$  - deformation

$\rho_w$  - wagging

$\rho_r$  - rocking

$\rho_t$  - twisting

as - asymmetric

s - symmetric

2. Reference to other chapters and paragraphs in this work

Example: [VIII.3.4] refers to chapter VIII, paragraph 3.4.

3. IR - infrared

XRD - X-ray diffraction

R - Raman

FT-IR - Fourier-transform infrared

4. Superscripts

IR - infrared active

R - Raman active

IR/R - infrared and Raman active

O - infrared and Raman inactive

**GENERAL INTRODUCTION**

The following solid state reactions were studied by means of vibrational spectroscopic methods:

(1) The thermal decomposition of  $(\text{NH}_4)_2\text{CrO}_4$  to  $(\text{NH}_4)_2\text{Cr}_2\text{O}_7$  [III],  
(2) the thermal decomposition of  $(\text{NH}_4)_2\text{Cr}_2\text{O}_7$  to  $\text{Cr}_2\text{O}_3$  [IV, V, VI],  
and (3) the photoisomerization of  $[\text{Co}(\text{NH}_3)_5\text{NO}_2]\text{Cl}_2$  to  $[\text{Co}(\text{NH}_3)_5\text{ONO}]\text{Cl}_2$  [VII]. The determination of the nature, properties and behaviour of the solids involved in these reactions mainly involved infrared and Raman measurements of the reactants at room-temperature and various high temperatures in the case of the thermal decomposition reactions, and the reactant before and after radiation in the case of the photochemical reaction. Spectra of the various products and possible intermediates were recorded as well. In order for these spectra to be interpreted the optically active vibrational modes of the compound involved have to be determined and assigned to the various infrared and Raman bands. Of the various available methods to determine the vibrational modes the following two are described in this work and illustrated by examples: the correlation method [I.1] and factor group analysis [I.2]. The reaction kinetics of two of the reactions, the thermal decomposition of  $(\text{NH}_4)_2\text{CrO}_4$  [III.4] and the photoisomerization of  $[\text{Co}(\text{NH}_3)_5\text{NO}_2]\text{Cl}_2$  [VII.3], were studied by Raman and infrared methods respectively and therefore some of the general theory on reaction kinetics necessary to interpret the data were included as well [II]. Various aspects of the above-mentioned reactions of solid  $(\text{NH}_4)_2\text{CrO}_4$ ,  $(\text{NH}_4)_2\text{Cr}_2\text{O}_7$  and  $[\text{Co}(\text{NH}_3)_5\text{NO}_2]\text{Cl}_2$  were investigated, including the determination of possible intermediate species and products under different conditions, reaction kinetics, as well

as the structure, crystallographic properties, infrared and Raman spectra, a vibrational analysis and even single crystal preparation of the reactants and products. A comparison of  $(\text{NH}_4)_2\text{CrO}_4$  with  $\text{K}_2\text{CrO}_4$  [III.3] and  $(\text{NH}_4)_2\text{Cr}_2\text{O}_7$  with  $\text{K}_2\text{Cr}_2\text{O}_7$  [VI] were included in the study of the behaviour of the two ammonium salts because of the lack in hydrogen bonding in the potassium salts.

## CHAPTER I

### METHODS OF VIBRATIONAL ANALYSIS

In the interpretation of vibrational spectra it is of great importance to determine the optically active vibrational modes in a crystal. The methods used for that purpose during this study include the correlation method and factor group analysis as described respectively by Fateley [1] and Adams [2] and are described in more detail below.

#### 1. THE CORRELATION METHOD

##### 1.1 Introduction

The derivation of vibrational selection rules for solids as described by Fateley [1] will be outlined in the following section. A demonstration of the method is given by calculating IR and Raman active modes for  $\text{Cr}_2\text{O}_3$ . Fateley adapted the same method for chain type structures. A description of this is included with an illustration of its use on  $\text{CrO}_3$ .

##### 1.2(a) Use of the correlation method

The first goal is to determine the number of lattice vibrations in a crystal (the external vibrations). The crystal structure of the compound must be known before such a determination can be carried out, or, a structure can be assumed and predictions can be made for the vibrations which

can be compared with observations to prove the structure acceptable or not. The crystallographic unit cell is used to obtain the Bravais space cell which in turn provides the irreducible representation for the lattice modes. For a crystal structure designated by a symbol containing P (primitive) the crystallographic unit cell and the Bravais cell are identical, but in others the crystallographic unit cell contains between two and four Bravais cells, resulting in two to four times as many lattice vibrations for a crystal. This can be eliminated by the use of eq. (I-1) where the number of molecules in a crystallographic unit cell,  $Z$ , is divided by the number of lattice points (LP) in the cell to obtain the number of molecules per Bravais cell,  $Z^B$ .

$$Z^B = \frac{Z}{(\text{LP})} \dots\dots\dots(\text{I-1})$$

The number of lattice points in different crystallographic structures are shown in Table (I.1) [1].

**Table (I.1)**

Crystal structure	LP
A	2
B	2
C	2
F	4
I	2
P	1
R	3 or 1



Before demonstrating the method by applying it to  $\text{Cr}_2\text{O}_3$ , the terms which will be used are first of all defined.  $R^Y$  and  $t^Y$  represent the number of rotations and translations in a site species and can take values of 0, 1, 2 or 3 depending on the number of rotations/translations contained in the site species  $y$ . This information can be obtained from the character tables in ref. 1 where rotations and translations are respectively identified as  $R_x, R_y, R_z$  and  $T_x, T_y, T_z$ . The degrees of rotational ( $f_R^Y$ ) and vibrational freedom ( $f^Y$ ) present in each site species  $y$  are calculated through the use of equations (I-2a) and (I-2b) [1]:

$$f_R^Y = R^Y \cdot n \dots\dots\dots (I-2a)$$

$$f^Y = t^Y \cdot n \dots\dots\dots (I-2b)$$

where  $n$  is the number of equivalent atoms/ions/molecules with the same site species.

The degrees of freedom,  $a_y$ , of each site species contributed to the factor group species  $x$  are determined with eq. (I-3) [1]:

$$a_y = \sum_x \frac{C_x}{f^Y} \dots\dots\dots (I-3)$$

where  $C_x$  represents the degeneracy of the  $x$ -species of the factor group with values shown in Table (I.2) [1].

**Table (I.2)**

Species	Usual values of C <sub>x</sub>
A	1
B	1
E	2
F	3
G	4
H	5

Next the site symmetry which is a subgroup of the full symmetry of the Bravais unit cell must be determined for each atom. This information is usually provided with the crystallographic structure of a compound. All the possible site symmetries for the space groups are tabulated in ref. 1, e.g. for  $D_{3d}^6$  all the available sites are  $D_3(2)$ ;  $C_3(2)$ ;  $C_3(4)$ ;  $C_i(6)$ ;  $C_2(6)$ ;  $C_1(12)$ . Most of the site symmetries will not be occupied in a specific crystal. The number in parentheses represents the number of equivalent atoms which could have that particular symmetry, for example in  $Cr_2O_3$  there are four equivalent chromium and six equivalent oxygen atoms occupying the  $C_3$  and  $C_2$  sites respectively. In the case of  $K_2Cr_2O_7$  (space group  $C_{2h}^5$ ),  $4C_i(2)$  indicates that there are four different  $C_i$  sites of which each could be occupied by 2 equivalent atoms. The correlation of the site group to the factor group, which describes the crystal symmetry, can now commence. Correlation tables relate the site groups to the factor group, which results in an identification of the species of lattice vibration in

the crystal and a prediction of infrared and Raman activity.

To avoid any errors, equations (I-4a) and I-4b) can be used to check the method during the correlation process.

$$\sum_Y f_Y = 3 n_{\text{site}} \dots\dots\dots(I-4a)$$

$$\sum_X a_X C_X = 3 n_{\text{factor group}} \dots\dots\dots(I-4b)$$

where  $a_X = \sum_Y a_{YX}$ , the number of lattice vibrations of the equivalent set of atoms in species  $x$  of the factor group.

The irreducible representation of each equivalent set of atoms is obtained through the use of eq. (I-5).

$$\Gamma_{\text{eq.set}} = \sum_X a_X \cdot X \dots\dots\dots(I-5)$$

The total irreducible representation of the crystal,  $\Gamma_{\text{cryst}}$ , is a combination of the irreducible representation of every equivalent set of atoms,  $\Gamma_{\text{eq.set}}$ , and gives the number of lattice vibrations in each species of the factor group.

$$\Gamma_{\text{cryst}} = \Gamma_{\text{eq.set}_1} + \Gamma_{\text{eq.set}_2} + \dots\dots\dots(I-6)$$

Acoustical modes have the same character as the translation

and can therefore be identified from the character table of the factor group species. It can then be subtracted from eq. (I-6) to obtain the irreducible representation of the lattice vibrations in the crystal:

$$\Gamma_{\text{vib}}^{\text{cryst}} = \Gamma^{\text{cryst}} - \Gamma^{\text{acoust}} \dots\dots\dots(\text{I-7})$$

1.2(b) Example: Cr<sub>2</sub>O<sub>3</sub>

Cr<sub>2</sub>O<sub>3</sub> belongs to space group D<sub>3d</sub><sup>6</sup> (R $\bar{3}$ c) with z = 6 [3], but the number of molecules per Bravais cell are two (z<sup>B</sup> = 2). Four chromium and six oxygen atoms occupy the C<sub>3</sub> and C<sub>2</sub> sites respectively.

Fig. (I.1a) Determination of  $\Gamma_{\text{eq.set}}$  for Cr in Cr<sub>2</sub>O<sub>3</sub> using the Fateley method

4 Cr in C <sub>3</sub>							
fY	tY	C <sub>3</sub>	→ D <sub>3d</sub>	C <sub>x</sub>	a <sub>x</sub>	= a <sub>A<sub>1</sub></sub>	+ a <sub>E</sub>
4	1(T <sub>Z</sub> )	A	→ A <sub>1g</sub>	1	1	= 1	+ 0
			→ A <sub>2g</sub>	1	1	= 1	+ 0
			→ A <sub>1u</sub>	1	1	= 1	+ 0
			→ A <sub>2u</sub>	1	1	= 1	+ 0
8	2(T <sub>X</sub> , T <sub>Y</sub> )	E	→ E <sub>g</sub>	2	2	= 0	+ 2
			→ E <sub>u</sub>	2	2	= 0	+ 2

$\Gamma_{\text{Cr}} = A_{1g} + A_{2g} + A_{1u} + A_{2u} + 2E_g + 2E_u$  [from eq. (I-5)]

The degrees of freedom of the site species,  $a_{A_1}$  and  $a_E$  in Fig. (I.1(a)) were determined as follows from eq. (I-3):

$$fY = 4 = a_{A_1}(C_{A_{1g}} + C_{A_{2g}} + C_{A_{1u}} + C_{A_{2u}}) = 4a_{A_1}$$

From this:  $a_{A_1} = 1$

$$fY = 8 = a_E(C_{E_g} + C_{E_u}) = 4a_E$$

From this:  $a_E = 2$

**Fig. (I.1(b))** Determination of  $\Gamma_{\text{eq.set}}$  for O in  $\text{Cr}_2\text{O}_3$  using the Fateley-method

<u>6 O in C<sub>2</sub></u>						
fY	tY	C <sub>2</sub> → D <sub>3d</sub>	C <sub>x</sub>	a <sub>x</sub>	= a <sub>A</sub>	+ a <sub>B</sub>
6	1(T <sub>z</sub> )	A → A <sub>1g</sub>	1	1	= 1	+ 0
		→ A <sub>1u</sub>	1	1	= 1	+ 0
12	2(T <sub>x</sub> , T <sub>y</sub> )	B → E <sub>g</sub>	2	3	= 1	+ 2
		→ E <sub>u</sub>	2	3	= 1	+ 2
		→ A <sub>2g</sub>	1	2	= 0	+ 2
		→ A <sub>2u</sub>	1	2	= 0	+ 2
$\Gamma_{\text{O}} = A_{1g} + A_{1u} + 3E_g + 3E_u + 2A_{2g} + 2A_{2u}$ [from eq. (I-5)]						

The degrees of freedom of the site species,  $a_A$  and  $a_B$  in Fig. (I.1(b)) were determined as follows from eq. (I-3):

$$fY = 6 = a_A(C_{A_{1g}} + C_{A_{1u}} + C_{E_g} + C_{E_u}) = 6a_A$$

$$\text{From this: } a_A = 1$$

$$fY = 12 = a_B(C_{E_g} + C_{E_u} + C_{A_{2g}} + C_{A_{2u}}) = 6a_B$$

$$\text{From this: } a_B = 2$$

In order to obtain all the crystal vibrations, the following procedure is followed:

$$\begin{aligned} \Gamma_{\text{cryst}} &= \Gamma_{\text{cr}} + \Gamma_{\text{O}} && [\text{From eq. (I-6)}] \\ &= 2A_{1g} + 3A_{2g} + 2A_{1u} + 3A_{2u} + 5E_g + 5E_u \end{aligned}$$

$$\Gamma_{\text{acoust}} = A_{2u} + E_u$$

$$\begin{aligned} \Gamma_{\text{vib}}^{\text{cryst}} &= \Gamma_{\text{cryst}} - \Gamma_{\text{acoust}} && [\text{eq. (I-7)}] \\ &= 2A_{1g}^{(R)} + 3A_{2g}^{\text{O}} + 2A_{1u}^{\text{O}} + 2A_{2u}^{(\text{IR})} + 5E_g^{(R)} + 4E_u^{(\text{IR})} \end{aligned}$$

### 1.3 Molecular crystals : intramolecular vibration

The method in 1.2(a) can be extended to include intramolecular vibration of molecular crystals, e.g.  $(\text{NH}_4)_2\text{Cr}_2\text{O}_7$ . The intramolecular vibrations of the  $\text{NH}_4^+$  and  $\text{Cr}_2\text{O}_7^{2-}$  ions are obtained by using the molecular symmetry of the particular ion. This is then correlated to the site species which can in turn be integrated into the factor group. This will be shown for  $(\text{NH}_4)_2\text{CrO}_4$  in (III.3.3.2) and  $(\text{NH}_4)_2\text{Cr}_2\text{O}_7$  in (IV.3.2).

## 1.4 Chain structures

### (a) Use of the correlation method

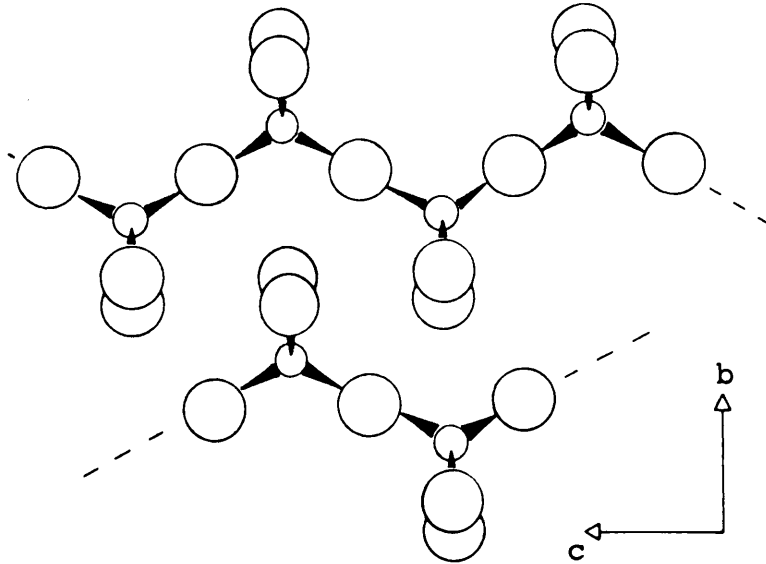
The method for chain structures differ from the others in that a line group which is a subgroup of the space group is chosen. The site group of each atom is then correlated with the line group to obtain the irreducible representation. The total irreducible representation is the sum of that of the various atoms. The irreducible representation of translation for the line group and the libration of the chain structure (only one rotation is possible about a chain axis) are used to obtain the irreducible representation for the intramolecular vibrations of the line group:

$$\Gamma_{\text{line group}}^{\text{intramol. vib}} = \Gamma_{\text{line group}}^{\text{tot}} - \Gamma_{\text{line group}}^{\text{transl}} - \Gamma_{\text{line group}}^{\text{lib}} \dots (I-8)$$

### (b) Example: CrO<sub>3</sub>

CrO<sub>3</sub> has a chain/layered structure and belongs to space group  $C_{2v}^{16}$  (C2cm) with  $Z = 4$  [4]. A typical CrO<sub>3</sub> chain is shown in Fig. (I.1). The line group is  $C_{2v}$  since it consists of the following symmetry operations : E,  $C_2$ ,  $\sigma_v$  and  $\sigma_v'$  with no perpendicular  $C_2$  axes or  $\sigma_h$ . The Cr, O(3) and O(4) atoms are situated on the  $C_s$  site

**Fig. (I.1)** Projection of a  $\text{CrO}_3$  chain in (100) showing the position of an adjacent chain. Small circles represent chromium atoms and large circles oxygen atoms.



and O(1) on  $C_2$ . There are two molecules per Bravais cell ( $z^B = 2$ ).

**Fig. (I.2(a))** Use of the Fateley method [1] to determine  $\Gamma_{\text{eq.set}}$  for O(1) in  $\text{CrO}_3$

<u>2 O(1) in <math>C_2</math></u>						
fY	tY	$C_2 \longrightarrow C_{2Y}$	$C_X$	$a_X = a_A + a_B$		
2	1( $T_Z$ )	A $\longrightarrow$ A <sub>1</sub>	1	1 = 1	+	0
		$\searrow$ A <sub>2</sub>	1	1 = 1	+	0
4	2( $T_X, T_Y$ )	B $\longrightarrow$ B <sub>1</sub>	1	2 = 0	+	2
		$\searrow$ B <sub>2</sub>	1	2 = 0	+	2
$\Gamma_{\text{O}(1)} = A_1 + A_2 + 2B_1 + 2B_2$						



The degrees of freedom of the site species,  $a_A$  and  $a_B$ , were determined as follows, using eq. (I-3):

$$fY = 2 = a_A(C_{A_1} + C_{A_2}) = 2a_A$$

From this:  $a_A = 1$

$$fY = 4 = a_B(C_{B_1} + C_{B_2}) = 2a_B$$

From this:  $a_B = 2$

**Fig. (I.2(b))** Use of the Fateley method [1] to determine  $\Gamma_{\text{eq.set}}$  for Cr, O(3) and O(4) in  $\text{CrO}_3$

2 Cr, 2 O(3) and 2 O(4) in $C_S$							
$fY$	$tY$	$C_S$	$\sigma(YZ)$	$C_{2V}$	$C_X$	$a_X$	$= a_{A'} + a_{A''}$
12	$2(T_X, Y_Y)$	$A'$	$\longrightarrow$	$A_1$	1	6	$= 6 + 0$
			$\searrow$	$B_2$	1	6	$= 6 + 0$
6	$1(T_Z)$	$A''$	$\longrightarrow$	$B_1$	1	3	$= 0 + 3$
			$\searrow$	$A_2$	1	3	$= 0 + 3$
$\Gamma_{\text{Cr, O(3), O(4)}} = 6A_1 + 3A_2 + 3B_1 + 6B_2$							

The degrees of freedom of the site species,  $a_{A'}$  and  $a_{A''}$ , were determined as follows:

$$fY = 12 = a_{A'}(2)$$

From this:  $a_{A'} = 6$

$$fY = 6 = a_{A''}(2)$$

From this:  $a_{A''} = 3$

$$\begin{aligned}\Gamma_{\text{line group}}^{\text{tot}} &= \Gamma_{\text{O}(1)} + \Gamma_{\text{Cr}, \text{O}(3), \text{O}(4)} \\ &= 7A_1 + 4A_2 + 5B_1 + 8B_2\end{aligned}$$

$$\Gamma_{\text{line group}}^{\text{trans}} = A_1 + B_1 + B_2$$

$$\Gamma_{\text{line group}}^{\text{lib}} = B_1$$

$$\begin{aligned}\Gamma_{\text{line group}}^{\text{intramol. vib.}} &= [\Gamma_{\text{O}(1)} + \Gamma_{\text{Cr}, \text{O}(3), \text{O}(4)}] - \Gamma_{\text{line group}}^{\text{trans}} \\ &\quad - \Gamma_{\text{line group}}^{\text{lib}}\end{aligned}$$

from eq. (I-8)

$$\text{Then } \Gamma_{\text{line group}}^{\text{intramol. vib.}} = 6A_1 + 4A_2 + 3B_1 + 7B_2$$

## 2. FACTOR GROUP ANALYSIS

### 2.1 Introduction

While factor group analysis is generally performed by an operation on all atoms in the primitive unit cell at the same time, Adams and Newton [2] simplified the procedure by separating operations on complete sets of equivalent points (Wyckoff sites) which allowed tabulation of the results for general use. A factor group analysis can now be performed on any solid by reading the appropriate rows in the tables provided by Adams and Newton [2].

### 2.2 The Method of analysis

The analysis for a non-primitive unit cell with the Adams-

tables [2] is automatically an analysis for the primitive cell: the number in each set of Wyckoff sites has been reduced to the number in the primitive cell since factor group analysis always deals with the smallest unit cell. Both internal and external(lattice)modes are present in molecular and complex ionic crystals. Translatory modes(T) are calculated by considering translatory independent components so that  $(T + T_A)$  is obtained by the summation of rows representing the centres of gravity of all molecules or ions (monatomic or complex). Rotatory modes(R) are obtained in a similar way but here only polyatomic groups are considered. The internal modes for  $\text{Cr}_2\text{O}_7^{2-}$  in  $(\text{NH}_4)_2\text{Cr}_2\text{O}_7$  are determined as an example. As before structural information is needed before values can be read from the Adams-tables [2].

$(\text{NH}_4)_2\text{Cr}_2\text{O}_7$  consists of  $\text{NH}_4^+$  and  $\text{Cr}_2\text{O}_7^{2-}$  ions and belongs to space group No. 15,  $\text{C}_{2h}^6$  with  $Z = 4$  [5].  $\text{NH}_4^+$ , Cr, O(1), O(2) and O(3) all occupy 4 F-sites while O(4) atoms are situated on the 2 E-sites.

### 2.3 Layer structures

Once again some structural information on the compound is needed before a vibrational analysis can be performed on a layer compound. While infinite layers and linear chains do not have any degree of rotational freedom, chains in which all of the atoms are not co-linear have one about the direction of the chain axis. It is also important to know how many layers or chains are present per unit cell, as only one

**Fig. I.3** Factor group analysis of the internal modes of  $\text{Cr}_2\text{O}_7^{2-}$  in  $(\text{NH}_4)_2\text{Cr}_2\text{O}_7$

Space group No 15	$A_g$	$B_g$	$A_u$	$B_u$
$\text{NH}_4^+$ (4F)	3	3	3	3
Cr (4F)	3	3	3	3
3 O (4F)	9	9	9	9
O (2E)	1	2	1	2
N(Total)	16	17	16	17
T + TA	4	5	4	5
$R(\text{Cr}_2\text{O}_7^{2-})$	1	2	1	2
$N_{\text{INT}}(\text{Cr}_2\text{O}_7^{2-})$	11	10	11	10
$\Gamma_{\text{int}}^{\text{Cr}_2\text{O}_7^{2-}} = 11A_g + 10B_g + 11A_u + 10B_u$				

layer/chain, results in the only translatory modes being of the acoustic type. The procedure can be illustrated by the following example:  $\text{CrO}_3$  is effectively an infinitely long  $\text{Cr}_2\text{O}_7^{2-}$  chain [6] and belongs to space group No. 40,  $C_{2v}^{16}$  with  $Z = 4$  [4]. An illustration of a  $\text{CrO}_3$  chain will be shown in Chapter V when the structure will be discussed in greater detail. The first step is to define the 'polymer site group', a subgroup of the space group with the same symmetry elements as in the chain. In  $\text{CrO}_3$  it is  $C_{2v}$ , but none of the sets of Wyckoff sites in space group  $C_{2v}^{16}$  are isomorphous with this polymer site symmetry. This will be true for chains which do have either glide planes or screw axes. In these cases such a set of Wyckoff sites are found in a different space group belonging to the same factor

group. In  $\text{CrO}_3$  this space group is no. 38,  $C_{2v}^{14}$ . ( $T + T_A$ ) is obtained from the Adams-tables [2] by using space group no. 38.  $\text{CrO}_3$  has only one rotational mode\* which is determined by subtracting values of  $R(x) + R(y)$  in one table from that of  $R(x, y, z)$  in another to leave the value of  $R(y)$  as  $B_1$ .

**Fig. (I.4)** Factor group analysis of  $\text{CrO}_3$

Space group no. 40	$A_1$	$A_2$	$B_1$	$B_2$
Cr 4(B)	2	1	1	2
O(4) 4(B)	2	1	1	2
O(3) 4(B)	2	1	1	2
O(1) 4(A)	1	1	2	2
N(Total)	7	4	5	8
$T + T_A$ (no. 38)	1	0	1	1
$R(y)$ (no. 38)*	0	0	1	0
	6	4	3	7
$\Gamma^{\text{vib}} = 6A_1^{\text{IR/R}} + 4A_2^{\text{R}} + 3B_1^{\text{IR/R}} + 7B_2^{\text{IR/R}}$				

It is evident that the same result has been obtained with this method of analysis as in the Fateley method applied to the  $\text{CrO}_3$  molecule.

## CHAPTER II

### REACTION KINETICS THEORY

#### 1. INTRODUCTION

In subsequent sections, the kinetic data for a decomposition reaction are obtained by the isothermal heating of the reactant at various pre-determined temperatures. The decreasing or increasing intensity of a specific infrared or Raman band of the reactant is then determined at regular time intervals to produce  $\chi_r$  against  $t$  plots.  $\chi_r$  is the fraction reactant present at time  $t$ . A repetition of this procedure at different temperatures allows the activation energy to be calculated from the Arrhenius equation if the reaction is isokinetic.

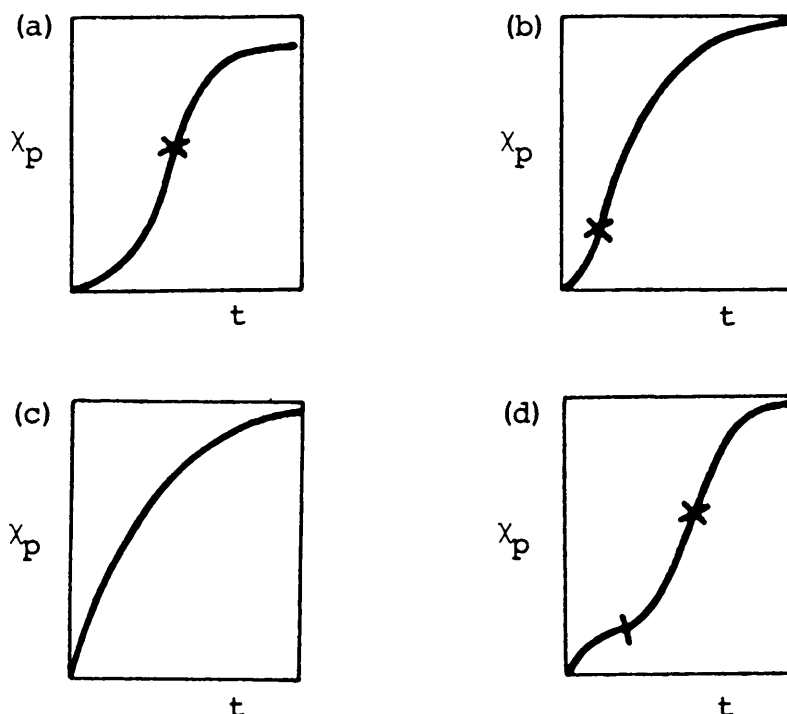
However, before these results can be described, some basic principles of the kinetics of solid state reactions must be considered very briefly.

#### 2. THE $\ln.\ln$ METHOD

The shape of the  $\chi_r$  against  $t$  plot can vary depending on the changing geometry, especially at the reaction interface. One, or up to four expressions may be found to describe the reaction at different stages of the decomposition such as an initial, accelerating and decelerating stage. Some typical plots of the fraction product present at time  $t$ ,  $\chi_p$ , against time are shown in Fig. (II.1(a-d)). One method to identify the rate law

**Fig. (II.1(a-d))** Typical  $\chi_p$  against time plots for the thermal decomposition of solids:

- (a) A sigmoid curve
  - (b) Short induction period with a mostly decreasing rate
  - (c) No induction period
  - (d) Very long induction period
- ( $\chi$ - The position of the maximum decomposition rate) [6]



providing the most satisfactory fit is based on the use of the generalised Avrami-Erofe'ev equation:

$$1-(\chi_p) = \exp(-kt^n) \dots\dots\dots(II-1)$$

where  $\chi_p$  is the fraction product present at time  $t$

Then  $\ln(1-\chi_p) = -kt^n,$

$$\ln[-\ln(1-\chi_p)] = n \ln t + \ln k, \text{ and}$$

$$\ln\left[\ln \frac{1}{(1-\chi_p)}\right] = n \ln t + \ln k$$

$$\text{But } \chi_p = 1 - \chi_r \dots\dots\dots(\text{II-2})$$

where  $\chi_r$  is the fraction  
reactant present at time  $t$

$$\text{Then } \ln[\ln(1/\chi_r)] = n \ln t + \ln k \dots\dots\dots(\text{II-3})$$

$\ln[\ln(1/\chi_r)]$  is plotted against  $\ln t$  and  $n$  is determined from the slope. (This is the  $\ln.\ln$  method of analysis). This provides straight lines of various fixed slopes for every different kinetic expression. Values of  $n$  have been determined for the rate equations which have found application in kinetic studies of solid phase reactions [6]. These are presented in Table (II.1).

Table (II.1)

<u>Rate equation</u>	<u>Slope*</u>
Three-dimensional diffusion: $[1-(1-\chi_p)^{1/3}]^2 = kt$	0,53
Ginstling-Brounshtein: $[1-(2\chi_p/3)]-(1-\chi_p)^{2/3} = kt$	0,55
Two-dimensional diffusion: $(1-\chi_p)\ln(1-\chi_p) + \chi_p = kt$	0,55
One-dimensional diffusion: $\chi_p^2 = kt$	0,58
1 <sup>st</sup> order $1-\chi_p = \exp(-kt)$	1,00
<u>Mampel intermediate law</u>	
Contracting volume $1-(1-\chi_p)^{1/3} = kt$	1,04
Contracting area $1-(1-\chi_p)^{1/2} = kt$	1,08
Zero-order	1,18
Avrami-Erofe'ev $(1-\chi_p)^{1/2} = kt$	2,00
$(1-\chi_p)^{1/3} = kt$	3,00
$(1-\chi_p)^{1/4} = kt$	4,00
Note: $1-\chi_p = \chi_r$	
*The slope in each case was determined theoretically from data in [6].	



The experimental slope is compared with that of the various theoretical expressions to determine the most suitable equation to describe the decomposition reaction.

The reactions can be divided according to their dependence on the maximum rate of decomposition. This maximum rate is defined in [6] as:

$$\left(\frac{d\chi_p}{dt}\right)_{\max}$$

But  $\chi_p = 1 - \chi_r$

$$\text{Then } \left(\frac{d\chi_p}{dt}\right)_{\max} = \frac{d(1-\chi_r)}{dt}$$

$$= \frac{-d\chi_r}{dt}$$

$$\text{and } \left(\frac{d\chi_p}{dt}\right)_{\max} = \left(\frac{-d\chi_r}{dt}\right)_{\max} \dots\dots\dots(\text{II-4})$$

The following three groups of reactions are recognised by the location of  $\left(\frac{-d\chi_r}{dt}\right)_{\max}$ :

Firstly a reaction obeyed up to the maximum decomposition rate which points to a relationship concerned with growth of nuclei. Secondly, obedience both sides of  $\left(\frac{-d\chi_r}{dt}\right)_{\max}$  are concerned with nuclei growth and thirdly obedience beyond  $\left(\frac{-d\chi_r}{dt}\right)_{\max}$  which is a  $\chi_r$  against  $t$  relationship concerned with nuclei interference or a decreasing reaction interface.

### 3. THE MAMPEL INTERMEDIATE LAW

Where the reaction is initiated by the development of a large number of closely spaced nuclei on all surfaces or on specific crystallographic surfaces, the kinetic characteristics are determined by the geometry of advance of the reaction interface from these boundaries in the direction of the centres of the particles. There is an initial rapid and preferential advance of the reaction interface. The Mampel intermediate law [7,8] which states the general form of two- and three-dimensional reactions as:

$$1-(1 - \chi_p)^{\frac{1}{n}} = kt$$

$$1-(\chi_r)^{\frac{1}{n}} = kt \dots\dots\dots(\text{II-5})$$

is only observed beyond the maximum decomposition rate.  $\left(\frac{-d\chi_r}{dt}\right)_{\text{max}}$  is then usually observed in the early stages of the reaction, thus at lower  $\chi_p$ - or higher  $\chi_r$ -values. This results in a short induction period. The decomposition rate is deceleratory after the maximum reaction rate. An example of such a curve is shown in Fig. (II.1(b)). It is an intermediate law because it holds over the middle range of  $\chi_r$ -values. If surface nucleation occurs, followed by growth over the surface and advance of the interface towards the center of supposed spherical particles, the reaction is said to follow the contracting sphere model. Similarly, if the reaction occurs at all faces of a cube it is said to follow the contracting cube model. Both these models are described by equation (II-6), which is referred to as the contracting volume equation.

$$1 - (1 - \chi_p)^{1/3} = kt \quad (n = 3)$$

$$\text{or} \quad 1 - (\chi_r)^{1/3} = kt \quad \dots\dots\dots(\text{II-6})$$

When the reaction is initiated at all surfaces of a cylinder, two-dimensional growth occurs and the reaction is said to follow the contracting cylinder model which is described by the contracting area equation, (II-7).

$$1 - (1 - \chi_p)^{1/2} = kt \quad (n = 2)$$

$$\text{or} \quad 1 - (\chi_r)^{1/2} = kt \quad \dots\dots\dots(\text{II-7})$$

The general form of these reactions is expressed by equation (II-5).  $n$  is the number of dimensions in which the interface is said to advance. With linear progression in a single direction,  $n$  equals 1. A deviation from idealized representations is expected in real systems as this is an indication of a strained and distorted reaction interface which develops because the volume of solid reactant is almost always significantly different from the volume of the product which is formed [6].

Variation in the average particle size may cause the value of  $\chi_r$  to decrease relative to that obtained for that of uniform particle size as a more rapid reaction is expected for smaller particles. Later  $\chi_r$  may decrease slower than for a uniform system due to the slower reaction expected for larger particles. In general the rate coefficient,  $k$ , and the exponent,  $n$ , are dependent on particle size and shape for decreasing interface reactions.

#### 4. THE ARRHENIUS EQUATION

When the rate coefficients and exponents have been determined for various temperatures and the reaction is found to be isokinetic at various temperatures, the Arrhenius equation (II-8) can be used to determine the activation energy,  $E$ , from the slope and the pre-exponential factor,  $A$ , from the intercept when  $\ln k$  is plotted against  $1/T$ .  $T[\text{K}]$  is the reaction temperature.

$$\ln k = \frac{-E}{RT} + \ln A \quad \dots\dots\dots(\text{II-8})$$

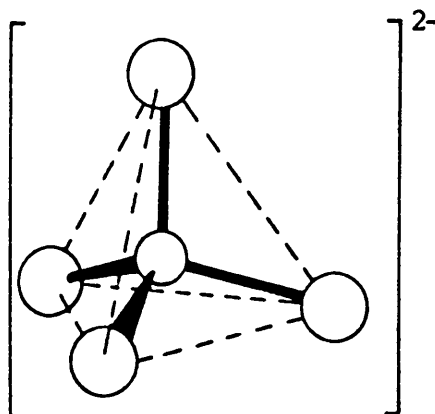
CHAPTER IIITHE DECOMPOSITION OF THE SOLID  $(\text{NH}_4)_2\text{CrO}_4$ 1. INTRODUCTION

$(\text{NH}_4)_2\text{CrO}_4$  decomposes to  $(\text{NH}_4)_2\text{Cr}_2\text{O}_7$  and eventually to  $\text{Cr}_2\text{O}_3$ , the most stable oxide of chromium, at higher temperatures. This decomposition reaction is used to investigate the potential of Raman spectroscopy as a tool in the study of solid state reactions, particularly with reference to reaction kinetics. Other aspects of interest include the existence of so-called intermediate species and a possible proton transfer mechanism.

2. CRYSTALLOGRAPHIC PROPERTIES

Ammonium chromate has a monoclinic crystal structure and belongs to space group  $C_{2h}^3$  ( $C2/m$ ) with  $Z = 4$  [9,10]. It contains isolated, almost regular  $\text{CrO}_4^{2-}$  tetrahedra and ammonium ions occupying eight coordinate positions. A representation of a typical  $\text{CrO}_4^{2-}$  tetrahedron are given in Fig. (III.1). The oxygen coordi-

Fig. (III.1) The  $\text{CrO}_4^{2-}$  tetrahedron



nation around each ammonium ion can be described as symmetrically bicapped trigonal prismatic [10]. The Cr,  $\text{NH}_4^+(1)$ ,  $\text{NH}_4^+(2)$ , O(1) and O(2) atoms all occupy 4i-sites with site symmetry  $C_s$ , while O(3) atoms are situated on 8j-sites with  $C_1$ -symmetry. Each of the four Cr-O bonds in a tetrahedral chromate group equals  $1,658 \pm 0,004 \text{ \AA}$ , with O-Cr-O bond angles:

$$\begin{aligned} \text{O}(1) - \text{Cr} - \text{O}(2) & : 110,9^\circ \\ \text{O}(1) - \text{Cr} - \text{O}(3) & : 108,5^\circ \\ \text{O}(2) - \text{Cr} - \text{O}(3) & : 109,3^\circ \\ \text{O}(3) - \text{Cr} - \text{O}(3') & : 110,2^\circ \quad [9] \end{aligned}$$

The unit cell parameters as obtained by Stephens and Cruickshank [9] and Gatehouse and Leverett [10] are compared in Table (III.1).

Table (III.1) Unit cell parameters of  $(\text{NH}_4)_2\text{CrO}_4$

	S + C [9]	G + L [10]
a	12,21 Å	12,300 Å
b	6,258	6,294
c	7,630	7,664
$\beta$	115,2°	115,6°

### 3. INFRARED AND RAMAN SPECTRA

#### 3.1 Previous studies

Infrared and Raman spectra of various chromates including ammonium chromate have been reported [11-16]. Campbell [11]

recorded infrared spectra of different chromates which he grouped in two types, the first having peaks from 850 to 980  $\text{cm}^{-1}$  but not between 700 and 800  $\text{cm}^{-1}$  and the second having sets of peaks in both regions. The second type showed remarkable similarities with dichromate spectra and although some of the chromates might have contained dichromate ions (especially the ammonium salt) it seemed unlikely that all did. The infrared spectrum of  $(\text{NH}_4)_2\text{CrO}_4$  was an intermediate between the two types. It was interpreted as being the result of hydrogen bonds removing the tetrahedral symmetry of the  $\text{CrO}_4^{2-}$  ion, leaving it with a lower symmetry. The absorption near 1700  $\text{cm}^{-1}$ , the splitting of the 1400  $\text{cm}^{-1}$  peak and the lack of isomorphism with the  $\text{K}_2\text{CrO}_4$  spectrum also indicate strong hydrogen bonding according to Waddington's criteria [17]. Muller *et. al.* [12] reported that the distinction of chromates from dichromates is not always possible by infrared spectroscopy as a dichromate-like spectrum can arise from a chromate with a distorted  $\text{CrO}_4^{2-}$  tetrahedron: Longer Cr-O bonds result in a stretching frequency similar to that of the dichromate Cr-O-Cr bridge vibration.

Assignment of the Raman active modes for a chromate ion from the literature are shown in Table (III.2).

### 3.2 Experimental

Campbell [11] reported that pelletizing of  $(\text{NH}_4)_2\text{CrO}_4$  causes appreciable conversion to  $(\text{NH}_4)_2\text{Cr}_2\text{O}_7$ . It was also observed in the present study that  $(\text{NH}_4)_2\text{CrO}_4$  decomposes under pressure therefore making it impossible to record spectra in

**Table (III.2)** Values of the Raman active modes for chromate ions (in solution) obtained from the literature

Assignment	Raman modes in $\text{cm}^{-1}$		
	Dupuis [13]	Michel [14]	Stammreich [15]
$\nu_2$ (E)	350	348	348
$\nu_4$ ( $F_2$ )	390	371	368
$\nu_1$ ( $A_1$ )	855	846	847
$\nu_3$ ( $F_2$ )	855	887	884

the form of KBr-discs. It was thus decided to record a diffuse reflectance infrared spectrum of  $(\text{NH}_4)_2\text{CrO}_4$  in the mid-infrared region instead of a transmission spectrum, using the reflection cell described in Chapter (VIII). The Raman spectrum was recorded at room-temperature between 20 and  $1000 \text{ cm}^{-1}$ .

### 3.3 Results and discussion

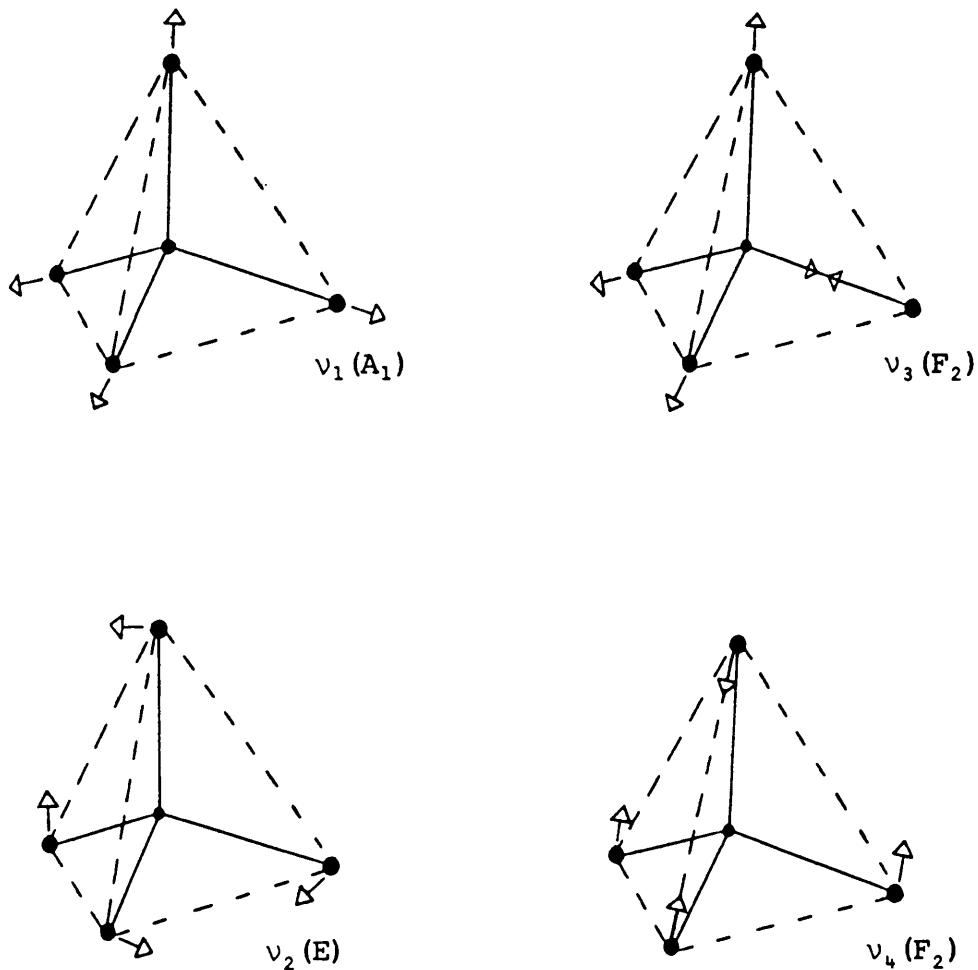
#### 3.3.1 Vibrational analysis

The normal modes of the tetrahedral chromate ion,  $A_1 + E + 2F_2$ , are all Raman active with  $F_2$  modes infrared active as well. These modes are shown in Fig. (III.2).

A factor group analysis using the Adams method [I-2] is shown in Fig. (III.3).

The correlation of 'free'  $\text{CrO}_4^{2-}$  ions in  $(\text{NH}_4)_2\text{CrO}_4$  and



**Fig. (III.2)** The normal modes in the tetrahedral  $\text{CrO}_4^{2-}$ -ion**Fig. (III.3)** Factor group analysis of  $(\text{NH}_4)_2\text{CrO}_4$   
(Adams method [I-2])

Space group No. 12	$A_g$	$B_g$	$A_u$	$B_u$
$\text{NH}_4^+$ (2I)	4	2	2	4
Cr (2I)	2	1	1	2
O (2I)	2	1	1	2
O (4J)	3	3	3	3
N(Total)	11	7	7	11
T + TA	4	2	2	4
$R(\text{CrO}_4^{2-})$	1	2	2	1
$N_{\text{INT}}(\text{CrO}_4^{2-})$	6	3	3	6
$\Gamma_{\text{INT}}^{\text{CrO}_4^{2-}} = 6A_g^{\text{IR/R}} + 3B_g^{\text{IR/R}} + 3A_u^{\text{IR}} + 6B_u^{\text{IR}}$				

$K_2CrO_4$  with site group  $C_s$  and factor groups  $C_{2h}$  and  $D_{2h}$  respectively will be shown in the next section (3.3.2) with the assignment of the bands.  $K_2CrO_4$  was chosen for comparison with the ammonium salt because the former does not contain any hydrogen bonding.

### 3.3.2 Description of the spectra

The Raman spectra of  $K_2CrO_4$  and  $(NH_4)_2CrO_4$  are shown in Fig. (III.4(a)) and (III.4(b)), with the infrared spectrum of  $K_2CrO_4$  in Fig. (III.5(a)) and the diffuse reflectance spectrum (mid-infrared) of  $(NH_4)_2CrO_4$  in Fig. (III.5(b)). The assignment of the modes for  $K_2CrO_4$  [16], including the correlation of chromate ions with the site- and factor group, are shown in Fig. (III.6). These values were used with the site- and factor group correlation to assign the vibrational modes of  $(NH_4)_2CrO_4$  in Fig. (III.7). Rotation and translation modes are compared with that of the dichromate in Table (III.3).

**Table (III.3)** Comparison of the rotational and translational modes of  $(NH_4)_2CrO_4$  and  $(NH_4)_2Cr_2O_7$

	$(NH_4)_2CrO_4$	$(NH_4)_2Cr_2O_7$ [IV.3.3]
Translation	98 $cm^{-1}$ 95 88	105 $cm^{-1}$ 98 94
Rotation	76 56 41	61 44 28

**Fig. (III.4(a))** The Raman spectrum of  $K_2CrO_4$

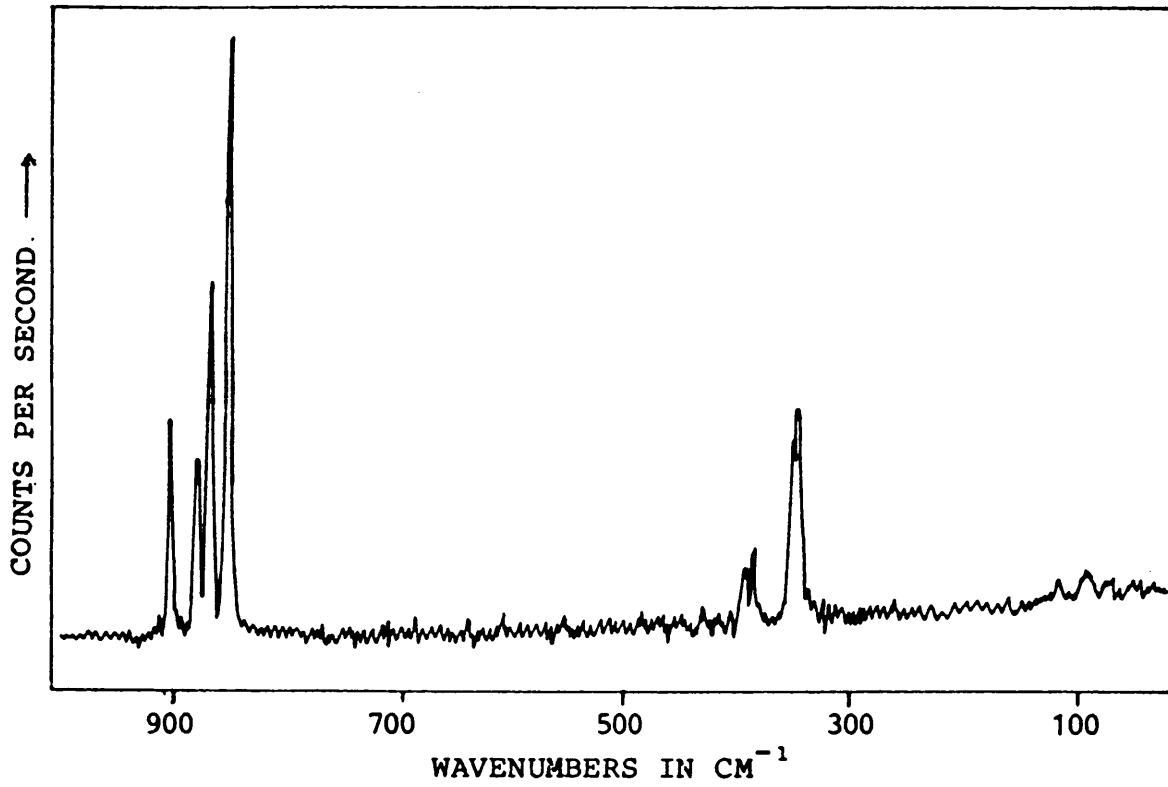


**Fig. (III.4(b))** The Raman spectrum of  $(NH_4)_2CrO_4$

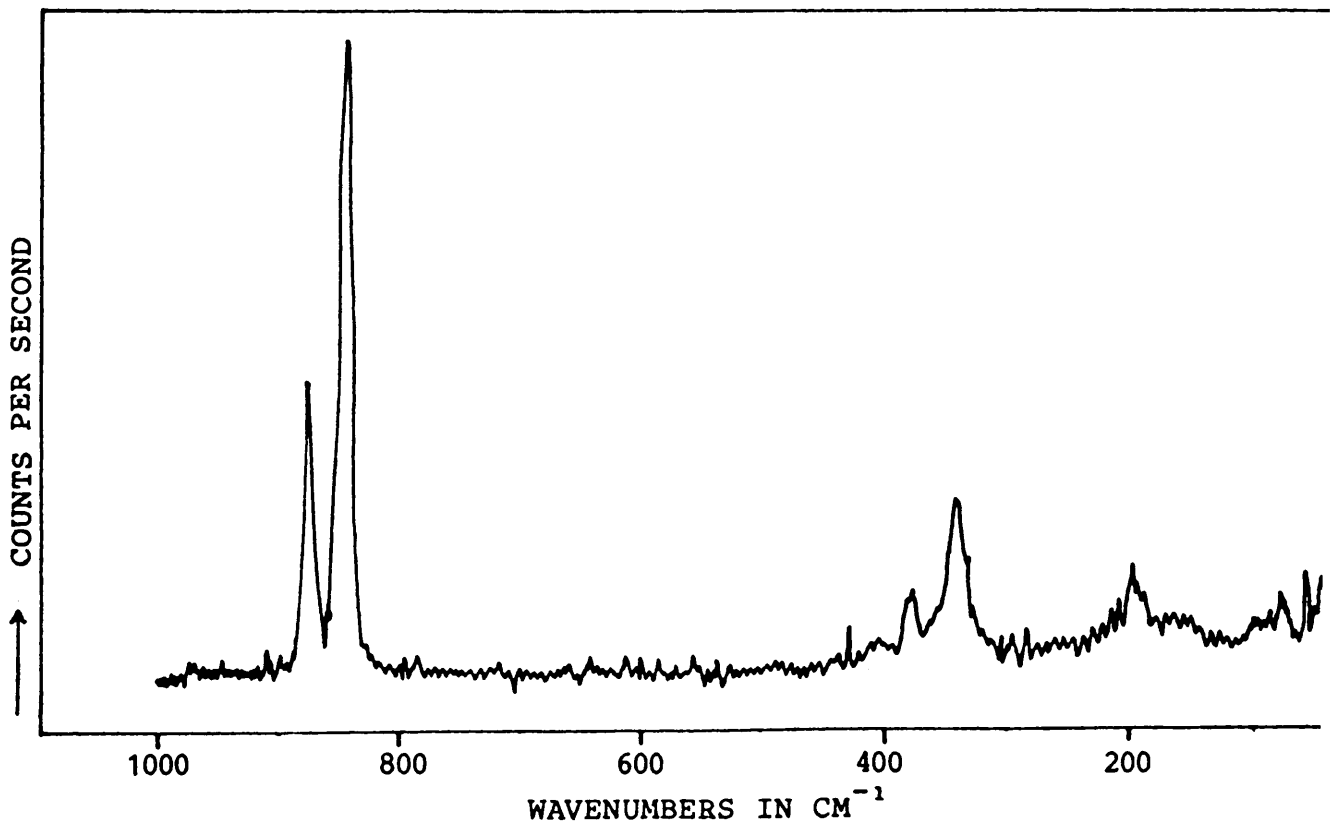


**Fig. (III.5(a))** The mid-IR spectrum of  $K_2CrO_4$

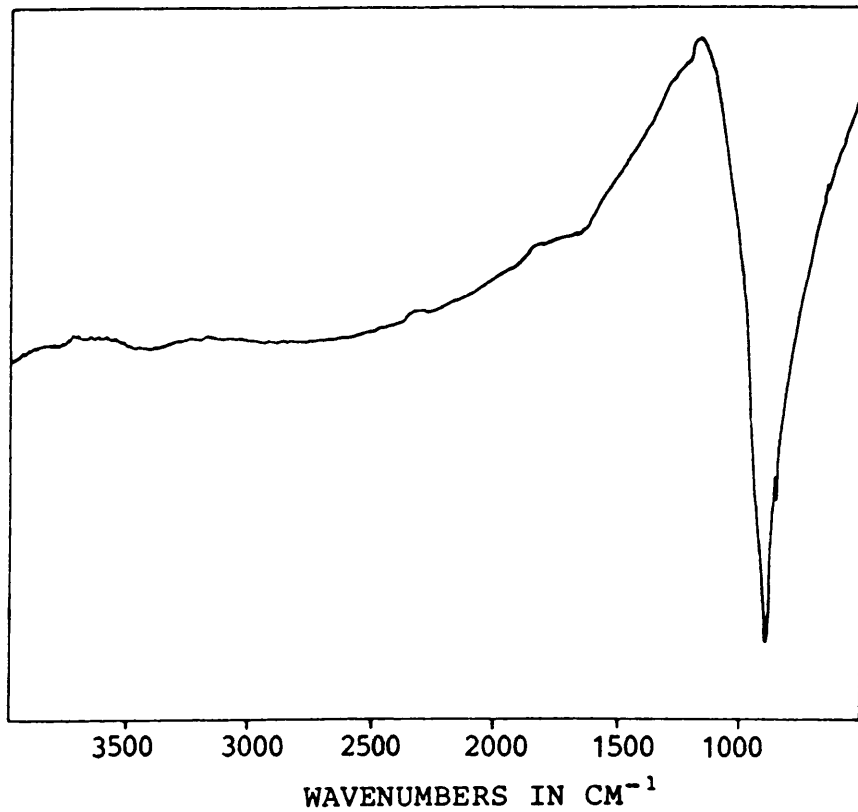


**Fig. (III.5(b))** The mid-IR reflectance spectrum of  $(NH_4)_2CrO_4$

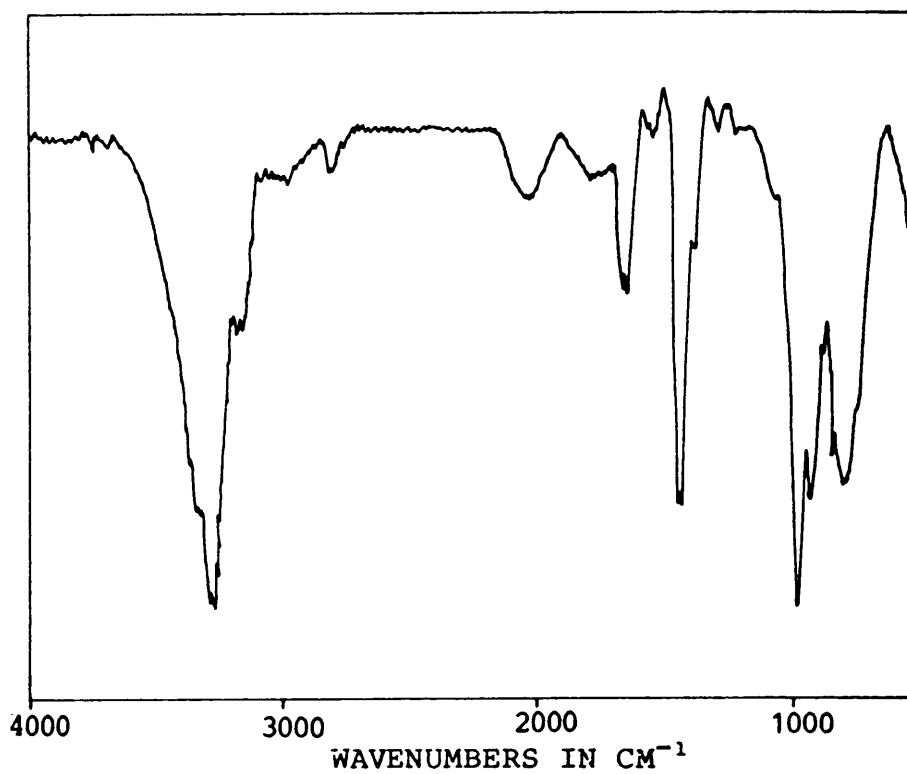


**Fig. (III.6)** Site and factor group correlation of  $\text{CrO}_4^{2-}$  in potassium chromate

<u>Symmetry of 'free' ion</u>		<u>Site group</u>	<u>Factor group</u>	<u>Bands in <math>\text{cm}^{-1}</math> [16]</u>	
<u><math>T_d</math></u>		<u><math>C_s</math></u>	<u><math>D_{2h}</math></u>	<u>Raman</u>	<u>IR</u>
$F_2$	(884 $\text{cm}^{-1}$ )	$2A'$	$2A_g$	905/868	
			$2B_g$	919/884	-
$F_2$	(884 $\text{cm}^{-1}$ )	$A''$	$2B_{1u}$		905/879
			$2B_{3u}$		929/888
			$B_{1g}$	881	-
			$B_{3g}$	877	-
$A_1$	(847 $\text{cm}^{-1}$ )	$A'$	$A_u$		877
			$B_{2u}$		877
			$A_g$	852	-
			$B_{2g}$	852	-
$F_2$	(368 $\text{cm}^{-1}$ )	$A'$	$B_{1u}$		851
			$B_{3u}$		851
			$2A_g$	397/387	
			$2B_{1g}$	398/388	-
$F_2$	(368 $\text{cm}^{-1}$ )	$A''$	$2B_{1u}$		386
			$2B_{3u}$		398
			$B_{1g}$	388	-
			$B_{3g}$	393	-
$E$	(348 $\text{cm}^{-1}$ )	$A'$	$A_u$		385
			$B_{2u}$		385
			$A_g$	347	-
			$B_{2g}$	353	-
$E$	(348 $\text{cm}^{-1}$ )	$A''$	$B_{1u}$		-
			$B_{3u}$		-
			$B_{1g}$	348	-
			$B_{3g}$	351	-
$E$	(348 $\text{cm}^{-1}$ )	$A''$	$A_u$		-
			$B_{2u}$		-

**Fig. (III.7)** Site and factor group correlation of  $\text{CrO}_4^{2-}$  in ammonium chromate

<u>T<sub>d</sub></u>		<u>C<sub>s</sub></u>	<u>C<sub>2h</sub></u>	<u>Raman</u>	<u>IR</u>
(876 cm <sup>-1</sup> )	F <sub>2</sub>	→ 2A'	→ 2A <sub>g</sub> → 2B <sub>u</sub>	876	- 984/935
		→ A''	→ B <sub>g</sub> → A <sub>u</sub>	-	864
(845 cm <sup>-1</sup> )	A <sub>1</sub>	→ A'	→ A <sub>g</sub> → B <sub>u</sub>	845	847 -
(378 cm <sup>-1</sup> )	F <sub>2</sub>	→ 2A'	→ 2A <sub>g</sub> → 2B <sub>u</sub>	379/376	
		→ A''	→ B <sub>g</sub> → A <sub>u</sub>	395	
(342 cm <sup>-1</sup> )	E	→ A'	→ A <sub>g</sub> → B <sub>u</sub>	340	
		→ A''	→ B <sub>g</sub> → A <sub>u</sub>	346	

Rotations

<u>C<sub>s</sub></u>		<u>C<sub>2h</sub></u>
A' (R <sub>z</sub> )	→	A <sub>g</sub> B <sub>u</sub>
2A'' (R <sub>x</sub> , R <sub>y</sub> )	→	2B <sub>g</sub> 2A <sub>u</sub>

Translations

<u>C<sub>s</sub></u>		<u>C<sub>2h</sub></u>
2A' (T <sub>x</sub> , T <sub>y</sub> )	→	2A <sub>g</sub>
A'' (T <sub>z</sub> )	→	B <sub>g</sub> A <sub>u</sub>

The site and factor group correlation for the ammonium ion in ammonium chromate are presented in Fig. (III.8) with tentative assignment of the infrared bands in Table (III.4).

**Fig. (III.8)** Site and factor group correlation of  $\text{NH}_4^+$  in  $(\text{NH}_4)_2\text{CrO}_4$

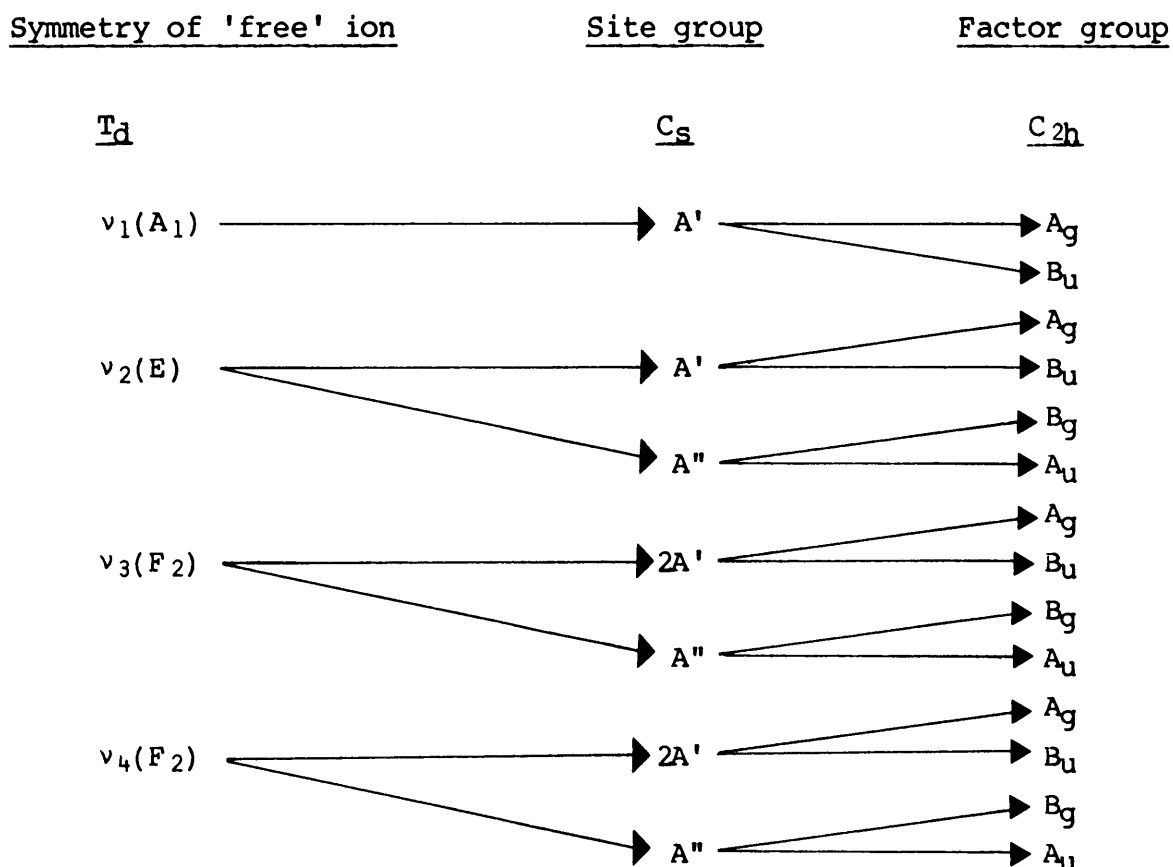


**Table (III.4)** Tentative assignment of IR-active ammonium vibrations in ammonium chromate

Wavenumbers in $\text{cm}^{-1}$	Assignment
3321 sh. ]	$\nu_3$
3250 s.b. ]	
3203 m.	$\nu_2 + \nu_4$
3057 w.	$\nu_1$
2806 w.	$2\nu_4$
1757 w.	$\nu_4 + \nu_6$
1653 m.sp.	$\nu_2$
1446 s.sp. ]	$\nu_4$
~1407 sh. ]	

#### 4. THERMAL DECOMPOSITION

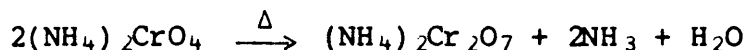
##### 4.1 Literature on the products, mechanism and kinetics of the decomposition of $(\text{NH}_4)_2\text{CrO}_4$

Different authors studied the decomposition of  $(\text{NH}_4)_2\text{CrO}_4$  as a precursor to the decomposition of  $(\text{NH}_4)_2\text{Cr}_2\text{O}_7$  by means of TG, DTA, DTG, X-ray diffraction, mass spectrometry and microscopic methods [18-20].

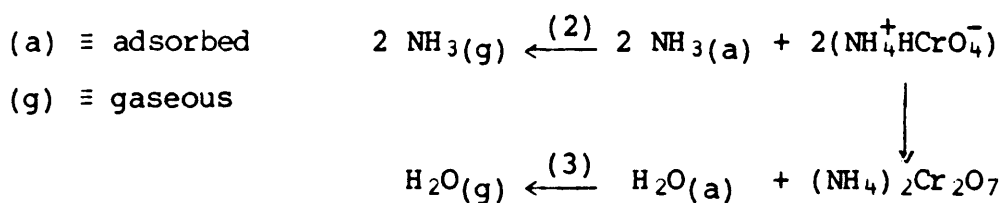
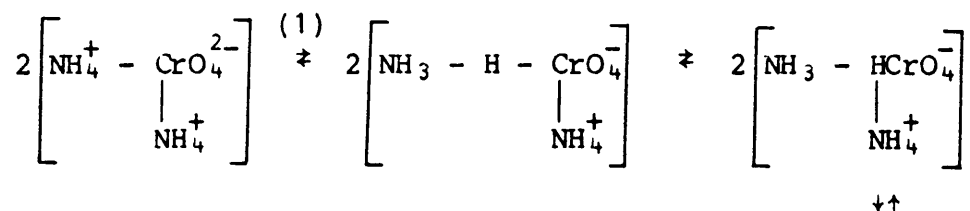
A study by means of the first four methods mentioned was carried out by Ill-Huyn Park [18] in order to determine the composition, structure and temperature range of each intermediate. An examination of the kinetics of some of the reaction steps was included in the study. Four reaction steps were found of which the first is the decomposition to  $(\text{NH}_4)_2\text{Cr}_2\text{O}_7$ . The three succeeding steps are similar to the three steps found in the decomposition of the dichromate resulting in products consisting of brown  $\text{CrO}_3$  (473-503 K), a black mixture of  $\text{CrO}_3$  and  $\text{Cr}_2\text{O}_3$  (533-548 K) and finally dark green  $\text{Cr}_2\text{O}_3$  (683-708 K). The reaction kinetics of the second step in the chromate decomposition was compared to that of the first step in the dichromate decomposition and similar results were obtained. Although the bright orange ammonium dichromate was obtained from yellow ammonium chromate by heating the latter to 393 K, it is known that ammonium chromate decomposes slowly to form ammonium dichromate even at room-temperature [18].



Constituents of gases evolved during this thermal decomposition were studied by Ill-Huyn Park by means of an omegatron mass spectrometer [19]. In the first decomposition step percentages  $\text{NH}_3$  and  $\text{H}_2\text{O}$  were determined. From this it was established that the following reaction



does not take place as the theoretical ratio  $\text{NH}_3 : \text{H}_2\text{O}$  of 2 : 1 does not appear until the chromate is heated up to 363 K and the ratio is much larger below 363 K. This suggests that  $\text{NH}_3$  is eliminated rapidly in the initial stages of the reaction, whereas the amount of  $\text{H}_2\text{O}$  evolved gradually increases as the reaction proceeds so that  $\text{NH}_3$  is eliminated before  $\text{H}_2\text{O}$  is formed. The following proton transfer mechanism was proposed [19]:



(1) Proton transfer from  $\text{NH}_4^+$  to  $\text{CrO}_4^{2-}$

(2)  $\text{NH}_3$  becomes free (no coulombic interaction) and desorption takes place.

(3) Desorption of  $\text{H}_2\text{O}$ .

Rajam and Galwey [20] obtained kinetic results by using a constant volume system in which the pressure of ammonia evolved during  $(\text{NH}_4)_2\text{CrO}_4$  decomposition was determined as a function of time. This showed that the decomposition of  $(\text{NH}_4)_2\text{CrO}_4$  to  $(\text{NH}_4)_2\text{Cr}_2\text{O}_7$  obeys the contracting cylinder equation:

$$1 - (1 - \alpha)^{1/2} = kt$$

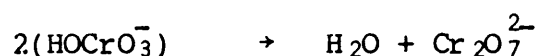
where  $\alpha$  is the fraction of product present at time  $t$  and  $k$  the rate constant.

A microscopic study was used in the characterization of textural changes during deamination. By studying cross section surfaces evidence was obtained that the reaction interface advances progressively inwards from the original crystal surfaces.

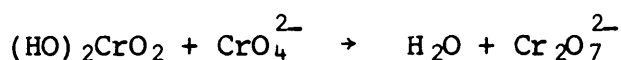
The reaction was found to be endothermic and two distinct chemical steps seem to contribute to the mechanism. On energetic grounds and by analogy with the decomposition of other ammonium salts the first step is assumed to be reversible proton transfer:



This is followed by water elimination:



or alternatively two proton transfer steps:



Rajam and Galwey [20] also found that low temperature  $\alpha$  against time plots (333–348 K) were more deceleratory than the requirement for the contracting cylinder equation. At these temperatures there was no evidence of an initial acceleratory process. Rate constants for the reaction of crystals (ca. 1 x 1 x 10 mm) at 381 K varied between  $5,83 \times 10^{-4}$  and  $7,50 \times 10^{-4} \text{ s}^{-1}$  for different amounts of sample. The activation energy,  $E$ , was determined as  $97 \pm 5 \text{ kJ}\cdot\text{mol}^{-1}$  and the frequency factor  $A[\text{s}^{-1}]$  was  $\log A = 10,3$ . The rate constants for powdered samples at 333 K varied between  $1,33 \times 10^{-4}$  and  $4,00 \times 10^{-4} \text{ s}^{-1}$ . The apparent activation energy was  $90 \pm 9 \text{ kJ}\cdot\text{mol}^{-1}$  for powdered samples and  $70 \pm 5 \text{ kJ}\cdot\text{mol}^{-1}$  for compressed samples [20].

## 4.2 Experimental work

### 4.2.1 Decomposition products

Raman spectra were recorded at 298, 323, 353, 373, 383 and 393 K between 20 and  $1000 \text{ cm}^{-1}$ , using the high temperature cell described in (VIII.2) to heat the samples of  $(\text{NH}_4)_2\text{CrO}_4$ . The  $(\text{NH}_4)_2\text{CrO}_4$  was also decomposed for various periods of time at 393 K, and the products were investigated by wet analysis methods, X-ray powder diffraction and UV/visible diffuse reflectance spectra.

### 4.2.2 Reaction kinetics

Raman measurements were made using the high temperature cell described in (VIII.2) to heat the samples of

Analytical Grade  $(\text{NH}_4)_2\text{CrO}_4$ . Both powdered (ca.  $0,1 \times 0,08 \times 0,04$  mm) and small microcrystals (ca.  $1,0 \times 0,2 \times 0,1$  mm) of  $(\text{NH}_4)_2\text{CrO}_4$  contained in glass tubes of diameter 3 mm were used for measurements and the intensity of the  $\nu_s(\text{Cr-O})$  band was recorded every 45 seconds for periods up to 600 seconds. These isothermal kinetic measurements were made at 343, 348, 353, 358 and 363 K, the temperature being correct within 5 K.

### 4.3 Results and discussion

#### 4.3.1 Decomposition products

Wet analysis results showing the percentages N and H present in samples decomposed for various periods at 393 K are shown in Table (III.2).

Table (III.2) Percentage N and H during decomposition

	% N	% H
$(\text{NH}_4)_2\text{CrO}_4$ (theoretical)	18,42	5,30
3h (393 K)	11,78	3,70
18h (393 K)	11,69	3,76
48h (393 K)	11,50	3,38
$(\text{NH}_4)_2\text{Cr}_2\text{O}_7$ (theoretical)	11,12	3,20

X-ray powder diffraction results showing the d-values (in Å) of the same decomposition products are presented in Table (III.3), and the diffuse reflectance electronic

**Table (III.3)** XRD : some of the d-values (in Å) of  $(\text{NH}_4)_2\text{CrO}_4$  and  $(\text{NH}_4)_2\text{Cr}_2\text{O}_7$  compared with some decomposition products. (Relative intensities in brackets.)

$(\text{NH}_4)_2\text{CrO}_4$	393 K (18h)	393 K (48h)	$(\text{NH}_4)_2\text{Cr}_2\text{O}_7$
	7,288(1)	7,284(1)	
6,991(4)	6,545(3)	6,552(3)	6,621(2)
5,532(10)	5,068(10)	5,072(10)	5,066(5)
4,788(4)	4,849(10)	4,852(10)	4,922(0)
4,106(0)	4,067(3)	4,072(4)	
3,729(2)	3,761(2)	3,761(2)	3,759(1)
3,457(10)	3,644(5)	3,646(5)	
	3,480(3)	3,480(3)	3,487(0)
	3,424(5)	3,425(5)	3,427(1)
3,397(0)	3,380(4)	3,381(4)	
	3,352(4)	3,354(4)	3,350(2)
	3,314(3)	3,315(3)	3,312(10)
	3,254(5)	3,254(5)	3,256(2)
3,177(2)	3,179(2)	3,181(2)	
	3,044(2)	3,046(2)	3,042(1)
	2,964(2)	2,966(2)	
2,824(5)	2,847(2)	2,850(1)	
	2,883(1)	-	
2,767(8)	2,784(1)	2,784(1)	2,783(1)
2,494(0)	2,461(1)	2,463(1)	2,485(0)
	2,342(1)	2,342(1)	2,341(0)
2,024(1)	2,052(1)	2,052(1)	2,052(1)
	1,995(1)	1,998(1)	1,996(0)
1,921(0)	1,921(1)	-	1,922(0)

spectra are shown in Fig. (III.3) with the absorption band maxima given in Table (III.4). The  $29412\text{ cm}^{-1}$  band in  $(\text{NH}_4)_2\text{CrO}_4$  is assigned to the low energy  ${}^1\text{T}_2$  state ( $1t_1\dots 2e$ ). The  $24096\text{ cm}^{-1}$  band is probably the electric dipole forbidden  ${}^1\text{T}_1$  by analogy with permanganate [21].

**Fig. (III.3)** Diffuse reflectance electronic spectra of  
 (a)  $(\text{NH}_4)_2\text{CrO}_4$  and (b)  $(\text{NH}_4)_2\text{Cr}_2\text{O}_7$  compared with  
 that of the following products:  
 (c)  $(\text{NH}_4)_2\text{CrO}_4$  18 hours at 393 K  
 (d)  $(\text{NH}_4)_2\text{CrO}_4$  48 hours at 393 K.

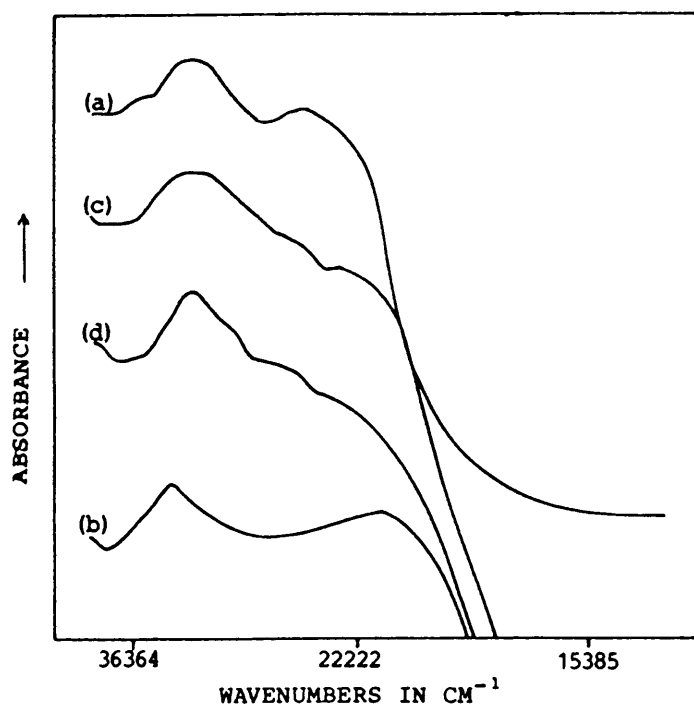


**Table (III.4)** Positions of absorption band maxima (in  $\text{cm}^{-1}$ ) in the diffuse reflectance electronic spectra of  $(\text{NH}_4)_2\text{CrO}_4$  and some of its decomposition products.

$(\text{NH}_4)_2\text{CrO}_4$	Products at 393 K		$(\text{NH}_4)_2\text{Cr}_2\text{O}_7$
	18h	48h	
$29\ 412\ \text{cm}^{-1}$	$29\ 412\ \text{cm}^{-1}$	$29\ 851\ \text{cm}^{-1}$	$30\ 303\ \text{cm}^{-1}$
$24\ 096\ \text{cm}^{-1}$	$24\ 096\ \text{cm}^{-1}$	$24\ 096\ \text{cm}^{-1}$	
	$21\ 978\ \text{cm}^{-1}$	$21\ 978\ \text{cm}^{-1}$	$21\ 978\ \text{cm}^{-1}$

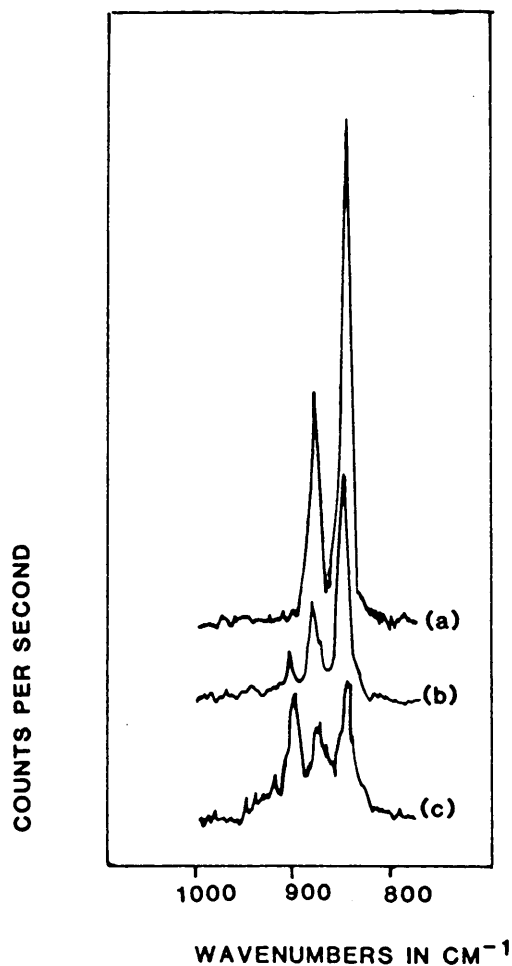
Raman spectra recorded up to 393 K indicated the direct formation of  $(\text{NH}_4)_2\text{Cr}_2\text{O}_7$  from  $(\text{NH}_4)_2\text{CrO}_4$ . Percentages N and H present in the samples decrease during the formation of  $(\text{NH}_4)_2\text{Cr}_2\text{O}_7$ . These atoms are removed from the solid when  $\text{NH}_3$  and  $\text{H}_2\text{O}$  gases evolve from the reaction [4]. From X-ray powder diffraction and diffuse reflectance spectra results it is clear that although the direct decomposition of  $(\text{NH}_4)_2\text{CrO}_4$  to  $(\text{NH}_4)_2\text{Cr}_2\text{O}_7$  proceeds even at room temperature [18], traces of the reactant are still present after 48 hours at 393 K. All the results indicate that no further decomposition takes place up to this temperature.

#### 4.3.2 Reaction kinetics

The Raman spectra of pure  $(\text{NH}_4)_2\text{CrO}_4$  and some of its decomposition products (in the frequency range  $800\text{--}1000\text{ cm}^{-1}$ ) are shown in Fig. (III.4). From this it is evident that the bands at  $845\text{ cm}^{-1}$  ( $\nu_{\text{g}}\text{-CrO}_4^{2-}$ ) and at  $902\text{ cm}^{-1}$  ( $\nu_{\text{g}}\text{-Cr}_2\text{O}_7^{2-}$ ) are well separated, and it is therefore justified to assume that the intensity of the  $845\text{ cm}^{-1}$  band in  $(\text{NH}_4)_2\text{CrO}_4$  will accurately reflect the amount of  $(\text{NH}_4)_2\text{CrO}_4$  in the decomposition reaction.

Isothermal kinetic results at various temperatures between 343 and 363 K are summarized in Appendix A, Tables (A1) to (A4) and (A5) to (A8) for microcrystals and powders respectively. These results are graphically represented in Fig. (III.5(a)) (microcrystals) and in Fig. (III.5(b)) (powders)

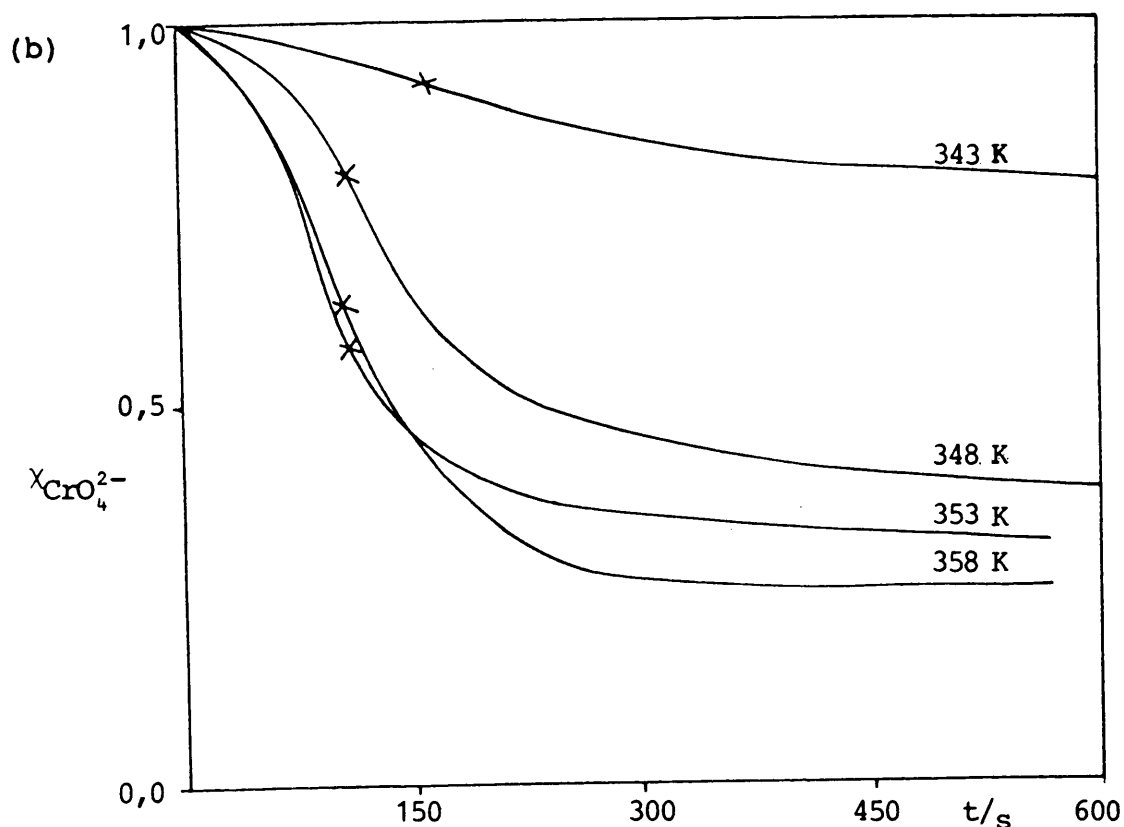
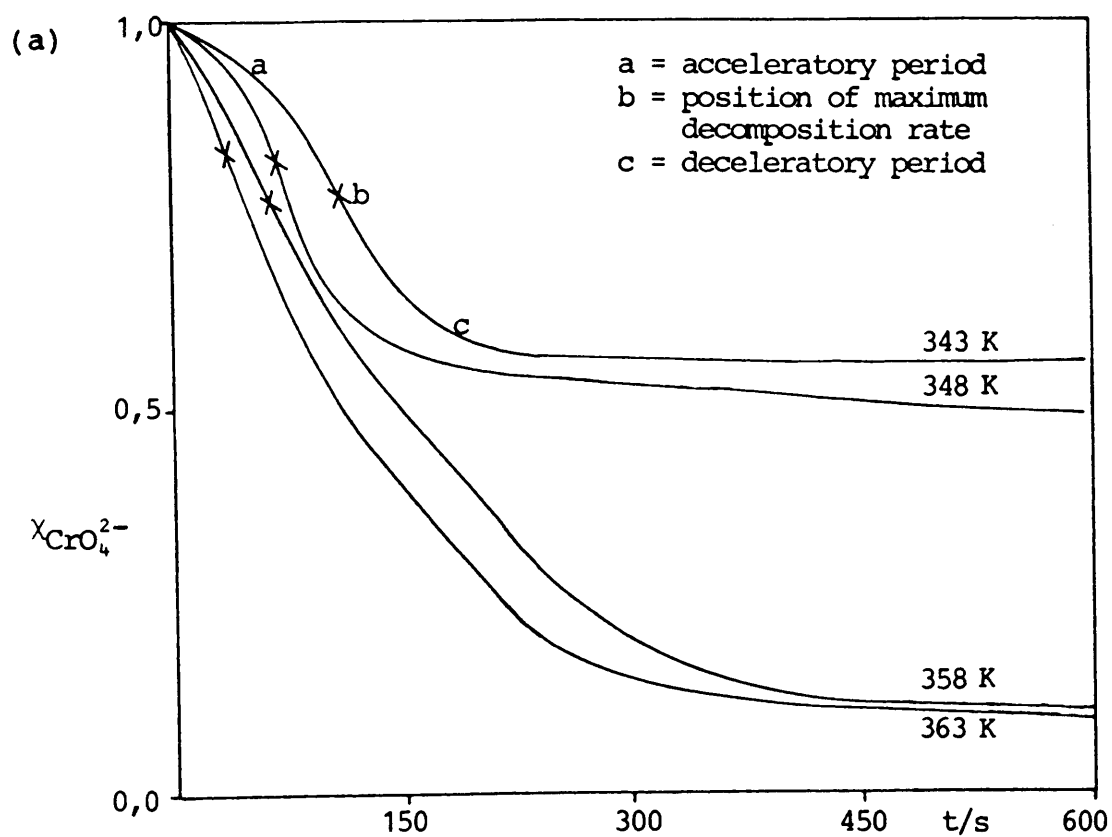
**Fig. (III.4)** Raman spectra of decomposing  $(\text{NH}_4)_2\text{CrO}_4$ .  
 (a)  $\nu_1(\text{A}_1)$  ( $845 \text{ cm}^{-1}$ ) and  $\nu_3(\text{F}_2)$  ( $876 \text{ cm}^{-1}$ ) of ammonium chromate,  
 (b) Smaller relative intensity for  $\nu_1(\text{A}_1)$  of  $(\text{NH}_4)_2\text{CrO}_4$ , and  
 (c)  $\nu_S(\text{CrO}_3)(\text{Ag})$  of  $(\text{NH}_4)_2\text{Cr}_2\text{O}_7$  increasing in relative intensity.



with the different stages of the reaction indicated on the graph obtained at 343 K in Fig. (III.5(a)). The maximum decomposition rate (indicated on each graph in Figures (III.5(a)) and (III.5(b))) is obtained sooner at higher temperatures and this point is reached during the early stages of the reaction in each case, the periods ranging from 45 to 135 seconds at the various temperatures after the initiation of the reaction. No induction period was



**Fig. (III.5)** The fraction  $(\text{NH}_4)_2\text{CrO}_4$  during decomposition ( $x_{\text{CrO}_4^{2-}}$ ) against time  $t$  at different temperatures:  
 (a) Microcrystals  
 (b) Powder



observed in the reaction; a short acceleratory period is observed at lower temperatures, this is however absent at 363 K. Acceleratory periods have not been detected by Rajam and Galwey [20] in the decomposition reaction of  $(\text{NH}_4)_2\text{CrO}_4$ , even at temperatures as low as 348 K. However, these authors used a warm-up period of a few minutes and it is possible that this could be the reason for not observing this period. The acceleratory period usually represents the growth of nuclei which are formed during an induction period. This could perhaps be accompanied by further nucleation and this period extends to the maximum rate of reaction. The reaction is decelerating after the maximum decomposition rate has been reached.

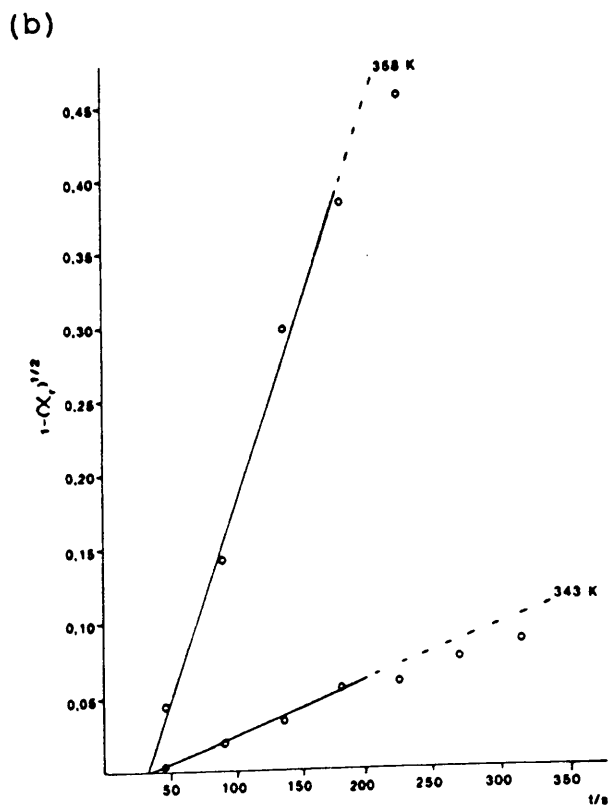
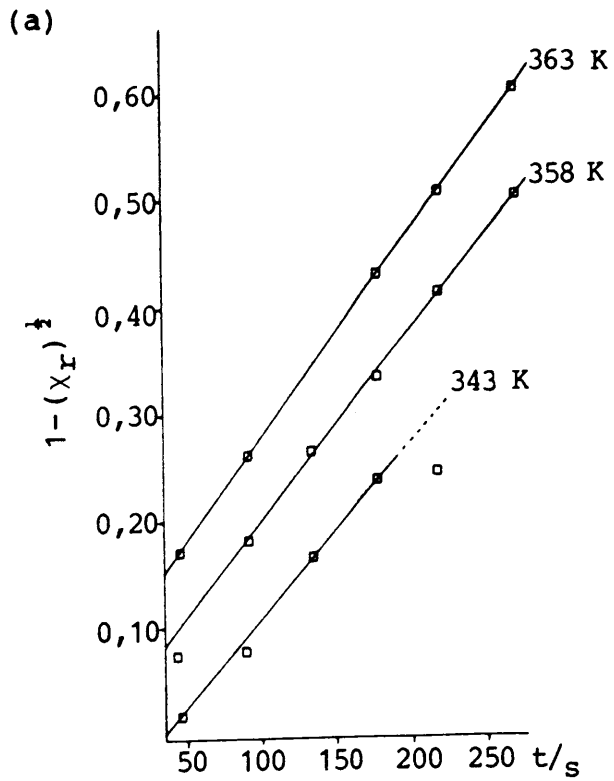
The  $\ln.\ln$  method of analysis was used to determine the kinetic expression which describes the reaction best. Accordingly, values of  $n$  were determined from  $\ln[(\ln^1/\chi_{\text{CrO}_4^{2-}})]$  vs.  $\ln$  time plots at various temperatures over intermediate ranges of the reaction. These results are summarized in Table (A9) in Appendix A. Straight lines were obtained beyond  $(-d\chi_{\text{CrO}_4^{2-}}/dt)_{\text{max}}$ . In the case of microcrystalline samples values of  $n$  could not be accurately determined at 343 and 348 K since the  $(-d\chi_{\text{CrO}_4^{2-}}/dt)_{\text{max}}$ -values were not sufficiently separated from the points at which the reaction is regarded to be complete. The values of  $n$  determined at 358 and 363 K for microcrystals are equal to 1,09 and 1,03 showing that the Avrami-Erofe'ev [22-25] or Mampel [26] intermediate law is followed. The values of  $n$  can however not be used to dis-

tinguish between the contracting volume equation,  $1-(\chi_r)^{1/3} = kt$ , or the contracting cylinder equation,  $1-(\chi_r)^{1/2} = kt$  which should give rise to values of 1,04 and 1,08 respectively [6]. In the case of powdered  $(\text{NH}_4)_2\text{CrO}_4$  the values of  $n$  vary between 0,81 and 1,10 in the temperature range concerned. These results once again indicate that the intermediate law is followed.

The obedience of the results to the contracting cylinder equation,  $1-(\chi_r)^{1/2} = kt$  are shown in Fig (III.6(a)) for microcrystals and Fig. (III.6(b)) for powder samples. Close agreement between theory and experiment was observed at higher temperatures, particularly in the case of microcrystals. In the case of powdered  $(\text{NH}_4)_2\text{CrO}_4$ , a slight decrease has been observed in the rate of the reaction at later stages as is clearly evident in Fig. (III.6(b)) in the case of a powdered sample at 343 K. Evidence has been provided [20] that this reduction in rate is caused by the accumulation of gaseous products. The linear kinetic plots for powdered  $(\text{NH}_4)_2\text{CrO}_4$  intercept the time axis at  $t = 30 \pm 10$ s. As has already been remarked there are indications of an initial acceleratory process at lower temperatures in the decomposition reaction of powdered samples. In the case of microcrystals, the intercepts with the time axes occur at approximately  $t = 0$ , indicating that there is no warm-up period for the reaction here.

In Table (A9) the values for the rate constants are given with the correlation coefficients for linear regression. Both the contracting cylinder and area equations have been

**Fig. (III.6)** The obedience of results to the contracting cylinder equation: (a) Microcrystals  
(b) Powder



used to calculate values of  $k$  at various temperatures for both microcrystals and powders. The results are virtually identical for the two and these results can therefore not be used to distinguish between these equations. However, assuming that the contracting cylinder equation is the appropriate one to represent the kinetics of this decomposition,  $k$  varies from  $4,84 \pm 0,9 \times 10^{-4}$  at 343 K to  $1,98 \pm 0,04 \times 10^{-3} \text{ s}^{-1}$  at 363 K for microcrystals and from  $8,35 \pm 0,2 \times 10^{-5}$  at 343 K and  $1,77 \pm 0,01 \times 10^{-3} \text{ s}^{-1}$  at 358 K for powdered  $(\text{NH}_4)_2\text{CrO}_4$ . The value of  $k$  at 343 K for microcrystals is of the same order of magnitude as that of  $1,33 \times 10^{-4} \text{ s}^{-1}$  reported by Rajam and Galwey [20] for 'crystallites'. However, these authors showed that the reaction is influenced by sample weight and particle dimensions (the values of  $k$  being inversely proportional to the particle radius), and it could therefore be inappropriate to compare the values of  $k$  in two completely different sets of measurements.

Assuming that the decomposition of  $(\text{NH}_4)_2\text{CrO}_4$  to  $(\text{NH}_4)_2\text{Cr}_2\text{O}_7$  is isokinetic at various temperatures, the Arrhenius equation  $\ln k = -E/RT + \ln A$  can be used to determine the activation energy,  $E$ , and the pre-exponential factor  $A$  from the graph of  $\ln k$  against  $1/T$ . These values are summarized in Table (A10). The value of  $E$  of  $97 \pm 10 \text{ kJ}\cdot\text{mol}^{-1}$  and  $\log A(\text{s}^{-1})$  of  $11,29 \pm 1,45$  closely agree with the values of Rajam and Galwey [20] for this reaction. The activation energy for powders of  $(\text{NH}_4)_2\text{CrO}_4$  is almost half that of microcrystals, clearly demonstrating the influence of particle size on this decomposition reaction.

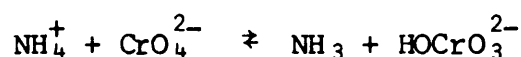
## 4.4 Conclusions

### 4.4.1 Decomposition products

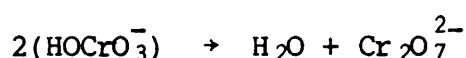
At temperatures up to 393 K  $(\text{NH}_4)_2\text{CrO}_4$  decomposes to  $(\text{NH}_4)_2\text{Cr}_2\text{O}_7$  only, and it seems to occur in a single step. Further decomposition steps coincide with the decomposition of  $(\text{NH}_4)_2\text{Cr}_2\text{O}_7$  [18,(IV.4)].

### 4.4.2 Reaction kinetics

The close agreement which has been obtained in the decomposition reaction of  $(\text{NH}_4)_2\text{CrO}_4$  between the values of  $\log A$  and  $E$  in the Raman measurements and the experiments in which the pressure of  $\text{NH}_3$  evolved was measured [20] clearly demonstrates the potential of Raman spectroscopy as a tool in the study of solid-state reactions. In addition to kinetic measurements, Raman spectroscopy provides direct evidence of structural changes during the course of the reaction. It was mentioned in (III.4.1) that the first step in the decomposition of  $(\text{NH}_4)_2\text{CrO}_4$  involves reversible proton transfer [20]



followed by water elimination



The complete Raman spectra over the range  $20 - 4000 \text{ cm}^{-1}$  were also recorded at regular time intervals at various

temperatures. However, these results fail to reveal any evidence of structural changes other than the disappearance and concomitant appearance of Cr-O modes characteristic of  $(\text{NH}_4)_2\text{CrO}_4$  and  $(\text{NH}_4)_2\text{Cr}_2\text{O}_7$  respectively. The  $\text{NH}_4^+$ -vibrations are extremely weak in both  $(\text{NH}_4)_2\text{CrO}_4$  and  $(\text{NH}_4)_2\text{Cr}_2\text{O}_7$  in the Raman effect and infrared measurements might reveal more direct evidence of structural changes in the  $\text{NH}_4^+$ -groups during the course of the reaction.

Generally speaking the kinetic results obtained by means of Raman measurements can be satisfactorily interpreted in terms of either the contracting cylinder  $1-(\chi_r)^{1/2} = kt$  or the contracting area  $1-(\chi_r)^{1/3} = kt$  equations. Based on microscopic evidence by Rajam and Galwey [20] the former law is the appropriate one. In the present Raman measurements the reaction could only be followed between 343 and 363 K because of instrumental limitations. The reaction is temperature-sensitive, at lower temperatures an initial acceleratory period is observed which is absent at higher temperatures. The reaction is furthermore dependant on particle size, E was found to be equal to  $97 \pm 12 \text{ kJ}\cdot\text{mol}^{-1}$  for microcrystals compared to  $49 \pm 0,9 \text{ kJ}\cdot\text{mol}^{-1}$  for finely divided powders.

**CHAPTER IV****THE DECOMPOSITION OF THE SOLID  $(\text{NH}_4)_2\text{Cr}_2\text{O}_7$** **1. INTRODUCTION**

The ammonium salt of dichromate consists of orange needle-like crystals. This is the product when chromic acid is added to ammonium hydroxide. These crystals can be used in leather tanning, the manufacturing of perfumes and photography [27]. It is well known that  $(\text{NH}_4)_2\text{Cr}_2\text{O}_7$  decomposes to  $\text{Cr}_2\text{O}_3$  but it seems uncertain which intermediate species, if any, are formed during the reaction [18,37-43].

**2. CRYSTALLOGRAPHIC PROPERTIES**

Ammonium dichromate has a monoclinic crystal structure and belongs to space group  $\text{C}_{2h}^6$  ( $\text{C}2/c$ ) with  $Z = 4$  [28]. The unit cell parameters are  $a = 13,16$ ;  $b = 7,54$ ;  $c = 7,74 \text{ \AA}$  and  $\beta = 93,2^\circ$ . The Cr, O(1), O(2) and O(3) atoms all occupy 8f-sites with  $\text{C}_1$  symmetry and O(4) atoms are situated on 4e-sites with  $\text{C}_2$  symmetry. The dichromate ion,  $\text{Cr}_2\text{O}_7^{2-}$ , consists of two distorted tetrahedra sharing a corner (an oxygen atom). The distortion of tetrahedra may be due to the formation of strong NH-O bonds although the accuracy of N-O distances determined is too low to decide whether this explanation is likely to be real. Cr-O distances are:

Cr-O(1)      1,55 Å

Cr-O(2)      1,57 Å

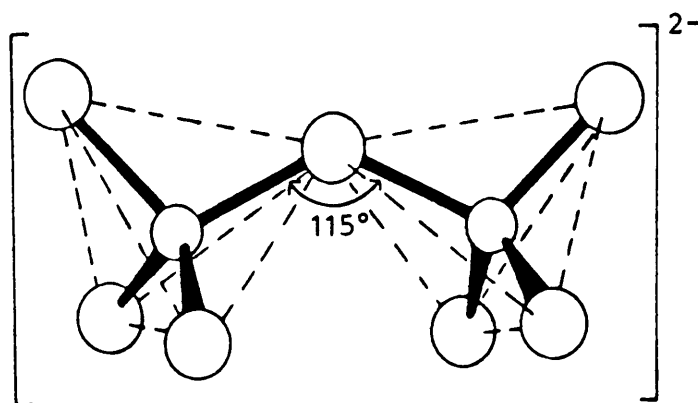


Cr-O(3) 1,78 Å

Cr-O(4) 1,91 Å

The shortest Cr-Cr distance is that of the chromium atoms in the Cr-O-Cr-bridge, being 3,2 Å. The dichromate ion are shown in Fig. (IV.1).

Fig. (IV.1) The  $\text{Cr}_2\text{O}_7^{2-}$  ion.



### 3. INFRARED AND RAMAN SPECTRA

#### 3.1 Previous studies

Both infrared and Raman spectra of  $(\text{NH}_4)_2\text{Cr}_2\text{O}_7$  have been reported with assignments. An early infrared spectrum was recorded by Miller *et. al.* [29] and band positions was reported without assignments. The first assignment of the dichromate spectrum was made by Stammreich *et. al.* [30]. Later studies gave additional information on the nature of the  $\text{Cr}_2\text{O}_7^{2-}$  vibrations [31-33]. The ammonium bands were assigned by Heyns [34]. Luu Dang Vinh [35] studied single crystals of  $(\text{NH}_4)_2\text{Cr}_2\text{O}_7$  by means of Raman spectroscopy, assigned the frequencies and identified the crystal vibrations.

### 3.2 Vibrational analysis

The determination of the total molecular vibrations of the dichromate ion,  $8A_1 + 5A_2 + 6B_1 + 8B_2$  (using the method described in ref. [36]), are shown in Table (IV.1).

**Table (IV.1)** Total molecular vibrations of  $\text{Cr}_2\text{O}_7^{2-}$

$C_{2v}$	E	$C_2$	$\alpha_V(xz)$	$\alpha_V^1(yz)$	
$\Gamma_{xyz}$	3	-1	1	1	
unmoved atoms	9	1	1	5	
$\Gamma_{tot}$	27	-1	1	5	$= 8A_1 + 5A_2 + 6B_1 + 8B_2$

Of these the following are rotation and translation modes :  $A_1 + A_2 + 2B_1 + 2B_2$ . This leaves the irreducible representation of molecular vibrations (normal modes) as:

$$\Gamma_{vib} = 7A_1 + 4A_2 + 4B_1 + 6B_2$$

All modes are both infrared and Raman active.

The molecular vibrations can be divided into stretching and bending vibrations which can in turn be divided in terminal and bridge stretches and  $\text{CrO}_3$ ,  $\text{O-CrO}_3$  and  $\text{Cr-O-Cr}$  bends.

An analysis of the  $\text{Cr-O}$  terminal and bridge stretching modes is presented in Table (IV.2)

**Table (IV.2)** Stretching analysis of Cr-O modes in  $\text{Cr}_2\text{O}_7^{2-}$ 

$C_{2v}$	E	$C_2$	$\alpha_V(xz)$	$\alpha'_V(yz)$	
$\Gamma_{\text{Cr-O}_t}$ stretch	6	0	0	2	$= 2A_1 + A_2 + B_1 + 2B_2$
$\Gamma_{\text{Cr-O}_b}$ stretch	2	0	0	2	$= A_1 + B_2$

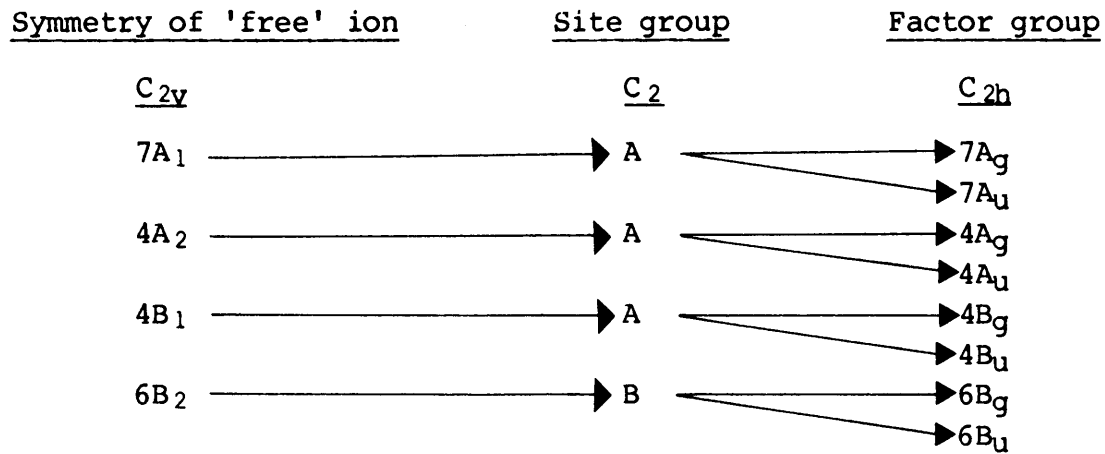
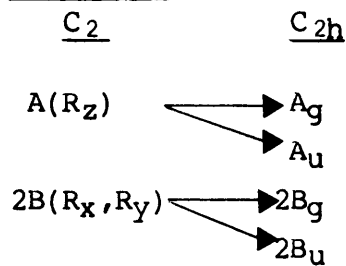
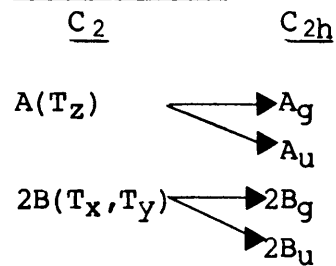
A bending analysis of  $\text{CrO}_3$  and  $\text{O-CrO}_3$  groups is presented in Table (IV.3). The Cr-O-Cr bending mode is the totally symmetric mode  $A_1$ .

**Table (IV.3)** Bending mode analysis of  $\text{Cr}_2\text{O}_7^{2-}$ 

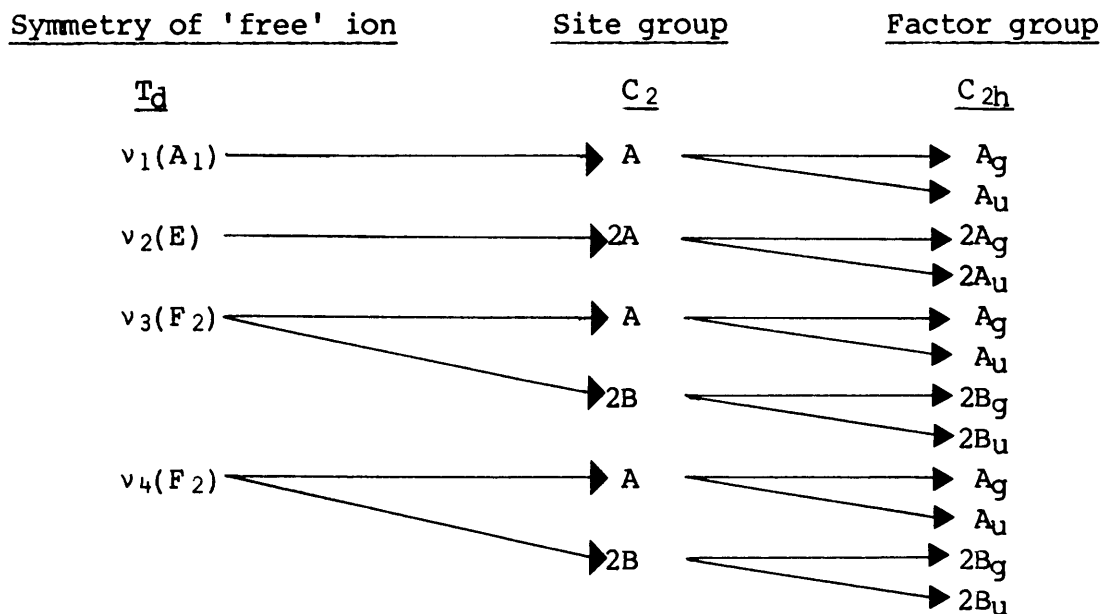
$C_{2v}$	E	$C_2$	$\alpha_V(xz)$	$\alpha'_V(yz)$	
$\Gamma_{\text{CrO}_3}$ bend	6	0	0	-2	$= A_1 + 2A_2 + 2B_1 + B_2$
$\Gamma_{\text{O-CrO}_3}$ bend	6	0	0	2	$= 2A_1 + A_2 + B_1 + 2B_2$

The correlation of the 'free'  $\text{Cr}_2\text{O}_7^{2-}$  and  $\text{NH}_4^+$  ions with site group  $C_2$  and factor group  $C_{2h}$  is shown in Fig. (IV.2(a)) and (IV.2(b)) respectively.

**Fig. (IV.2(a))** Site and factor group correlation of the  $\text{Cr}_2\text{O}_7^{2-}$  ion in  $(\text{NH}_4)_2\text{Cr}_2\text{O}_7$

RotationsTranslations

**Fig. (IV.2(b))** Site and factor group correlation of the  $\text{NH}_4^+$  ion in  $(\text{NH}_4)_2\text{Cr}_2\text{O}_7$



The internal modes of  $\text{Cr}_2\text{O}_7^{2-}$  in  $(\text{NH}_4)_2\text{Cr}_2\text{O}_7$  are confirmed by the factor group analysis using the Adams method [2] described in Fig. I.3 (I.2.2).

### 3.3 Description of the spectra

The Raman and mid-IR spectra of  $(\text{NH}_4)_2\text{Cr}_2\text{O}_7$  are shown in Fig. (IV.3) and (IV.4) respectively, with far-IR bands in

Fig. (IV.3) The Raman spectrum of  $(\text{NH}_4)_2\text{Cr}_2\text{O}_7$

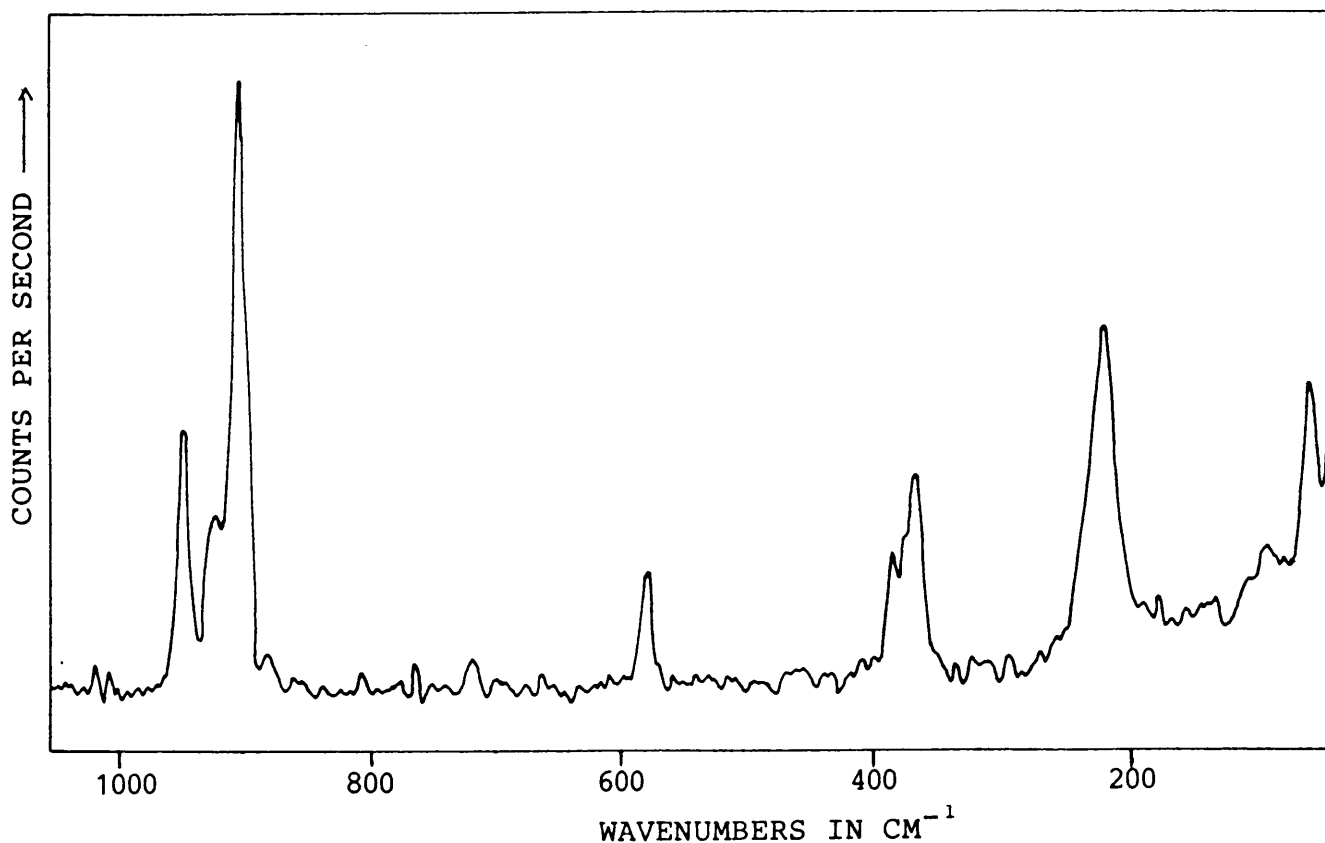
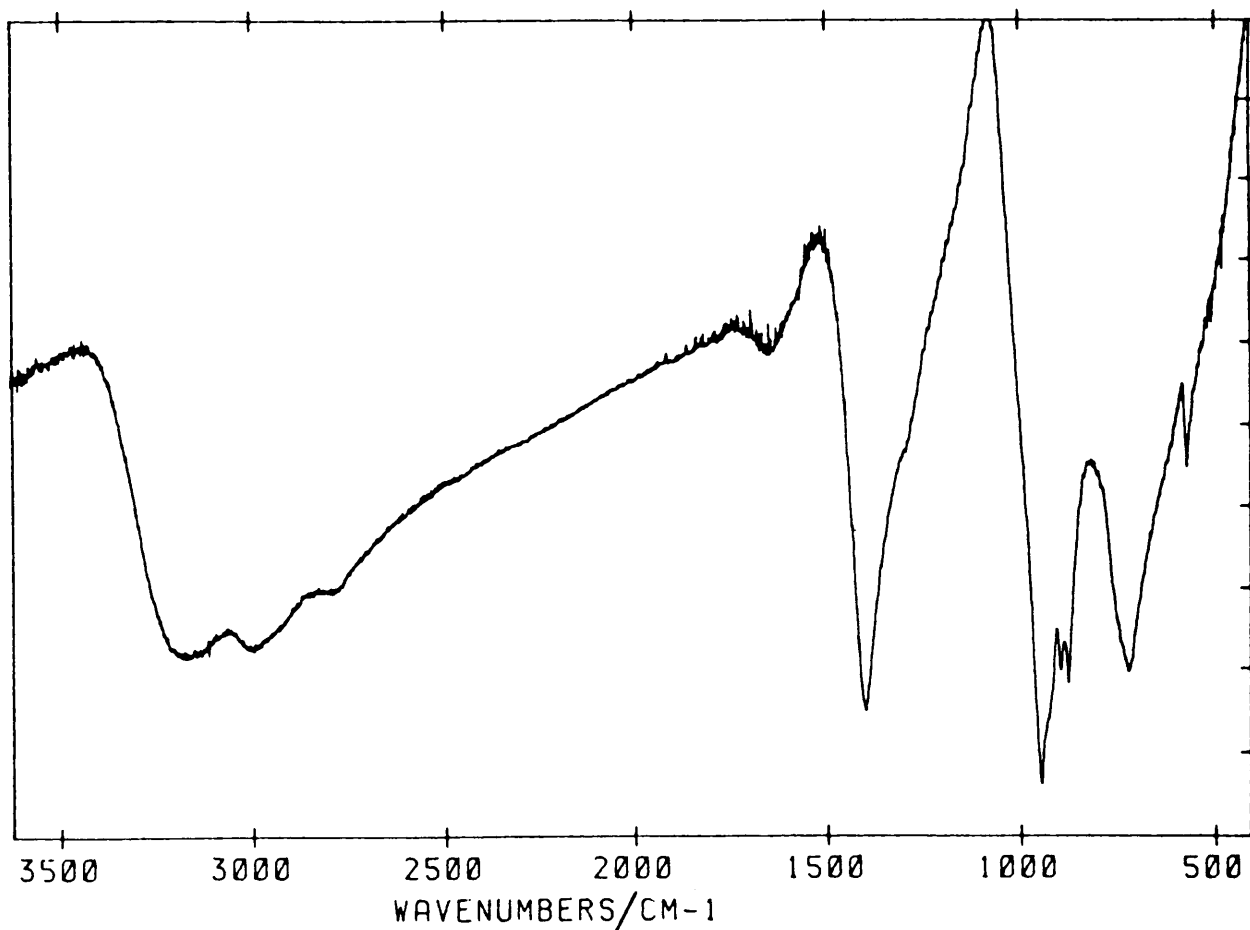
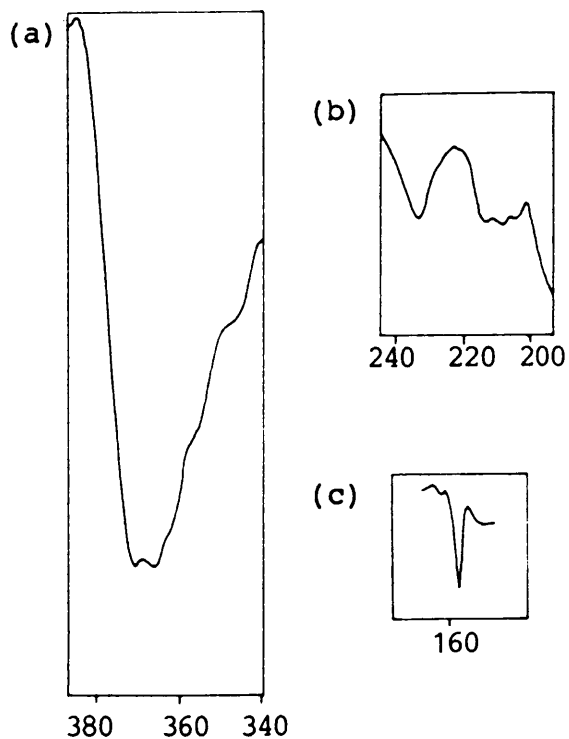


Fig. (IV.5(a-c)). The ammonium bands in the infrared spectrum are compared to the bands obtained and assigned by Heyns [34] at room-temperature in Table (IV.4).

**Fig. (IV.4)** The mid-IR spectrum of  $(\text{NH}_4)_2\text{Cr}_2\text{O}_7$ 

**Fig. (IV.5)** Some far-IR bands of  $(\text{NH}_4)_2\text{Cr}_2\text{O}_7$   
 (a)  $\delta_{\text{S}}(\text{CrO}_3)\text{Ag}$  ( $370 \text{ cm}^{-1}$ ) and  $\delta_{\text{AS}}(\text{CrO}_3)\text{Ag}$  ( $366 \text{ cm}^{-1}$ )  
 (b) O-CrO<sub>3</sub> bend(Ag) ( $234 \text{ cm}^{-1}$ ) and O-CrO<sub>3</sub> bend(Bg) ( $209 \text{ cm}^{-1}$ )  
 (c) O-CrO<sub>3</sub> bend(Ag) ( $157 \text{ cm}^{-1}$ )



**Table (IV.4)** Frequencies and assignment of the IR active ammonium vibrations in  $(\text{NH}_4)_2\text{Cr}_2\text{O}_7$

Frequency in $\text{cm}^{-1}$		
Heyns [34]	This work	Assignment [34]
3220 sh.	-	
~3130 b.	3128 s.b.	$\nu_3$
3020	2982 s.	$\nu_2 + \nu_4$
2860-2790	2787 sh.	$2\nu_4$
1400	1402 s.sp.	$\nu_4$

s = strong                      b = broad  
sh = shoulder                  sp = sharp

In Table (IV.5) the assignment of Raman bands by Luu Dang Vinh et. al. [35] are compared to the bands obtained from IR and Raman spectra in this study.

The IR spectrum and the thermal behaviour of Raman modes in  $(\text{NH}_4)_2\text{Cr}_2\text{O}_7$  will be compared to that of  $\text{K}_2\text{Cr}_2\text{O}_7$  in (VI.3.3) and (VI.4.3).

**Table (IV. 5)** Infrared and Raman bands of  $(\text{NH}_4)_2\text{Cr}_2\text{O}_7$  found during this study

sh = shoulder                      s = strong  
 w = weak                            b = broad  
 m = medium                        sp = sharp

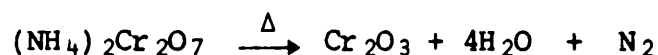
Assignment [35]				Frequency in $\text{cm}^{-1}$	
				Raman	IR
$\Gamma_{\text{CrO}_3}$ stretch	[ $\nu_{\text{as}}$	$B_g$	( $B_2$ )	950 sh.	949 s.sp.
		$A_g$	( $A_1$ )	946 m.	
		$B_g$	( $B_1$ )	919 w.	929 s.sh.
	[ $\nu_s$	$A_g$	( $A_2$ )	912 sh.	
		$A_g$	( $A_1$ )	902 s.sp.	898 s.sp.
		$B_g$	( $B_1$ )	878 w.	877 s.sp.
$\Gamma_{\text{Cr-O-Cr}}$ stretch	[ $\nu_{\text{as}}$	$B_g$	( $B_1$ )	720 w	724 s.b.
	[ $\nu_s$	$A_g$	( $A_1$ )	578 w.	573 m.s.p.
$\Gamma_{\text{CrO}_3}$ bend	[ $\delta_{\text{as}}$	$B_g$	( $B_1$ )	391 w.	
		$A_g$	( $A_1$ )	385 m.	
	[ $\delta_s$	$B_g$	( $B_1$ )	382 m.	
		$B_g$	( $B_2$ )	375 sh.	
	[ $\delta_{\text{as}}$	$A_g$	( $A_1$ )	373 m.	370 w.sh.
		$A_g$	( $A_2$ )	362 sh.	366 w.
$\Gamma_{\text{O-CrO}_3}$ bend	[	$A_g$	( $A_2$ )	236 sh.	234 w.
		$B_g$	( $B_2$ )	230 sh	
		$B_g$	( $B_1$ )	228 s	
		$B_g$	( $B_2$ )	198 w.	209 w.
		$A_g$	( $A_2$ )	160 w.	157 w.sp.
$\Gamma_{\text{Cr-O-Cr}}$ bend	[ $\delta$	$A_g$	( $A_1$ )	226 sh.	
Translations				105, 98, 94	
Rotations				61, 44, 28	



#### 4. THE THERMAL DECOMPOSITION OF $(\text{NH}_4)_2\text{Cr}_2\text{O}_7$

##### 4.1 Literature on the Products and Mechanism of the reaction

The thermal decomposition of  $(\text{NH}_4)_2\text{Cr}_2\text{O}_7$  is generally represented by the following simplified reaction [18].



Several authors [19,37-43] have studied the reaction, but the conclusions were often controversial and contradictory especially concerning the large variety of intermediate species which have been proposed.

Mahieu et. al. [37] studied the decomposition reaction by means of DTA and TGA. So-called "intermediate compounds" were determined by, amongst others, X-ray diffraction and magnetic susceptibility measurements. The decomposition seemed to occur in four consecutive reaction steps, occurring at 508, 533, 573 and 693 K respectively. Effluent gases analyzed by gas chromatography revealed that  $\text{N}_2$ ,  $\text{H}_2\text{O}$  and  $\text{NH}_3$  were released during the first two reaction steps,  $\text{N}_2$  and  $\text{H}_2\text{O}$  during the third step and  $\text{O}_2$  in the final decomposition step. X-ray diffraction results revealed that the final green solid product was crystalline  $\text{Cr}_2\text{O}_3$ , with the black intermediate products all being amorphous. Radio-active tracer techniques were used to determine the oxidation states at different stages of the reaction. The composition after the first stage was 39% Cr(III), 61% Cr(VI) and 66% Cr(III),

34% Cr(VI) after the second and third stages. However, the authors concluded from this that these ratios indicate the existence of Cr(V) after the first stage and Cr(IV) after the second and third stages! The following intermediate compounds were then proposed [37]:

Cr(V):       $\text{Cr}_2\text{O}_5$           at 503 K.

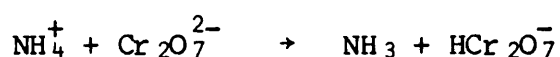
Cr(IV):       $[\text{CrO}_2]_6\text{H}_2\text{O}$       at 533 K.

Cr(IV):       $\text{CrO}_2$               at 573 K.

If  $\text{Cr}_2\text{O}_5$  did exist as an intermediate in this decomposition reaction, it would not coincide with an oxidation number of V, or even a combination of VI and III as  $\text{Cr}_2\text{O}_5$  is generally regarded as  $\text{CrO}_3 \cdot \text{CrO}_2$  [44], and thus a combination of oxidation number VI and IV would occur.

Simpson *et. al.* [38] also proposed  $\text{Cr}_2\text{O}_5$  as a possible intermediate. A kinetic study of the decomposition of single crystals of  $(\text{NH}_4)_2\text{Cr}_2\text{O}_7$  from 453 to 488 K was included in the study. Three consecutive stages were identified: An induction period corresponding to nucleation, an autocatalysis obeying the Prout-Tompkins equation,  $\log P/(p_f - p) = k \log t + \text{const.}$ , where  $p_f$  is the pressure at the end of the stage of gaseous products not absorbed by phosphoric oxide, and thirdly a zero-order rate process ascribed to a constant area of interface advance. (This is in contrast with the results obtained by Fischbeck and Spingler [41]. Their analysis of the sigmoid curve obtained between 461 and 491 K showed obedience to the power law with

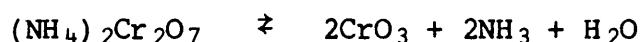
n = 4 during the acceleratory period followed by a contracting sphere mechanism). During the decomposition [38] the colour was reported to change to a deep-red which gradually darkened to a black amorphous solid. Black diamond-shaped nuclei developed on the crystal surfaces in the early stages of the reaction. The composition of the black solid forming at 469 K was determined as  $\text{Cr}_2\text{O}_3:0,88\text{H}_2\text{O}:0,047\text{N}_2\text{O}:0,15\text{O}_2$ . Infrared spectra showed the possible formation of an intermediate which may contain nitrite and nitrate groups, with electrical conductivity changes during the decomposition supporting the possibility. A possible structure for such an intermediate is suggested to consist of chains of alternating chromium and oxygen atoms to which nitrite( $\text{NO}_2^-$ ) and nitrate( $\text{NO}_3^-$ ) or even  $\text{NH}_2$ -groups are linked. According to infrared spectra the nitrite and nitrate groups present in the intermediate appear not to be co-ordinated to Cr(III) in a normal way.  $\text{NH}_3$  and  $\text{H}_2\text{O}$  inhibited the reaction as the evolution of these compounds occurred until completion of the acceleratory stage. In analogy with other compounds it was concluded that the first step is proton transfer [38]:



The thermal decomposition of ammonium chromate and ammonium dichromate were studied by Ill-Huyn Park [18,19] by means of TG, DTA, DTG and mass spectrometry. Four reaction steps were found in the decomposition of ammonium chromate and three steps in that of ammonium dichromate. All three steps in the decomposition of the latter were found to be exothermic.

According to weight loss percentages  $(\text{NH}_4)_2\text{Cr}_2\text{O}_7$  decomposes to brown  $\text{CrO}_3$  between 478 and 518 K, to black  $\text{CrO}_2$  between 533 and 558 K, and finally to dark green  $\text{Cr}_2\text{O}_3$  above 683 K. The black solid obtained between 478 and 518 K was however identified by X-ray diffraction as a mixture of  $\text{CrO}_3$  and  $\text{Cr}_2\text{O}_3$ . The gases that evolved from the reaction were identified as  $\text{N}_2$ ,  $\text{N}_2\text{O}$ ,  $\text{H}_2\text{O}$  and a small amount of  $\text{NH}_3$  [19].  $\text{CrO}_3$ , one of the products obtained from the decomposition, is a strong oxidizing agent. Therefore  $\text{NH}_3$  present will be easily oxidized to form  $\text{N}_2$  and  $\text{N}_2\text{O}$ , with Cr(VI) being reduced to Cr(III). In the final stages of the decomposition  $\text{O}_2$  is released above 673 K.

Galwey et. al. [42] examined previously decomposed crystals of  $(\text{NH}_4)_2\text{Cr}_2\text{O}_7$  by means of an electron microscope and found evidence that the reaction proceeds through the intervention of a melt. The darkening of  $(\text{NH}_4)_2\text{Cr}_2\text{O}_7$  during the decomposition reaction is ascribed to dissociative loss of ammonia and the ultimate yielding of  $\text{CrO}_3$  as a possible molten intermediate, since the melting point of  $\text{CrO}_3$  (468-469 K) is towards the lower end of temperatures used during the study. The following reaction was proposed as an initial reaction in the decomposition [42]:



The reaction is probably reversible. This would be followed by oxidation of  $\text{NH}_3$  or  $\text{NH}_4^+$ , yielding  $\text{N}_2$  and  $\text{N}_2\text{O}$  as gaseous products. The internal structure of the product in the reac-

tion of  $\text{CrO}_3$  with ca. 20%  $(\text{NH}_4)_2\text{CO}_3$  at 513 K closely resembled the structure of the product found when  $(\text{NH}_4)_2\text{Cr}_2\text{O}_7$  was heated to 478 K [42].

Results obtained during an infrared and X-ray diffraction study by Zaki and Fahim [43] showed that in contrast to results obtained by previous authors [18,19,42] the product in the first stage of the decomposition reaction of  $(\text{NH}_4)_2\text{Cr}_2\text{O}_7$  (458-488 K) exists mainly of a highly distorted  $\text{Cr}_2\text{O}_3$ -structured compound, together with small amounts of  $\text{CrO}_3$ . Infrared results indicated that  $\text{NH}_4^+$  and  $\text{H}_2\text{O}$  were present, probably as surface species. Although weight loss in the second step of the reaction (503-588 K) once again indicated the formation of  $\text{CrO}_2$ , X-ray diffraction results revealed the domination of a still highly strained  $\text{Cr}_2\text{O}_3$ -species at the expense of the  $\text{CrO}_3$ -species. No trace was found of the existence of  $\text{CrO}_2$ . The final product, existing of highly stoichiometric  $\alpha\text{-Cr}_2\text{O}_3$  is obtained at temperatures above 673 K [43].

A summary of the results obtained by the various authors for the decomposition of both  $(\text{NH}_4)_2\text{CrO}_4$  and  $(\text{NH}_4)_2\text{Cr}_2\text{O}_7$ , together with the different methods used, are shown in Table (IV.6).

#### 4.2 Experimental work

The Raman spectrum of  $(\text{NH}_4)_2\text{Cr}_2\text{O}_7$  recorded at room-temperature between 20 and  $1000\text{ cm}^{-1}$  are shown in Fig. (IV.3). Further Raman measurements were made after 30 minutes at each

Table (IV.6)

A summary of the results obtained by the various authors

Authors : Decomposition of :	Mahieu et. al. [37] $(\text{NH}_4)_2\text{Cr}_2\text{O}_7$	Simpson et. al. [38] $(\text{NH}_4)_2\text{Cr}_2\text{O}_7$	Park [18] $(\text{NH}_4)_2\text{CrO}_4$ and	Park [19] $(\text{NH}_4)_2\text{Cr}_2\text{O}_7$	Galwey and Rajam [20] $(\text{NH}_4)_2\text{CrO}_4$	Galwey et. al. [42] $(\text{NH}_4)_2\text{Cr}_2\text{O}_7$	Zaki and Fahim [43] $(\text{NH}_4)_2\text{Cr}_2\text{O}_7$
Methods of Analysis	DTA, TGA, XRD, magnetic susceptibility, gas chromatography	XRD, gas chromatography, IR, electrical conductivity	TG, DTA, DTG, XRD	Mass spectrometry	Electron microscopy	Electron microscopy	TG, DTA, XRD, IR
Reaction steps found	4	-	4	3	-	-	3
Products suggested at different temperatures	$\text{Cr}_2\text{O}_5$ (508 K) [ $(\text{CrO}_2)_6\text{H}_2\text{O}$ ] (533 K) $\text{CrO}_2$ (573 K) $\text{Cr}_2\text{O}_3$ (693 K)	$\text{Cr}_2\text{O}_5$  $\text{NH}_3$ -Cr-compound  $\text{Cr}_2\text{O}_3$	$(\text{NH}_4)_2\text{Cr}_2\text{O}_7$ $\text{CrO}_3$  $\text{CrO}_3/\text{Cr}_2\text{O}_3$  $\text{Cr}_2\text{O}_3$	$\text{CrO}_3$ (478-518 K) $\text{CrO}_3/\text{Cr}_2\text{O}_3$ (533-558 K) $\text{Cr}_2\text{O}_3$ (673 K $\rightarrow$ )	$(\text{NH}_4)_2\text{Cr}_2\text{O}_7$ (1st step)	$\text{CrO}_3$ -melt  $\text{NH}_3$ -Cr-compound  $\text{Cr}_2\text{O}_3$	$\text{Cr}_2\text{O}_3$ and traces $\text{CrO}_3$ (473-543 K) Strained $\text{Cr}_2\text{O}_3$ (503-588 K) $\alpha$ - $\text{Cr}_2\text{O}_3$ (673 K)

of the following temperatures: 323, 373, 423, 433, 443, 453, 463, 473, 483, 488, 493, 498, 503 and 518 K. Mid- and far-infrared spectra of the products obtained at 498, 503 and 518 K were recorded. Products prepared in the Raman high temperature cell by heating  $(\text{NH}_4)_2\text{Cr}_2\text{O}_7$  for short periods at 613 and 693 K, and for three hours at 693 K, were also investigated by means of FT-IR. Infrared spectra of untreated  $(\text{NH}_4)_2\text{Cr}_2\text{O}_7$ ,  $\text{CrO}_3$  and  $\text{Cr}_2\text{O}_3$  were also recorded for comparison with the various products obtained.

Samples of  $(\text{NH}_4)_2\text{Cr}_2\text{O}_7$  were decomposed at various temperatures for different periods of time and the products were investigated by wet analysis methods, X-ray powder diffraction and UV-diffuse reflectance spectra.

### 4.3 Results and Discussion

#### 4.3.1 Raman Spectroscopy results

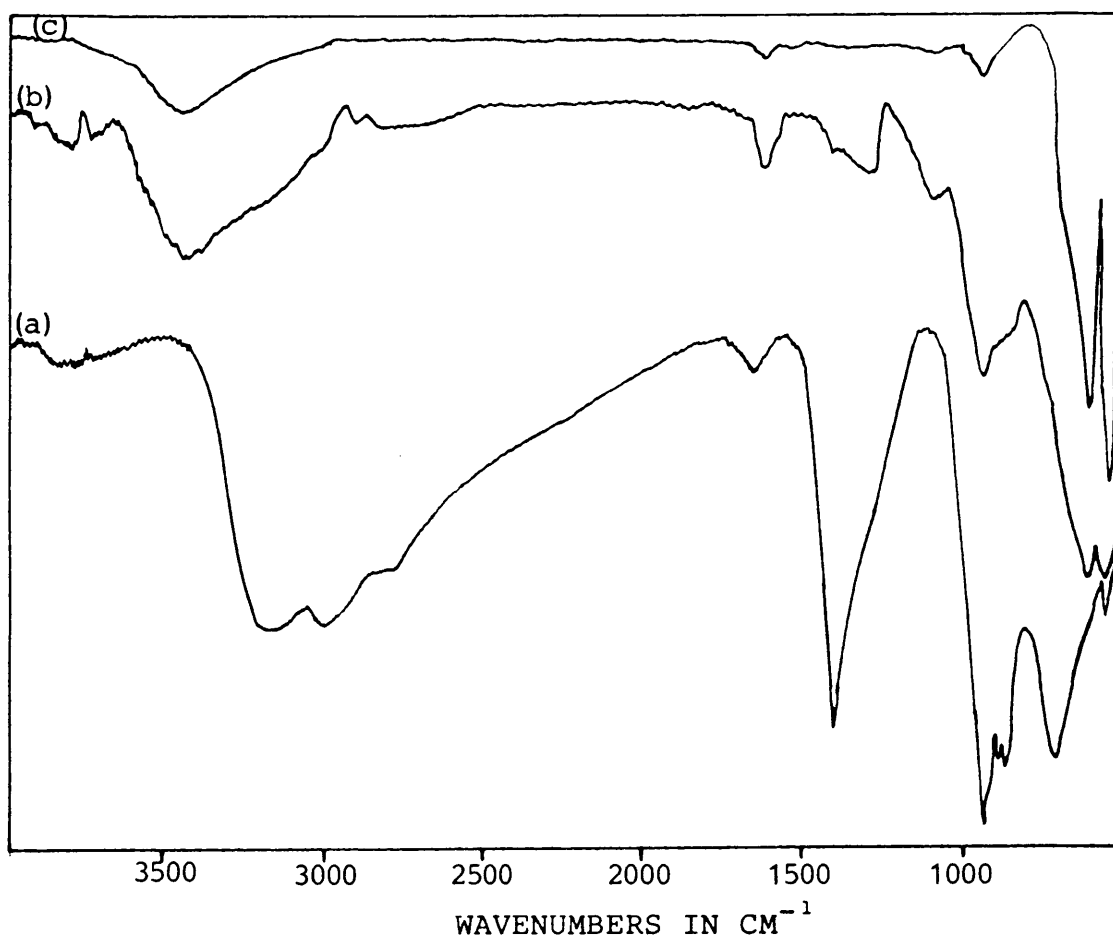
Raman spectra recorded up to 473 K indicated only the presence of  $(\text{NH}_4)_2\text{Cr}_2\text{O}_7$  up to this temperature. At higher temperatures the samples decomposed rapidly, turning black and no Raman measurements were made at these temperatures. The thermal behaviour of the Raman bands of this compound at temperatures up to 473 K are discussed in (VI.4).

#### 4.3.2 FT-IR

All the Infrared active bands of the products obtained are

compared with that of pure  $(\text{NH}_4)_2\text{Cr}_2\text{O}_7$ ,  $\text{CrO}_3$  and  $\text{Cr}_2\text{O}_3$  in Table (IV.7). The mid-infrared spectra of  $(\text{NH}_4)_2\text{Cr}_2\text{O}_7$  at different decomposition stages at relatively low temperatures are shown in Fig. (IV.6).

**Fig. (IV.6)** Infrared spectra of  
(a)  $(\text{NH}_4)_2\text{Cr}_2\text{O}_7$  and its decomposition products  
at (b) 498 K and (c) 503K.



(a) Rapid heating up to 498 K

A violent reaction yields a black- and green solid. Infrared spectra shows a weakening in the intensity of



**Table (IV.7)** IR-bands of some decomposition products of  $(\text{NH}_4)_2\text{Cr}_2\text{O}_7$  compared with pure  $(\text{NH}_4)_2\text{Cr}_2\text{O}_7$ ,  $\text{CrO}_3$ ,  $\text{Cr}_2\text{O}_3$  and a complex. All frequencies are in  $\text{cm}^{-1}$ .

$(\text{NH}_4)_2\text{Cr}_2\text{O}_7$	Products					$[\text{Cr}(\text{NH}_3)_6]\text{Cl}_3$ [46]	$\text{CrO}_3$	$\text{Cr}_2\text{O}_3$
	498 K	503 K	518 K	613 K	693 K			
3128 $\nu_3(\text{NH}_4^+)$ 1633 1402 $\nu_4(\text{NH}_4^+)$	3421 m.b. 1628 w. 1276 w.b.	3431 w.b. 1626 w.	3151 s.b. 1646 sh. 1387 sh. 1277	3432 w.b. 1670 w. 1120 w. 958 w. 949 w.	3446 w.b.	3330 1622 1334 1120 w.	1618 w. 959 944 907	
949 $\nu_{\text{as}}(\text{CrO}_3)$	947 m.							
898 $\nu_{\text{as}}(\text{CrO}_3)$ 724 $\nu_{\text{as}}(\text{Cr-O-Cr})$	621 m. 561 m.		899 745 s.b. 557 s.b.	616- 568 492 470 461	618s.sp. 558s.sp.	492 474 Cr-N 459	623s.sp 558s.sp	
		460 sh. 444 411 325			445 412 307 sp.	325 $\delta(\text{N-Cr-N})$	444 415	

w = weak  
m = medium  
s = strong  
sh = shoulder  
sp = sharp  
b = broad

the ammonium bands, with the appearance of ammonia bands [45] at 3421 and 1628  $\text{cm}^{-1}$ . A weak band at 1276  $\text{cm}^{-1}$  can be attributed to  $\text{NO}_2$  groups trapped in the solid during decomposition, as an infrared spectrum of  $[\text{Cr}(\text{NH}_3)_5\text{NO}_3](\text{NO}_2)_2$  has a band at 1277  $\text{cm}^{-1}$  [38] which is absent in other chromium complexes containing only  $\text{NH}_3$ ,  $\text{H}_2\text{O}$  and  $\text{NO}_3$  groups. There is a decrease in the intensity of the characteristic dichromate bands between 947 and 724  $\text{cm}^{-1}$ . The bands appearing at 621 and 561  $\text{cm}^{-1}$  are characteristic of  $\text{Cr}_2\text{O}_3$ .

(b) Rapid heating up to 503 K

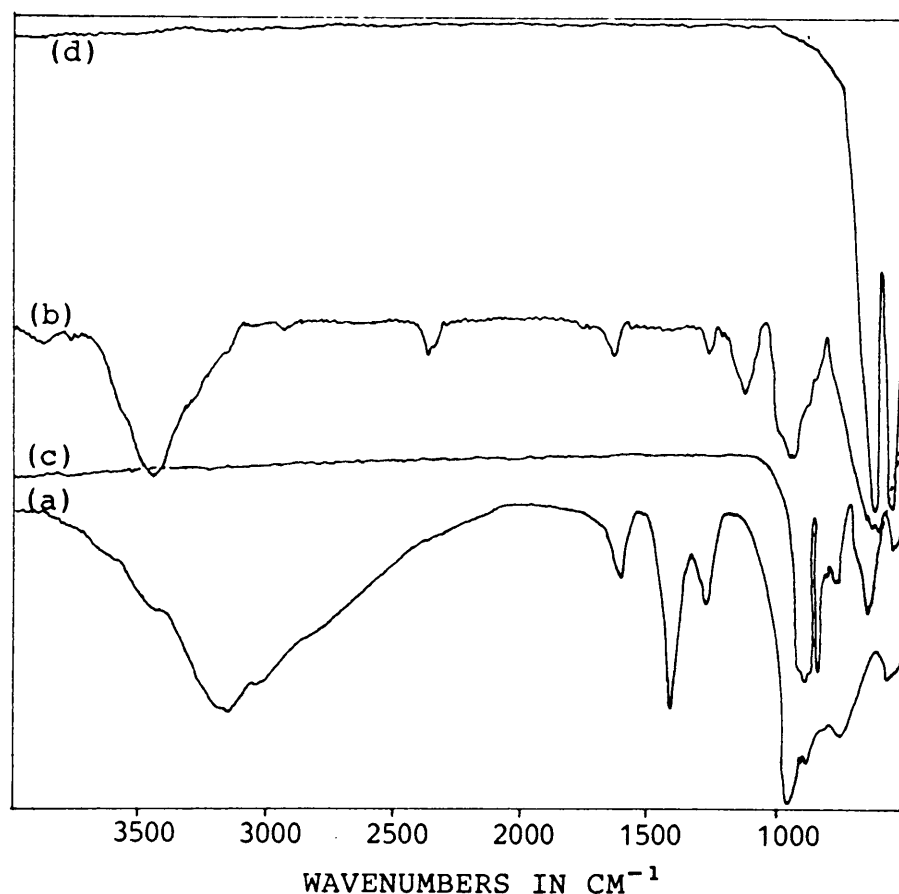
$\text{NH}_3$ -bands [46] are observed at 3431 and 1626  $\text{cm}^{-1}$  with no sign of  $\text{NH}_4^+$ -bands. In the far-infrared spectra the band observed at 460  $\text{cm}^{-1}$  in both the spectra of  $(\text{NH}_4)_2\text{Cr}_2\text{O}_7$  and its decomposition product at 498 K are absent, but two new bands appearing at 444 and 411  $\text{cm}^{-1}$  are also observed in the far-infrared spectra of  $\text{Cr}_2\text{O}_3$ .

Mid-infrared spectra of decomposition products obtained at 518 and 613 K are compared with the spectra of  $\text{CrO}_3$  and  $\text{Cr}_2\text{O}_3$  in Fig. (IV.7).

(c) Gradual heating up to 518 K

Gradual heating results in a slower reaction so that no violent reaction is visible. The product is a black solid. The ammonium bands are of a lower intensity

**Fig. (IV.7)** Infrared spectra of the decomposition products of  $(\text{NH}_4)_2\text{Cr}_2\text{O}_7$  at (a) 518 K and (b) 613 K, compared with the spectra of (c)  $\text{CrO}_3$  and (d)  $\text{Cr}_2\text{O}_3$ .



than those occurring from 3182 to 2787 and 1402  $\text{cm}^{-1}$  in the spectrum of untreated  $(\text{NH}_4)_2\text{Cr}_2\text{O}_7$ , and the bands have shifted to 3151 and 1387  $\text{cm}^{-1}$  respectively. A shoulder around 3400  $\text{cm}^{-1}$  and a new band at 1646  $\text{cm}^{-1}$  indicates the formation of  $\text{NH}_3$  [45], while the band at 1277  $\text{cm}^{-1}$  is again ascribed to  $\text{NO}_2^-$  [38] formation.

Dichromate bands are still present between 950 and 880  $\text{cm}^{-1}$  but the band at 724  $\text{cm}^{-1}$  now occurs at

745  $\text{cm}^{-1}$ . The broad band at 557  $\text{cm}^{-1}$  appears to be the band characteristic of  $\text{Cr}_2\text{O}_3$ .

(d) Gradual heating up to 613 K

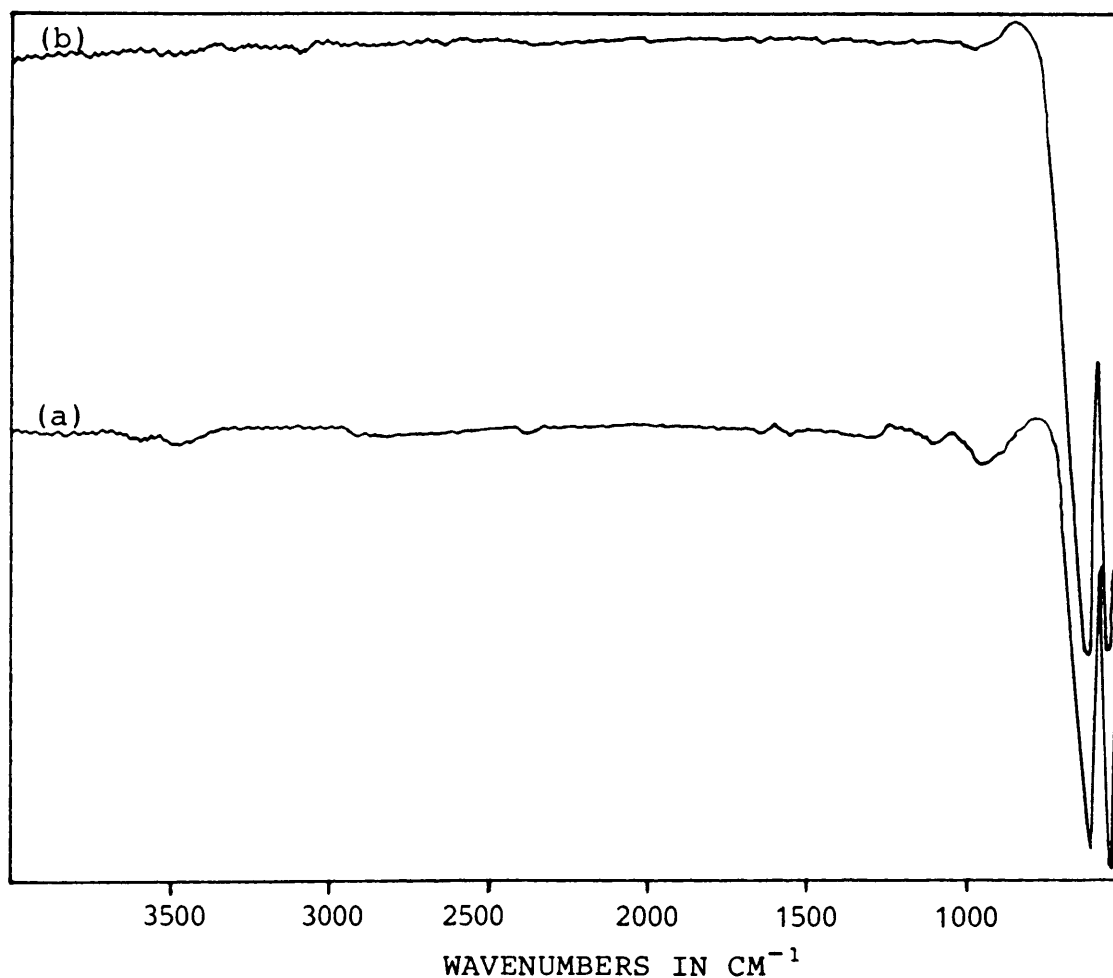
The presence of  $\text{NH}_3$  is indicated by the band at 3432  $\text{cm}^{-1}$ . A broad band, split in two at 568 and 616  $\text{cm}^{-1}$  indicate the existence of  $\text{Cr}_2\text{O}_3$ . A small amount of  $\text{CrO}_3$  could be present, as is indicated by the presence of the low-intensity bands at 958 and 949  $\text{cm}^{-1}$ . Nakamoto [46] reported a spectrum of the following Cr(III) complex:  $[\text{Cr}(\text{NH}_3)_6]\text{Cl}_3$ . The far-infrared bands of the product occurring at 492, 470 and 461  $\text{cm}^{-1}$ , is in concurrence with  $\nu(\text{Cr-N})$  bands reported at 492, 474 and 459  $\text{cm}^{-1}$ . The low-intensity band at about 1120  $\text{cm}^{-1}$  is present in both the spectrum of the product recorded here and that of the Cr(III)-complex reported by Nakamoto [46].

A spectrum of the product obtained from  $(\text{NH}_4)_2\text{Cr}_2\text{O}_7$  after 3 hours at 693 K are compared with that of  $\text{Cr}_2\text{O}_3$  in Fig. (IV.8).

(e) Product after 3 hours at 693 K

Strong, sharp  $\text{Cr}_2\text{O}_3$ -bands were observed at 618 and 558  $\text{cm}^{-1}$  in the mid-infrared and at 445, 412 and 307 in the far-infrared region.

**Fig. (IV.8)** Infrared spectra of (a) the decomposition product of  $(\text{NH}_4)_2\text{Cr}_2\text{O}_7$  obtained after 3 hours at 693 K and (b)  $\text{Cr}_2\text{O}_3$ .



$\text{NH}_3$ -bands of a very low intensity are still visible at  $3446 \text{ cm}^{-1}$ .

#### 4.3.3 Percentages N and H in products at various decomposition stages

Wet analysis results, showing the percentages N and H present in the various decomposed samples are presented in Table (IV.8).

**Table (IV.8)** Percentages N and H present during the decomposition of  $(\text{NH}_4)_2\text{Cr}_2\text{O}_7$ .

	%N	%H
$(\text{NH}_4)_2\text{Cr}_2\text{O}_7$ (theoretical values)	11,12	3,20
" 5h at 473 K	10,71	3,70
" Gradual heating		
up to 518 K	6,31	1,26
" Rapid heating		
up to 493 K	0,85	0,92
" 503-793 K	<0,3	<0,3

This reveals that the percentages N and H in the sample decrease at higher decomposition temperatures and with rapid heating until only  $\text{Cr}_2\text{O}_3$  is left. N- and H-atoms are probably released as part of the gasses evolving from the system, e.g.  $\text{N}_2\text{O}$ ,  $\text{N}_2$ ,  $\text{H}_2\text{O}$  and to a lesser extent,  $\text{NH}_3$  [18,19,37,38].

#### 5.3.4 X-ray Powder Diffraction

XRD-patterns have been used by several authors [18,37,38,43] to determine possible intermediate species in the decomposition reaction. The d-values (in Å) of some of the decomposition products obtained in this study are shown in Table (IV.9).

The bright orange  $(\text{NH}_4)_2\text{Cr}_2\text{O}_7$  sample changed to a deep orange colour after a few hours at 423 K. XRD indicated that only  $(\text{NH}_4)_2\text{Cr}_2\text{O}_7$  was present after 5 hours at this temperature. After 5 hours at 473 K  $(\text{NH}_4)_2\text{Cr}_2\text{O}_7$  appeared

**Table (IV.9)** XRD : Some of the d-values (in Å) of  $\text{CrO}_3$ ,  $\text{Cr}_2\text{O}_3$ , and  $(\text{NH}_4)_2\text{Cr}_2\text{O}_7$  compared with some of the decomposition products. Relative intensities are given in brackets.

$(\text{NH}_4)_2\text{Cr}_2\text{O}_7$	473 K	493 K	693 K	773 K	$\text{Cr}_2\text{O}_3$	$\text{CrO}_3$
6,991(2)	6,552(3)					
5,532(5)	5,072(10)					
4,922(0)	4,928(1)					
3,759(1)	3,762(3)	3,603(5)	3,617(5)	3,625(6)	3,627(6)	3,987(1)
3,487(0)	3,490(1)					
3,427(1)	3,428(4)					
3,312(10)	3,315(3)					
3,256(2)	3,260(2)					
3,042(1)	3,044(2)					
2,783(1)	2,785(1)	2,651(7)	2,659(8)	2,661(7)	2,662(10)	2,451(0)
2,462(0)	2,465(1)	2,469(10)	2,473(10)	2,476(10)	2,477(7)	2,254(2)
2,125(0)	2,126(0)	2,166(4)	2,170(4)	2,172(4)	2,173(3)	
2,052(1)	2,053(1)					
1,922(0)	1,924(0)					
1,829(0)	1,830(0)	1,809(3)	1,811(3)	1,812(3)	1,814(3)	1,841(1)
1,714(0)	1,714(0)	1,668(7)	1,669(8)	1,670(8)	1,671(9)	1,716(1)
1,492(1)	1,492(0)	1,461(2)	1,462(2)	1,463(2)	1,464(2)	1,437(1)
1,429(0)	1,431(0)	1,428(4)	1,429(4)	1,429(4)	1,430(3)	1,426(0)
				1,294(1)	1,295(2)	
				1,238(1)	1,239(1)	

to be black, but upon grinding the sample to a powder it had a dark brown colour and XRD showed that it still consisted of  $(\text{NH}_4)_2\text{Cr}_2\text{O}_7$  only. When the samples were heated rapidly to temperatures above 493 K, it decomposed violently to yield a black- and green powder. At higher decomposition temperatures more of the product had a green colour until after a few hours at 773 K when the sample was completely green. According to XRD results, as indicated in Table (IV.9), all samples heated to above 493 K consisted of  $\text{Cr}_2\text{O}_3$  only.

#### 4.3.5 Diffuse reflectance electronic spectra

Diffuse reflectance spectra have been reported for  $\text{CrO}_3$  and  $\text{Cr}_2\text{O}_3$  between 46063 and 47515  $\text{cm}^{-1}$  without assignments [47]. The diffuse reflectance spectra of  $\text{Cr}_2\text{O}_3$ ,  $\text{CrO}_3$ ,  $(\text{NH}_4)_2\text{Cr}_2\text{O}_7$  and some of its decomposition products obtained at different stages of the reaction (recorded in this study) are shown in Fig. (IV.9). The position of absorption band maxima are given in Table (IV.10). Only  $(\text{NH}_4)_2\text{Cr}_2\text{O}_7$  is present in the samples heated to 423 and 473 K, and  $\text{Cr}_2\text{O}_3$  is only present in samples decomposed at temperatures above 493 K. Traces of  $\text{CrO}_3$  could be present in the sample decomposed at 613 K as a low-intensity absorption band at 19048  $\text{cm}^{-1}$  coincides with a band in the spectrum of  $\text{CrO}_3$  [Fig. (IV.9)].



**Fig. (IV.9)** Diffuse reflectance electronic spectra of (a)  $(\text{NH}_4)_2\text{Cr}_2\text{O}_7$  and some of its decomposition products obtained at (b) 423 K, (c) 473 K, (d) 493 K, (e) 773 K, (f) 613 K and the spectra of (h)  $\text{CrO}_3$  and (i)  $\text{Cr}_2\text{O}_3$ .

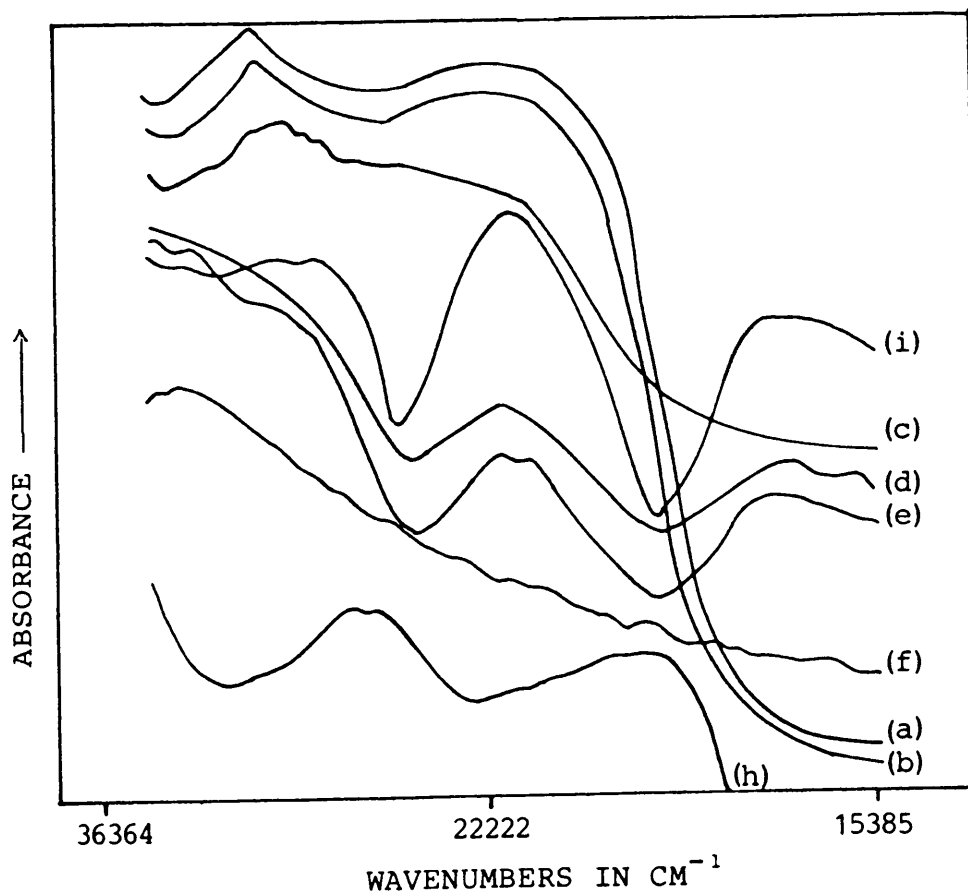


**Table (IV.10)** Diffuse reflectance electronic spectra: Positions of absorption band maxima of various decomposition products (in  $\text{cm}^{-1}$ ).

Pure $(\text{NH}_4)_2\text{Cr}_2\text{O}_7$	Decomposition products of $(\text{NH}_4)_2\text{Cr}_2\text{O}_7$					Pure $\text{CrO}_3$	Pure $\text{Cr}_2\text{O}_3$
	423 K	473 K	493 K	613 K	773 K		
30 303	29 851	29 412	30 769	35 714	35 714		35 714
			27 778	27 778	29 851		28 986
				25 000	27 778	26 667	27 778
21 978	21 978	21 978	21 739	21 739	21 739		21 739
			16 667	19 048	16 667	19 048	16 667

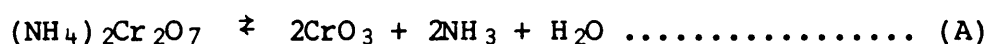
#### 4.4 Conclusions

With a complex process and a large variety of intermediate species being proposed by various authors, conclusions regarding the decomposition of  $(\text{NH}_4)_2\text{Cr}_2\text{O}_7$  were often controversial and contradictory. Some of the intermediates that have been proposed include  $\text{Cr}_2\text{O}_5$  [37,38],  $[(\text{CrO}_2)_6\text{H}_2\text{O}]$ ,  $\text{CrO}_2$  [37],  $\text{CrO}_3$  [18,19,42] and a  $\text{CrO}_3\text{-NH}_3$  complex [38,42]. Of these, the formation of  $\text{Cr}_2\text{O}_5$ , generally regarded as  $\text{CrO}_3\cdot\text{CrO}_2$ ,  $[(\text{CrO}_2)_6\text{H}_2\text{O}]$  and  $\text{CrO}_2$  seems unlikely. Infrared and Raman spectra were not included as methods of identification in the previous studies to confirm the existence of such intermediates. No evidence of the existence of any such compound as an intermediate was found in this study.

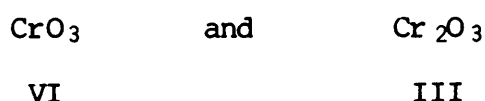
Raman spectra recorded up to 473 K showed the existence of only  $(\text{NH}_4)_2\text{Cr}_2\text{O}_7$  up to this temperature. Rapid heating of  $(\text{NH}_4)_2\text{Cr}_2\text{O}_7$  above 493 K causes a violent reaction to take place, yielding a black- and green solid. Infrared spectra indicate relatively few ammonium groups to be present after the reaction at 498 K, with no sign of these groups after the reaction at 503 K. Instead  $\text{NH}_3$ , and even traces of  $\text{NO}_2$  groups presumably trapped in the solid are observed. The green solid is  $\text{Cr}_2\text{O}_3$ .

When  $(\text{NH}_4)_2\text{Cr}_2\text{O}_7$  is heated gradually the subsequent reaction is not a violent one, even if the temperature is raised up to 613 K. Instead the orange crystals change to a dark red, brown and finally black colour. Ammonium bands in the infra-

red spectra shifted to lower wavenumbers, probably an indication of the groups being more free to rotate than before. When  $(\text{NH}_4)_2\text{Cr}_2\text{O}_7$  is heated gradually so that no violent reaction takes place, traces of  $\text{CrO}_3$  are likely to occur in the product as part of a  $\text{CrO}_3$ - $\text{Cr}_2\text{O}_3$  mixture because of a side reaction taking place in an open system. Such a reaction was proposed by Galwey et. al. [42] as an initial main reaction in the decomposition:



Galwey [42] suggested that the reaction could be reversible. Evidence of the existence of small amounts of  $\text{CrO}_3$  in the decomposition products was found by means of FT-IR and Diffuse Reflectance electronic spectra in the product obtained at 613 K with  $\text{Cr}_2\text{O}_3$  as the main product. The reversibility of reaction was investigated by treating solid  $\text{CrO}_3$  with various solutions, e.g.  $\text{NH}_3$ ,  $(\text{NH}_4)_2\text{CO}_3$  and  $\text{NH}_4\text{NO}_3$ . This yielded orange crystals in each case, identified by means of FT-IR as  $(\text{NH}_4)_2\text{Cr}_2\text{O}_7$ , leading to the conclusion that reaction (A) is reversible. The existence of  $\text{CrO}_3$  and  $\text{Cr}_2\text{O}_3$  in one product could result in a black colour of the product because of mixed valence oxides:



$\text{NO}_2$  and  $\text{NH}_3$  groups detected in decomposition products obtained at 498, 518 K and 498, 503, 518, 613, 693 K respectively, are probably present as surface species, but the

bands in the infrared spectra of the decomposition product obtained at 613 K coincide with that of  $\nu(\text{Cr-N})$  in the spectrum of the  $[\text{Cr}(\text{NH}_3)_6]\text{Cl}_3$ -complex indicating the possible existence of a  $\text{CrO}_3\text{-NH}_3$  or a  $\text{Cr-NH}_3$  complex.

The final product in the decomposition of  $(\text{NH}_4)_2\text{Cr}_2\text{O}_7$  is the most stable oxide of chromium,  $\alpha\text{-Cr}_2\text{O}_3$ .

## CHAPTER V

### FURTHER STUDY ON THE PRODUCTS OF THE DECOMPOSITION OF $(\text{NH}_4)_2\text{Cr}_2\text{O}_7$

#### 1. CrO<sub>3</sub>

##### 1.1 Introduction

CrO<sub>3</sub> is commonly called 'chromic acid' and it is generally prepared by the addition of H<sub>2</sub>SO<sub>4</sub>(c) to a saturated aqueous solution of a dichromate. CrO<sub>3</sub> is a strongly acidic and rather covalent oxide with a melting point of 470 K. Its strong oxidizing properties are widely used in organic chemistry [44]. CrO<sub>3</sub> melts with some decomposition, and if heated above 493–523 K it loses oxygen to give a succession of lower oxides until green Cr<sub>2</sub>O<sub>3</sub> is formed [44,48].

Traces of CrO<sub>3</sub> was found to be present during the decomposition of (NH<sub>4</sub>)<sub>2</sub>Cr<sub>2</sub>O<sub>7</sub> to Cr<sub>2</sub>O<sub>3</sub> [IV.4]. It is therefore appropriate to include CrO<sub>3</sub> in this study, especially since it is effectively an infinitely long Cr<sub>2</sub>O<sub>7</sub><sup>2-</sup> chain [11].

##### 1.2 Structure

The deep red lath-like crystals of CrO<sub>3</sub> are made up of infinite chains of corner-sharing CrO<sub>4</sub> tetrahedra running parallel to the c-axis [44]. A typical CrO<sub>3</sub> chain was shown in Fig. (I.1) in Chapter I. The tetrahedra lie on mirror planes, and adjacent tetrahedra in each chain are related by

twofold axes which pass through the bridging oxygen atoms [4]. The chain direction is often marked on the crystals by a heavy striation and the crystals break up easily into small needles parallel to the streaks. This agrees well with the fact that the bonds between the chains, both in the a- and b-direction must be rather weak [49]. Adjacent chains are not joined by chemical bonds and are held together only by Van der Waals forces. The preferential growth of CrO<sub>3</sub> in the c-direction to produce cylindrical crystals is thus readily understood [4]. The relatively low melting point (~470 K) is also explained by this structure [49].

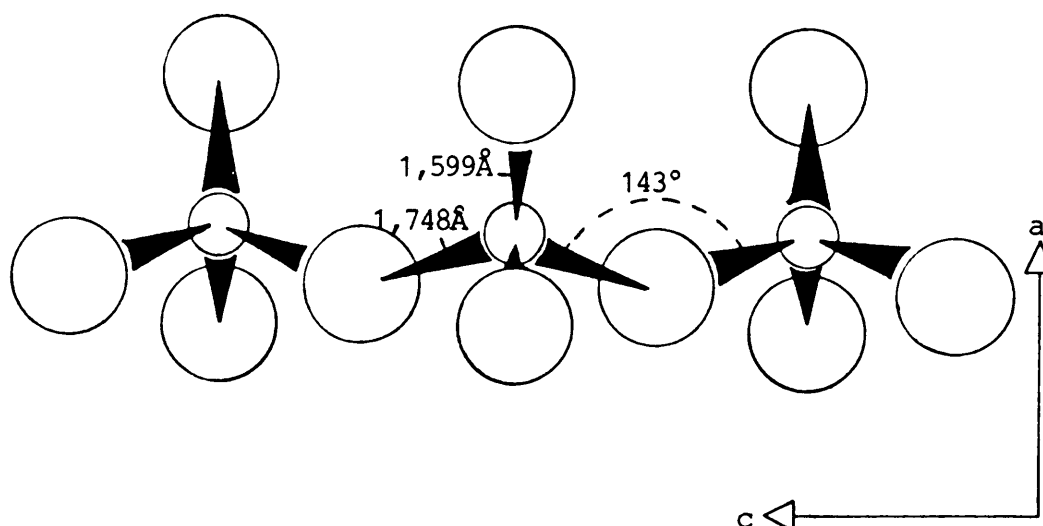
### 1.3 Crystallographic properties

CrO<sub>3</sub> has an orthorhombic crystal structure and belongs to space group  $C_{2v}^{16}$  (C2cm) with unit cell parameters  $a = 4,789$ ;  $b = 8,557$  and  $c = 5,743$  Å. The Cr, O(3) and O(4) atoms occupy 4b-sites with site symmetry  $C_s$ , while O(1) atoms are situated on 4a-sites with  $C_2$ -symmetry. The O(3) and O(4) atoms are bonded to only one chromium atom. This Cr-O bond length is 1,599 Å with the bridging Cr-O bond length 1,748 Å. The angle at the bridging oxygen atom O(1) is 143° [4]. This is illustrated in Fig. (V.1).

Each oxygen is surrounded by 12 other oxygen atoms, including those within the same tetrahedron. The distances between oxygen atoms from different tetrahedra are in the range 2,995 to 3,660 Å, while oxygen distances within the tetrahedron are between 2,564 and 2,871 Å. All O-Cr-O angles are within 0,9°

of the ideal tetrahedral value of  $109,5^\circ$  despite the difference in terminal and bridging Cr-O bond lengths [4].

**Fig. (V.1)** Projection of a  $\text{CrO}_3$ -chain on (010) showing terminal and bridging Cr-O bond distances and the Cr-O-Cr angle. Small circles represent chromium atoms and large circles oxygen atoms



#### 1.4 Preparation of single crystals of $\text{CrO}_3$

A saturated  $\text{Na}_2\text{Cr}_2\text{O}_7$  solution was prepared and concentrated  $\text{H}_2\text{SO}_4$  was added slowly. The solution changed from an orange to a deep red colour. The solution was evaporated slowly at room-temperature, and dark red cylindrical needles appeared after a few days. It was identified as  $\text{CrO}_3$  by means of Raman spectroscopy.

#### 1.5 Vibrational analysis

The internal modes of  $\text{CrO}_3$ ,  $6A_1 + 4A_2 + 3B_1 + 7B_2$ , were

determined by the Fateley method [1] in Fig. (I.2(a) and (b)) [I.1.4(b)] and the results were confirmed by a factor group analysis, using the Adams method [2], in Fig. (I.4) [I.2.3]. All the modes are Raman active and, with the exception of  $A_2$ , infrared active. Mattes [48] considered the  $\text{CrO}_2$  groups and the Cr-O chain in  $\text{CrO}_3$  separately:

<u>Vibrations</u>	<u><math>\text{CrO}_2</math> groups</u>	<u>Cr-O chain</u>
Stretch	$2A_1$ $2B_2$	$A_1$ $B_2$
Bend	$2A_1 + 2A_2 + 2B_1 + 2B_2$	$A_1 + A_2 + B_1 + 2B_2$
	<hr/>	<hr/>
	$4A_1 + 2A_2 + 2B_1 + 4B_2$	$2A_1 + 2A_2 + 2B_1 + 3B_2$

This gives a total of  $6A_1 + 4A_2 + 4B_1 + 7B_2$  which is in agreement with the internal modes determined here but including the  $B_1$  rotational mode.

## 1.6 Infrared and Raman spectra

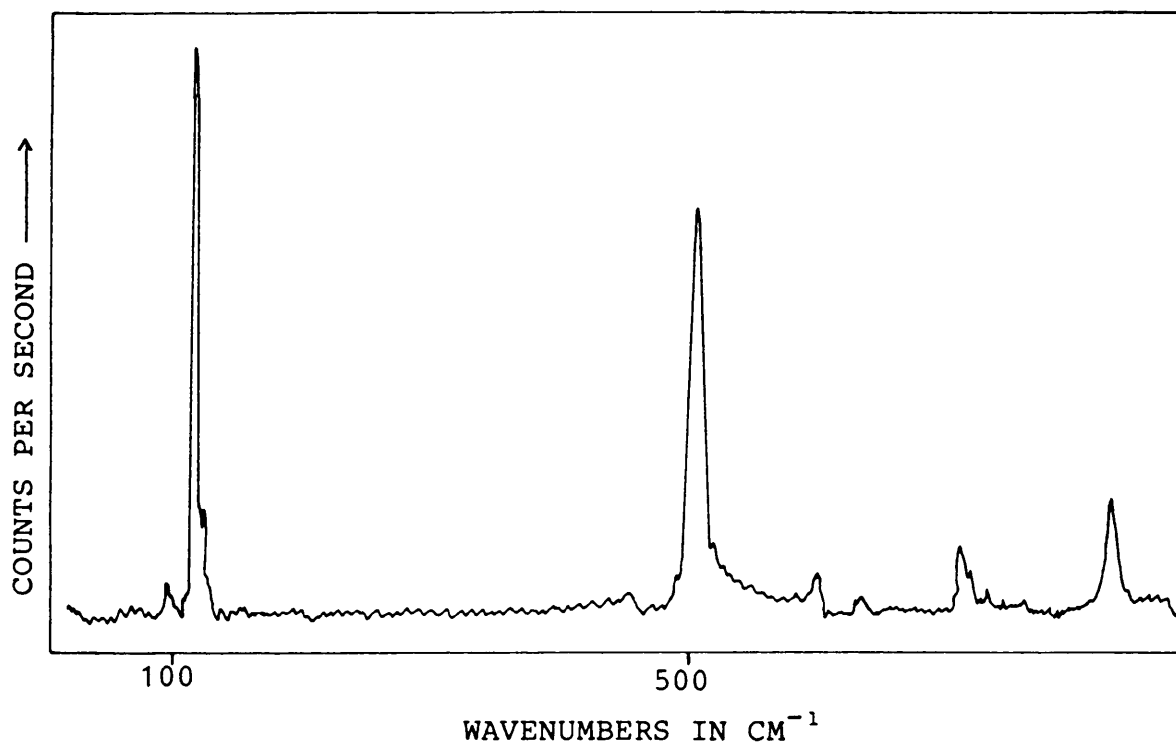
### 1.6.1 Previous studies

Several authors [11,13,15,30,50-52] reported infrared spectra of  $\text{CrO}_3$  but very little attention was given to assignments before Mattes [48] reported infrared and Raman spectra with assignments.

### 1.6.2 Description of the spectra

The Raman spectrum of  $\text{CrO}_3$  is shown in Fig. (V.2), with



**Fig. (V.2)** The Raman spectrum of  $\text{CrO}_3$ 

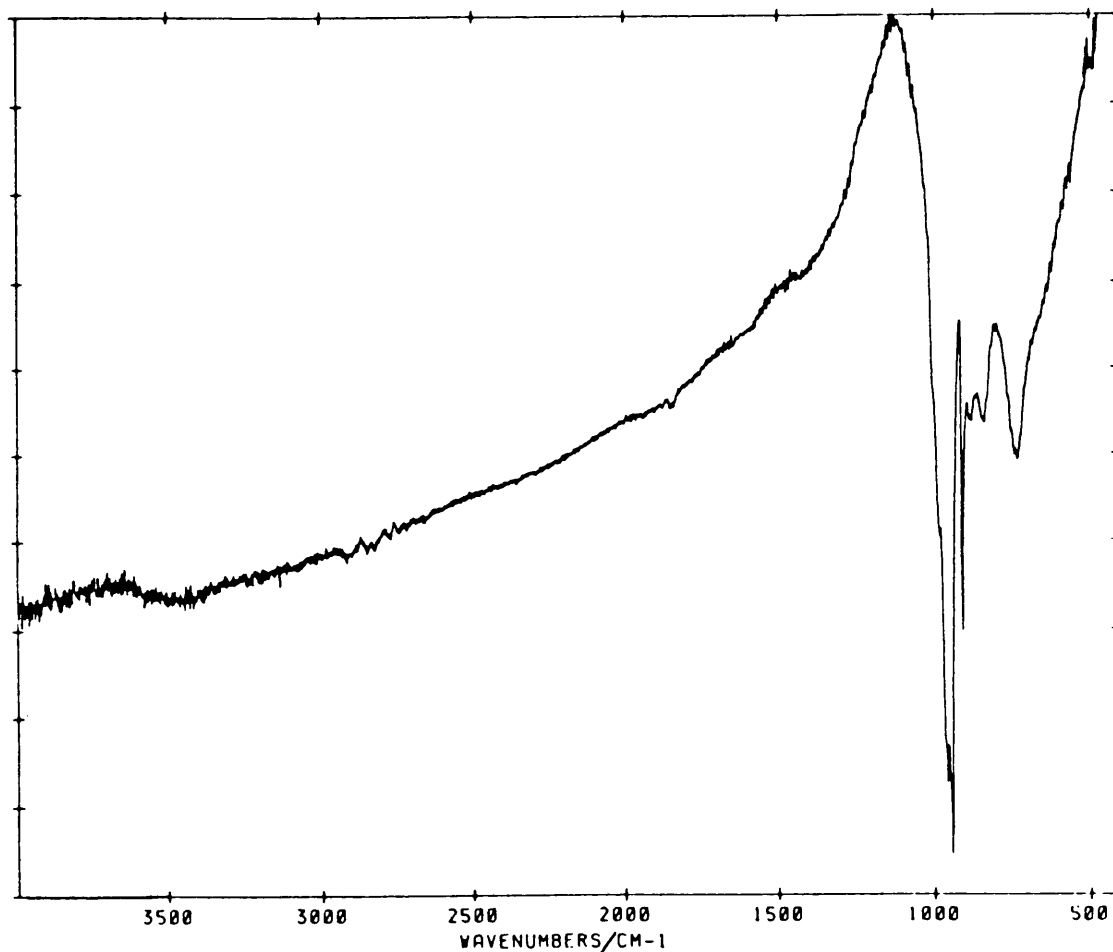
mid- and far-IR spectra in Fig. (V.3(a) and (b)). The band positions are shown in Table (V.1) with the assignments given by Mattes [48].

## 2. $\text{Cr}_2\text{O}_3$

### 2.1 Introduction

$\text{Cr}_2\text{O}_3$  is the most stable oxide of chromium and although it can be obtained conveniently by the heating of ammonium dichromate, it is also the final product in the combustion of the metal. It is a semiconductor and antiferromagnetic below 308 K [44].  $\text{Cr}_2\text{O}_3$  finds wide applications as a green pigment and as a catalyst in some organic reactions [44]. It is one

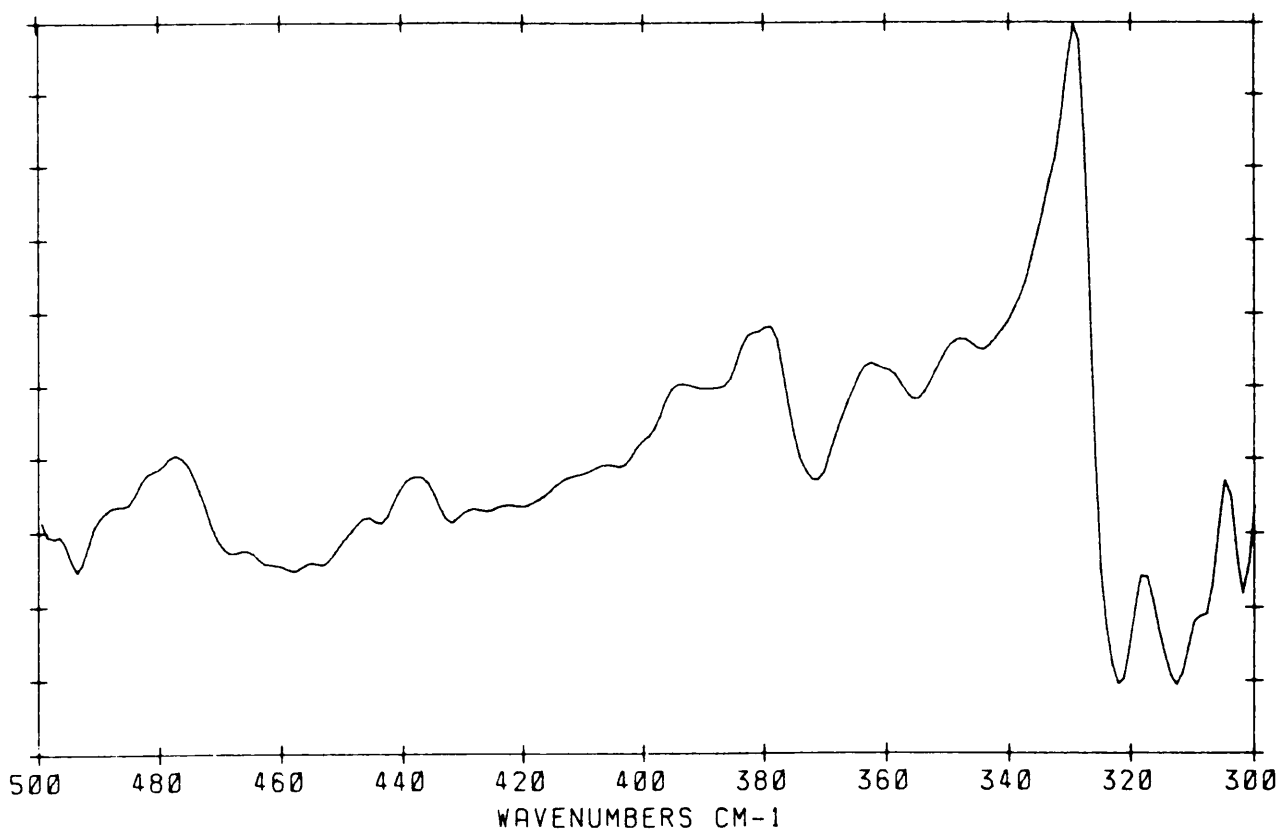
Fig. (V.3(a)) The mid-IR spectrum of  $\text{CrO}_3$



of the compounds in the  $\text{M}_2\text{O}_3$  series that has the corundum structure [44, 48].

## 2.2 The Corundum structure

An idealized corundum structure has oxygen in hcp positions with metal atoms in  $\frac{2}{3}$  of the octahedral holes. The location of the void positions is shifted by the distance and direction of one of the interoxygen vectors consistently from metal layer to metal layer. This results in four coordina-

**Fig. (V.3(b))** The far-IR spectrum of  $\text{CrO}_3$ 

tion at  $\frac{2}{3}$  of the corners of a trigonal prism, the vacant corners being diagonally opposed across a rectangular face prism. This coordination is distorted tetrahedral [44], and is shown in Fig. (V.4). True corundum structure is obtained from the idealized structure by movement of the metal atoms: the two metals sharing an edge on the trigonal prism ((a) and (b) or (c) and (d) in Fig. (V.4)) move apart and the two diagonally opposed on a rectangular face of the prism ((a) and (d) or (b) and (c)) move closer together. This results in a nearly regular tetrahedral coordination of oxygen [53].

**Table (V.1)** Positions of the vibrational modes in  $\text{CrO}_3$  found during this study

Frequency in $\text{cm}^{-1}$		
Raman	IR	Assignment [48]
1003 w.		$\nu_{\text{as}}(\text{CrO}_2)$
	986 sh.	
977 s.sp.		$\nu_{\text{s}}(\text{CrO}_2)$
969 sh.	959 s.sp.	
	944 s.sp.	
	907 m.sp.	$\nu_{\text{as}}(\text{CrOCr})B_2$
	879 w.	$B_1$
	839 w.	
	731 m.	
557 w.		$\nu_{\text{s}}(\text{CrOCr})A_2$
492 w.	494 w.	$A_1$
398 w.		$\delta(\text{CrO}_2)B_2$
375 w.	371 w.	$\rho(\text{CrO}_2 \parallel \text{OCrO})A_2$
334/336 w.		$B_1$
	322/312 w.	$\delta(\text{OCrO})B_2$
227 sh.		$\rho(\text{CrO}_2 \perp \text{OCrO})$
210 w.		$\tau(\text{CrO}_2)A_2/B_2$
95 m.		$\delta(\text{CrOCr})A_2$
63 w.		$A_1$

w = weak

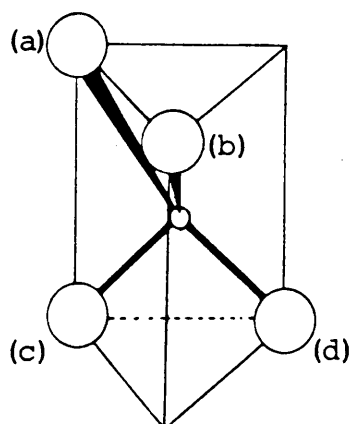
m = medium

s = strong

sh = shoulder

sp = sharp

**Fig. (V.4)** Idealized corundum structure : Metal atoms at  $^2_3$  of the corners of a trigonal prism



### 2.3 Crystallographic properties of $\text{Cr}_2\text{O}_3$

$\text{Cr}_2\text{O}_3$  belongs to space group  $D_{3d}^6$  ( $R\bar{3}c$ ) with six formula units in the hexagonal unit cell. The chromium atoms all occupy 4c-sites with site symmetry  $C_3$ , while the oxygen atoms are situated on 6e-sites with  $C_2$ -symmetry. The angle between the line connecting chromium atoms (Cr-O-Cr) range from  $82,3$  to  $133,1^\circ$  [3]. Each chromium atom is surrounded by six oxygen atoms which are not at the corners of a regular octahedron. Three of these oxygens lie slightly closer to the metal atom than the other three [54]. O-Cr-O angles range from  $81,4$  to  $167,0^\circ$  [3].

### 2.4 Vibrational Analysis

Internal modes of  $\text{Cr}_2\text{O}_3$ ,  $2A_{1g} + 3A_{2g} + 2A_{1u} + 2A_{2u} + 5E_g + 4E_u$ , were determined by the Fateley method [1] in Fig. (I.1(a)) [I.1.2(b)]. The results are confirmed by the factor group analysis (using the Adams method [2] in Fig. (V.5)).

**Fig. (V.5)** Factor group analysis of  $\text{Cr}_2\text{O}_3$  using the Adams method

Space group no. 167	$A_{1g}$	$A_{2g}$	$E_g$	$A_{1u}$	$A_{2u}$	$E_u$
Cr (4C)	1	1	2	1	1	2
O (6E)	1	2	3	1	2	3
N (total)	2	3	5	2	3	5
T + $T_A$	0	0	0	0	1	1
R	0	0	0	0	0	0
$N_{\text{Cr}_2\text{O}_3}$ internal	2	3	5	2	2	4

The  $A_{2u}$  and  $E_u$  modes are infrared active with the  $A_{1g}$  and  $E_g$  modes Raman active.

## 2.5 Infrared spectra

### 2.5.1 Previous studies

Various authors [50,52,55,56] reported infrared spectra without any assignment. Brown assigned Cr-O stretching and deformation modes on the basis of an octahedrally coordinated chromium ion. This resulted in 15 modes. Factor group analysis however revealed 18 internal modes for  $\text{Cr}_2\text{O}_3$  [57].

### 2.5.2 Description of the spectra

The mid-IR bands of  $\text{Cr}_2\text{O}_3$  are shown in Fig. (V.6(a)) with the strongest far-IR band in Fig. (V.6(b)). Bandpositions

**Fig. (V.6(a))** The mid-IR spectrum of  $\text{Cr}_2\text{O}_3$

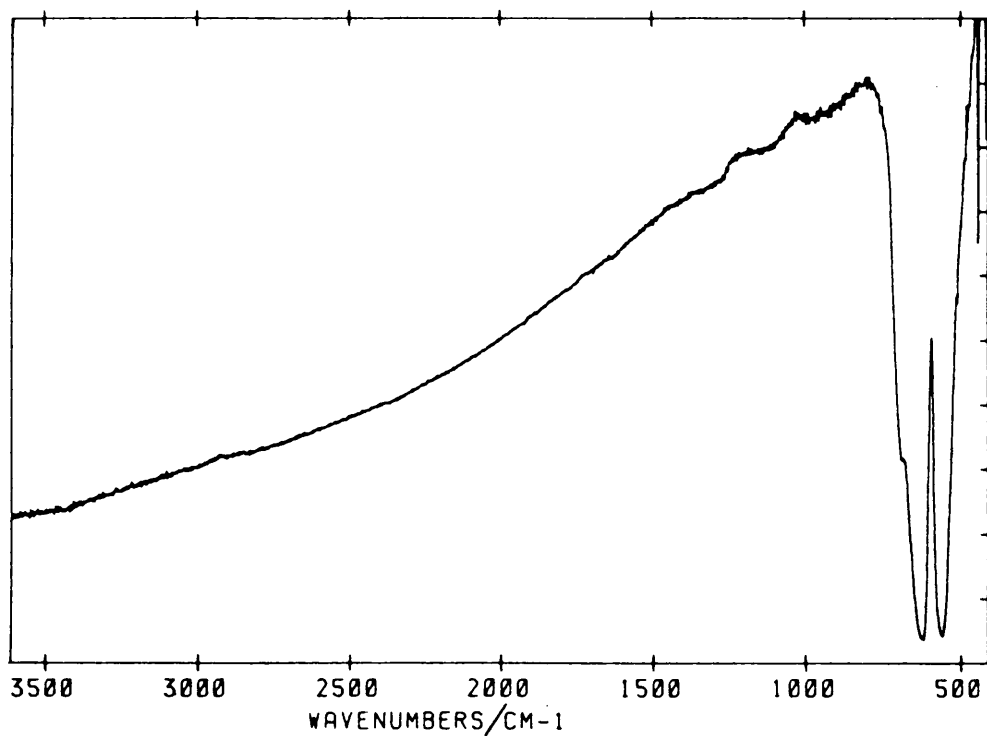
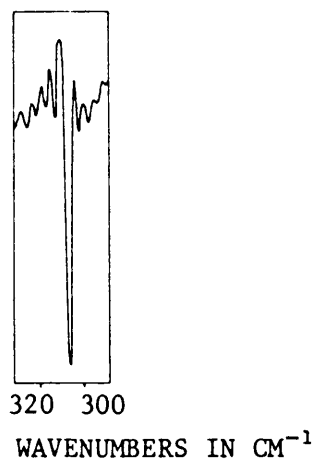


**Fig. (V.6(b))** The strongest far-IR band of  $\text{Cr}_2\text{O}_3$



are shown in Table (V.2) with assignments made by different authors.

**Table (V.2)** Infrared frequencies for Cr<sub>2</sub>O<sub>3</sub>

Frequency in cm <sup>-1</sup>	Assignments		
	[58]	CrO <sub>6</sub> [57]	
684 sh.			sh = shoulder
623 s.sp.	A <sub>2u</sub> and E <sub>u</sub>	ν <sub>3</sub>	s = strong
558 s.sp.	A <sub>2u</sub> and E <sub>u</sub>		m = medium
444 m.	E <sub>u</sub>		sp = sharp
415 m.	E <sub>u</sub>		
307 s.sp.		ν <sub>4</sub>	

The strong sharp band at 307 cm<sup>-1</sup> was reported only once before by Brown [55] at 306 cm<sup>-1</sup> who assigned it to the ν<sub>4</sub>(CrO<sub>6</sub>) mode [Table (V.2)].

### 3. COMPARISON BETWEEN THE CHROMIUM COMPOUNDS

The structures, bonding distances and angles, and some vibration, translation and rotation modes of (NH<sub>4</sub>)<sub>2</sub>CrO<sub>4</sub>, (NH<sub>4</sub>)<sub>2</sub>Cr<sub>2</sub>O<sub>7</sub>, CrO<sub>3</sub> and Cr<sub>2</sub>O<sub>3</sub> are compared in Table (V.3).

Wing et. al. [59] reported that the normal coordinated analysis of M-O bridge systems are strongly dependent on the M-O-M angle, allowing distinction to be made between M<sub>2</sub>O and M<sub>2</sub>O<sub>2</sub> bridges. In M<sub>2</sub>O the bridge is usually larger than 115°, and ν<sub>as</sub> and ν<sub>s</sub> are separated by at least 215 cm<sup>-1</sup>. In M<sub>2</sub>O<sub>2</sub> the separation is much smaller, and the bridge angle lies between 80 and 90°. Mattes [60] used this information on CrO<sub>3</sub>. The splitting of

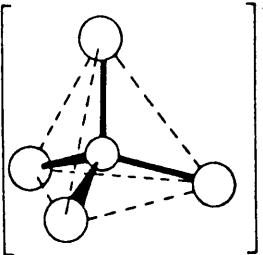
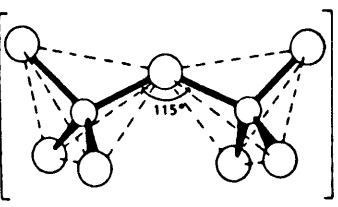
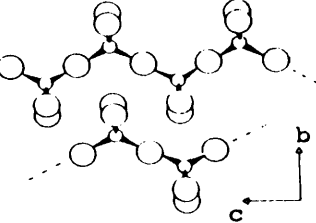
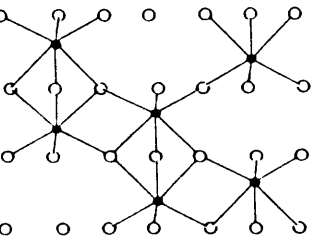


$\nu_{\text{as}}(\text{CrO}_2)$  and  $\nu_{\text{s}}(\text{CrO}_2)$  (at 1003 and 977  $\text{cm}^{-1}$  in this study) is small (26  $\text{cm}^{-1}$ ), showing that the O-Cr-O angle is close to  $90^\circ$ .

During this study a separation of 413  $\text{cm}^{-1}$  was found between  $\nu_{\text{as}}(\text{Cr-O-Cr})$  (907  $\text{cm}^{-1}$ ) and  $\nu_{\text{s}}(\text{Cr-O-Cr})$  (494  $\text{cm}^{-1}$ ). From this it can be concluded that the Cr-O-Cr angle is larger than  $115^\circ$ . It was indeed determined as  $143^\circ$  by Stephens et. al. [4].

In  $(\text{NH}_4)_2\text{Cr}_2\text{O}_7$  the  $\nu_{\text{as}}/\nu_{\text{s}}(\text{Cr-O-Cr})$  separation (724 and 573  $\text{cm}^{-1}$ ) is 141  $\text{cm}^{-1}$ , which is smaller than 215  $\text{cm}^{-1}$ , although not significantly so. This 'medium' splitting is probably because of the Cr-O-Cr angle of  $115^\circ$ .

**Table (V.3)** A comparison between the chromium compounds studied

	$(\text{NH}_4)_2\text{CrO}_4$	$(\text{NH}_4)_2\text{Cr}_2\text{O}_7$	$\text{CrO}_3$	$\text{Cr}_2\text{O}_3$
Structure				
<u>Bond distance</u>				<u>Average bond length:</u>
Cr-O(t)	1,658 Å [10]	1,633 Å [28]	1,599 Å [4]	2,00 Å [3]
Cr-O(b)	-	1,91 Å [28]	1,748 Å	
<u>Bond angles</u>				
O-Cr-O	109,7° [10]	-	-	81,4° to 167,0° [3]
Cr-O(b)-Cr	-	115° [28]	143° [4]	82,3° to 133,1° [3]
<u>Stretching</u> modes: $\nu_{as}/\nu_s$				
Cr-O(t)	876/845 $\text{cm}^{-1}$	946/902 $\text{cm}^{-1}$	1003/977 $\text{cm}^{-1}$	684/623 $\text{cm}^{-1}$
Cr-O-Cr	-	-	907/557 $\text{cm}^{-1}$	558/444 $\text{cm}^{-1}$
O-Cr-O	-	720/578 $\text{cm}^{-1}$	-	
<u>Bend/deform.</u> modes: $\delta_{as}/\delta_s$				
Cr-O-Cr	-	228 $\text{cm}^{-1}$	95 $\text{cm}^{-1}$	
O-Cr-O	378/342 $\text{cm}^{-1}$	391/382 $\text{cm}^{-1}$	398 $\text{cm}^{-1}$	307 $\text{cm}^{-1}$
<u>Translation</u>	98, 95, 88 $\text{cm}^{-1}$	105, 98, 94 $\text{cm}^{-1}$	-	
<u>Rotation</u>	76, 56, 41 $\text{cm}^{-1}$	61, 44, 28 $\text{cm}^{-1}$	63 $\text{cm}^{-1}$	

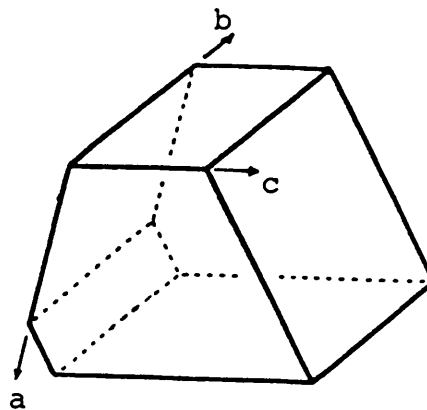
CHAPTER VIA COMPARISON BETWEEN  $K_2Cr_2O_7$  AND  $(NH_4)_2Cr_2O_7$ 1. INTRODUCTION

A study of potassium dichromate was included in order to compare the thermal behaviour of Raman modes with that of the ammonium salt. The potassium salt was preferred to the sodium salt because of the hygroscopic character of the latter which may influence thermal behaviour when the water in  $Na_2Cr_2O_7 \cdot 2H_2O$  is lost at higher temperatures.

2. CRYSTALLOGRAPHIC PROPERTIES OF  $K_2Cr_2O_7$ 

Potassium dichromate exhibits a triclinic crystal structure, space group  $P_1(C_1^1)$  with  $Z = 4$  at temperatures below 515 K.

Fig. (VI.1) Habit of triclinic  $K_2Cr_2O_7$  crystals [61].



The unit cell parameters are  $a = 13,37$ ;  $b = 7,38$ ;  $c = 7,45$ ;  $\alpha = 90,8^\circ$ ;  $\beta = 96,2^\circ$  and  $\gamma = 98,0^\circ$ . The  $Cr_2O_7^{2-}$  ions in the

primitive cell occupy two sets of nonequivalent sites. The dichromate ion consists of two nearly tetrahedral  $\text{CrO}_4$  groups joined through a shared oxygen atom. The ion is almost in the eclipsed configuration and is close to having  $C_{2v}$ -symmetry. The Cr-O(terminal) distance is 1,63 Å and the Cr-O(bridging) distance is 1,79 Å. All angles at the chromium atoms are tetrahedral except for the one O(bridging)-Cr-O(terminal) angle in each ion which is  $106^\circ$ . Angles at the bridging oxygen atoms are 124 and  $128^\circ$  [61].

Above 515 K  $\text{K}_2\text{Cr}_2\text{O}_7$  exhibits a monoclinic lattice, space group  $P_{21/c}$  ( $C_{2h}^5$ ). The  $\text{Cr}_2\text{O}_7^{2-}$  ions occupy four equivalent  $C_1$  sites [62].

### 3. VIBRATIONAL ANALYSIS AND INFRARED SPECTRA

#### 3.1 Previous studies on $\text{K}_2\text{Cr}_2\text{O}_7$

Infrared spectra of polymorphic  $\text{K}_2\text{Cr}_2\text{O}_7$  have been recorded by various authors [32,63,64]. The far-IR spectra of the crystalline powder in a polyethylene matrix between 40 and  $400\text{ cm}^{-1}$  was reported by Mathur et. al. [32], showing six new bands at 380, 168, 148, 134, 106 and  $64\text{ cm}^{-1}$  in addition to the mid-IR bands reported by Stammreich [30]. Carter et. al. [64] reported IR spectra of the triclinic structure only, as monoclinic  $\text{K}_2\text{Cr}_2\text{O}_7$  converted to the triclinic form upon grinding. Assignments were made with consideration of the factor group selection rules for the structure. The data was compared to that of the rubidium and cesium salts. Bates et. al. [63] reported the IR spectrum of crystalline  $\text{K}_2\text{Cr}_2\text{O}_7$  at 77 K.

### 3.2 Vibrational analysis of triclinic and monoclinic $K_2Cr_2O_7$

The normal modes of the  $Cr_2O_7^{2-}$  ion were determined in (VI.3.2) as  $7A_1 + 4A_2 + 4B_1 + 6B_2$ . The correlation of the 'free'  $Cr_2O_7^{2-}$  ion with site group  $C_1$  and factor group  $C_i$  for the triclinic structure is shown in Fig. (VI.2), and correlation to site group  $C_1$  and factor group  $C_{2h}$  for the monoclinic structure in Fig. (VI.3).

**Fig. (VI.2)** Site- and Factor group correlation of  $Cr_2O_7^{2-}$  in the Triclinic crystal structure of  $K_2Cr_2O_7$

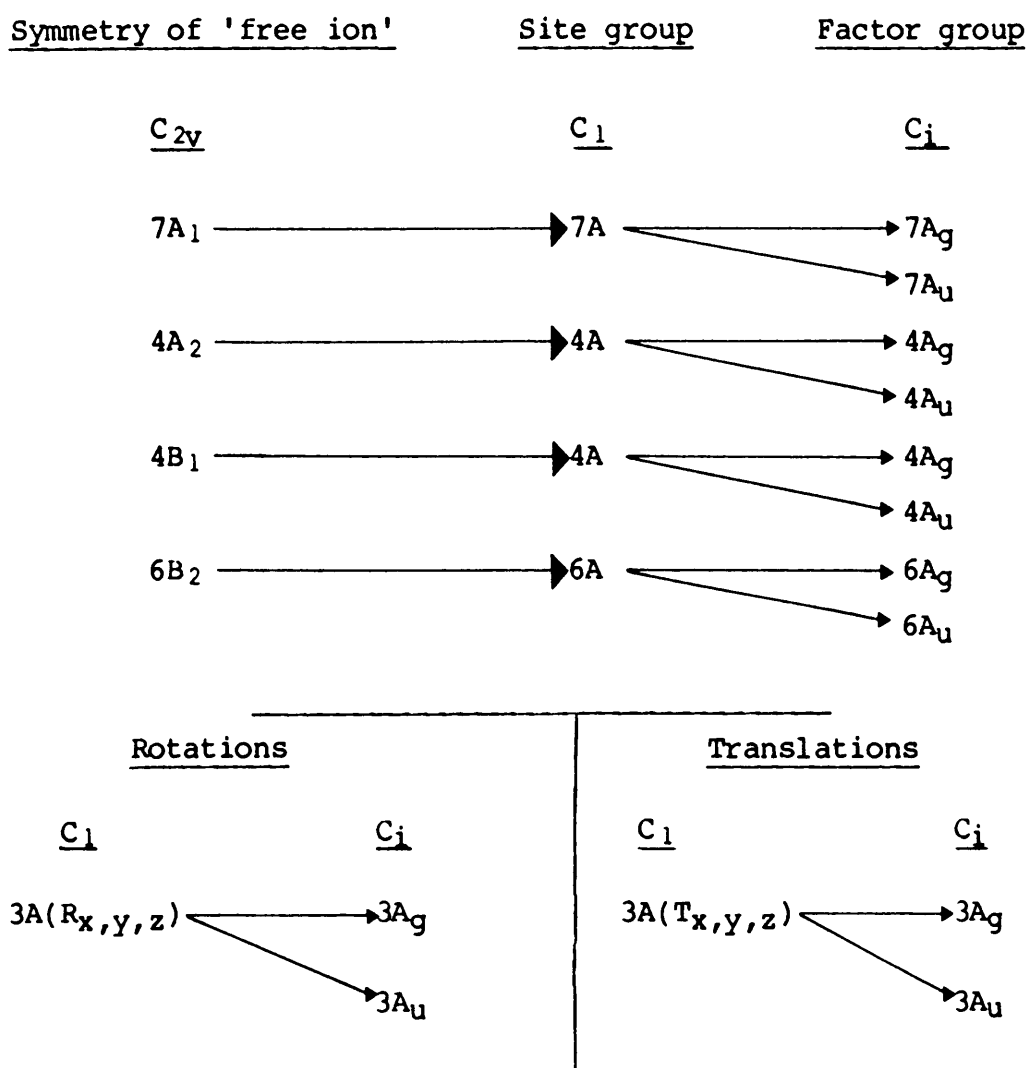
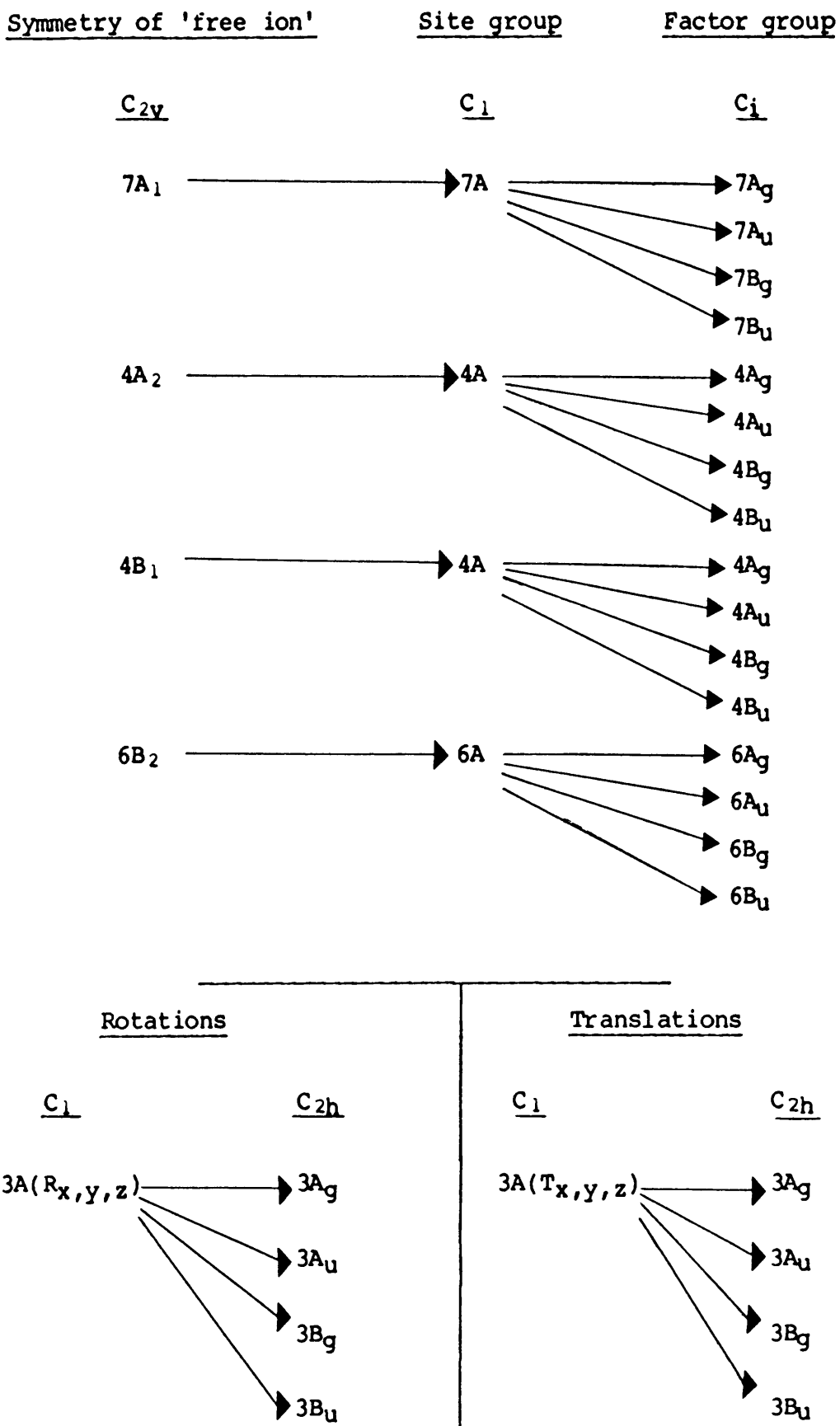


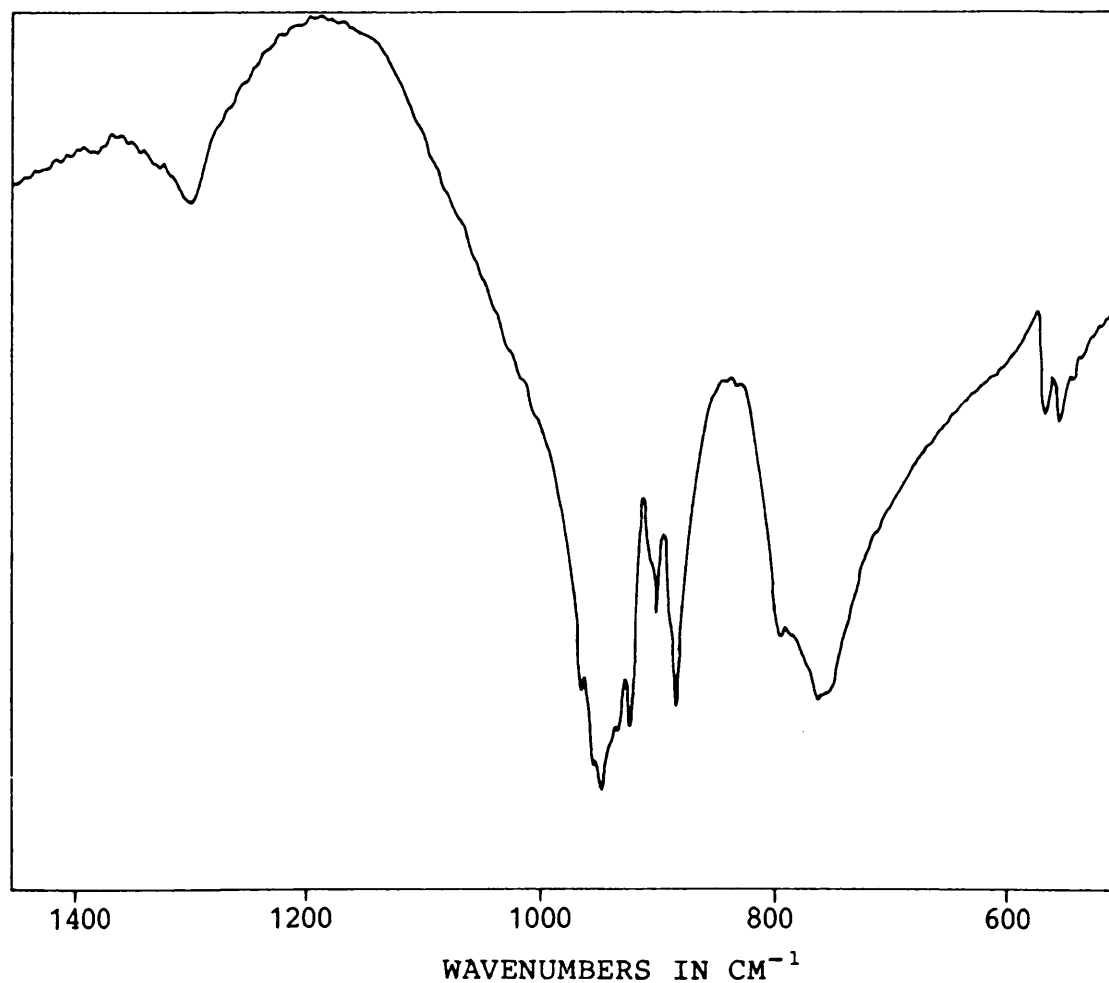
**Fig. (VI.3)** Site- and Factor group correlation of  $\text{Cr}_2\text{O}_7^{2-}$  in the Monoclinic crystal structure of  $\text{K}_2\text{Cr}_2\text{O}_7$

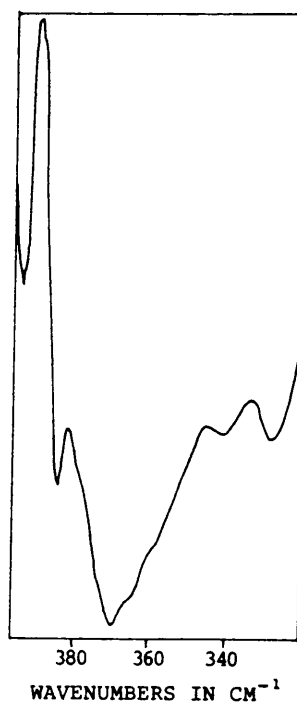


### 3.3 Description of the infrared spectra of $K_2Cr_2O_7$ and comparison with $(NH_4)_2Cr_2O_7$

The mid- and far-IR spectra of triclinic  $K_2Cr_2O_7$  (recorded at room-temperature) are shown in Fig. (VI.4) and (VI.5). Infrared active modes of  $K_2Cr_2O_7$  are compared to those of  $(NH_4)_2Cr_2O_7$  in Table (VI.1).

Fig. (VI.4) Mid-IR spectrum of  $K_2Cr_2O_7$



**Fig. (VI.5)** Far-IR spectrum of  $K_2Cr_2O_7$ **Table (VI.1)** IR modes of  $K_2Cr_2O_7$  and  $(NH_4)_2Cr_2O_7$ 

IR frequency in $cm^{-1}$		Assignment [64]
$K_2Cr_2O_7$	$(NH_4)_2Cr_2O_7$	
965 s.		CrO <sub>3</sub> asymmetric stretch
959 s.		
949 s.	949 s.sp.	
940 sh.		
934		
923 s.sp.	929 s.sh.	CrO <sub>3</sub> symmetric in-phase stretch
908 sh.		
902 m.sp.		
891 sh.	898 s.sp.	CrO <sub>3</sub> symmetric out-of-phase stretch
884 s.sp.	877 s.sp.	
792 m.b.		Cr-O-Cr asymmetric bridge stretch
761 s.	724 s.b.	
565 w.	573 m.	Cr-O-Cr symmetric bridge stretch
553 w.		
393		CrO <sub>3</sub> symmetric bend and CrO <sub>3</sub> scissor deformation
385		
369 m.	370 w.	
	366 w.	
	337 w.	
	234 w.	



#### 4. THERMAL BEHAVIOUR OF THE RAMAN MODES OF $K_2Cr_2O_7$

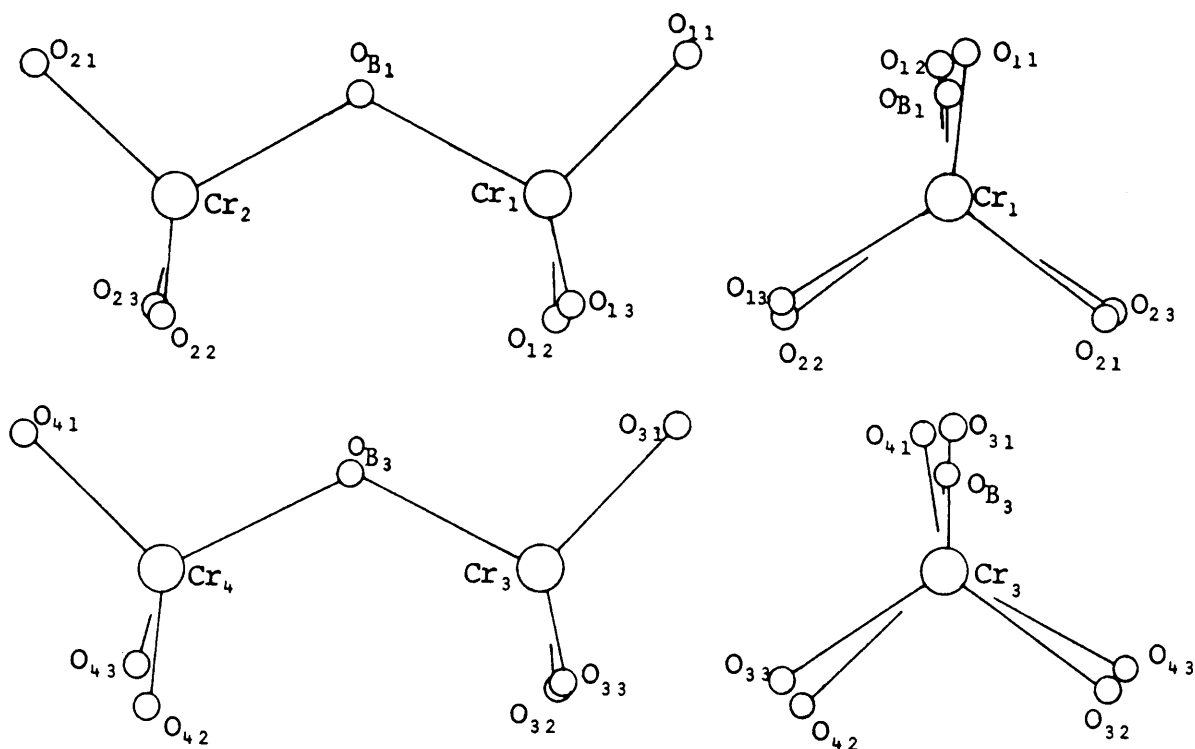
##### 4.1 Introduction

$K_2Cr_2O_7$ , with a melting point of  $398^\circ C$ , exhibits a triclinic crystal structure below  $241,6^\circ C$  (515 K) [65]. The solid-solid phase transition involves a transformation from a triclinic lattice, space group  $P\bar{1}(C_1^1)$  [61] to a monoclinic lattice, space group  $P2_1/c(C_{2h}^5)$  [62].

Raman spectra of the triclinic and monoclinic structure, including low temperature and molten  $K_2Cr_2O_7$  data, have been published [32,63,64]. Raman spectra recorded at 514, 541, 553 and 593 K have been reported [63], and groups of bands have been assigned according to symmetry species of a  $C_{2v}$  pointgroup [63] with approximate descriptions of the modes [32,64].

The  $Cr_2O_7^{2-}$  ions in the primitive cell of the triclinic crystal structure occupy two sets of nonequivalent sites. The two crystallographically independent ions are similar, deviating only slightly from  $C_{2v}$ -symmetry. Side and end views of the two independent ions are shown in Fig. (VI.6). Both ions are in similar environments [61]. The splitting of internal  $Cr_2O_7^{2-}$  modes observed in the Raman spectra of  $K_2Cr_2O_7$  below the transition temperature is caused by this two-site effect [63].

**Fig. (VI.6)** Side and end views of the two independent  $\text{Cr}_2\text{O}_7^{2-}$  ions in triclinic  $\text{K}_2\text{Cr}_2\text{O}_7$  [61].



In contrast to the low temperature form, the  $\text{Cr}_2\text{O}_7^{2-}$  ions occupy four equivalent  $C_1$  sites in the unit cell of the high temperature phase. Any observable splitting of internal  $\text{Cr}_2\text{O}_7^{2-}$  modes in the monoclinic form can thus only be caused by correlation field effects [63].

The thermal behaviour of Raman active modes of  $\text{K}_2\text{Cr}_2\text{O}_7$  at temperatures ranging from room-temperature (triclinic crystal structure) to above the phase transition temperature at 515 K (monoclinic crystal structure), can be compared with the thermal behaviour of Raman active modes of  $(\text{NH}_4)_2\text{Cr}_2\text{O}_7$  up to 473 K, as the latter does not undergo a phase transition, but decomposes at temperatures above 473 K (IV.4).

## 4.2 Experimental

The high temperature Raman cell was used to heat  $K_2Cr_2O_7$  and  $(NH_4)_2Cr_2O_7$  alternately in a glass tube, 3 mm in diameter. Raman spectra were recorded between 20 and  $1000\text{ cm}^{-1}$  at the following temperatures:

$K_2Cr_2O_7$  - 298, 323, 373, 423, 433, 443, 453, 473, 503, 523 and 533 K.

$(NH_4)_2Cr_2O_7$  - 298, 323, 373, 423, 433, 443, 453, 463 and 473 K.

Raman spectra could not be recorded of  $(NH_4)_2Cr_2O_7$  at higher temperatures as the samples decomposed rapidly above 473 K, turning black.

## 4.3 Results, discussion and comparison with $(NH_4)_2Cr_2O_7$

The Raman spectra of triclinic and monoclinic  $K_2Cr_2O_7$  are shown in Fig. (VI.7) and (VI.8) respectively. The lowest temperature at which a spectrum of the monoclinic structure was found, was 513 K. Complete results of the thermal behaviour of the Raman bands of  $K_2Cr_2O_7$  and  $(NH_4)_2Cr_2O_7$  at the various temperatures are presented in Table (VI.2)/Fig. (VI.9(a)) and (b) and Table (VI.3)/Fig. (VI.10) respectively. Values of  $dv/dT$  are given in Table (VI.4) together with assignment of the various modes, and the spectrum of  $K_2Cr_2O_7$  at 533 K is compared with that of  $(NH_4)_2Cr_2O_7$  at room-temperature, both exhibiting a monoclinic crystal structure.

**Fig. (VI.7)** Raman spectrum of  $K_2Cr_2O_7$  at 298 K (Triclinic form)

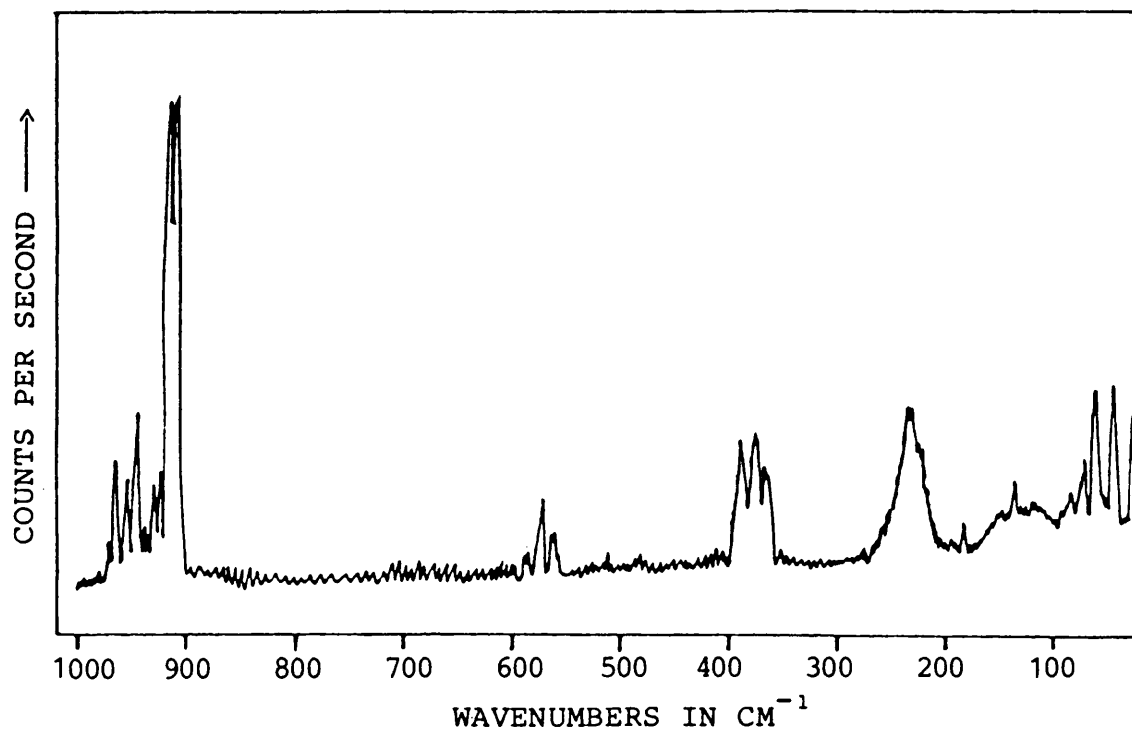


**Fig. (VI.8)** Raman spectrum of  $K_2Cr_2O_7$  at 513 K (Monoclinic form)

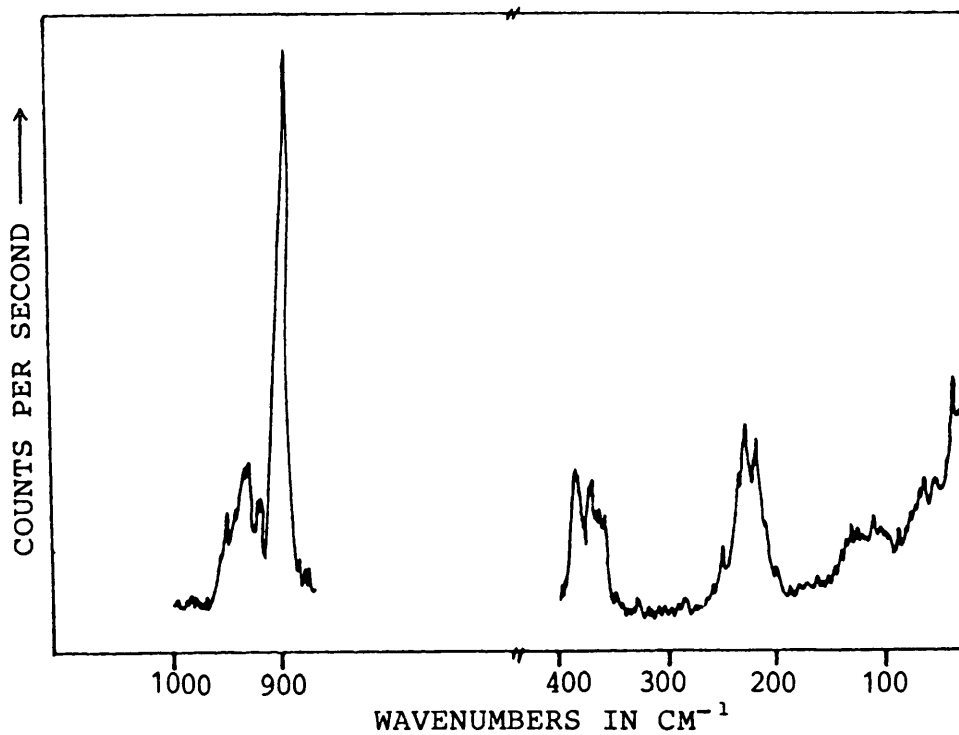


**Table (VI.2)** Thermal behaviour of Raman active modes of  $K_2Cr_2O_7$ 

Temp/K	$\nu/cm^{-1}$																	
298	23	45	67	216	357	360	370	382	557	568	908	912	921	928	944	952	960	967
323	23	45	67	216	357	361	371	384	555	567	905	912	920	926	941	949	958	962
373	23	45	67	218	360	362	370	382	553	565	906	910	920	926	941	949	557	-
423	23	45	67	215	356	362	371	383	551	564	905	910	920	926	941	949	957	-
433	23	45	-	218	358	363	369	383	-	565	904	910	918	926	940	948	954	963
443	23	42	-	216	-	362	368	382	-	563	904	909	919	925	940	948	955	962
453	23	44	67	215	358	363	369	383	552	564	905	909	919	924	939	948	955	959
473	23	44	66	217	357	-	369	382	-	560	904	906	917	924	939	948	956	-
503	22/24	43	65	217	357	367	369	384	-	-	908	909	915	925	939	945	953	-
513	-	45	-	-	-	-	-	-	-	-	902	-	918	-	938	-	-	-
523	22	-	67	216	357	-	370	384	-	-	902	-	918	925	938	945	953	958
533	22	43	-	219	356	-	371	383	-	-	902	-	916	-	938	-	953	-

**Table (VI.3)** Thermal behaviour of Raman active modes of  $(\text{NH}_4)_2\text{Cr}_2\text{O}_7$ 

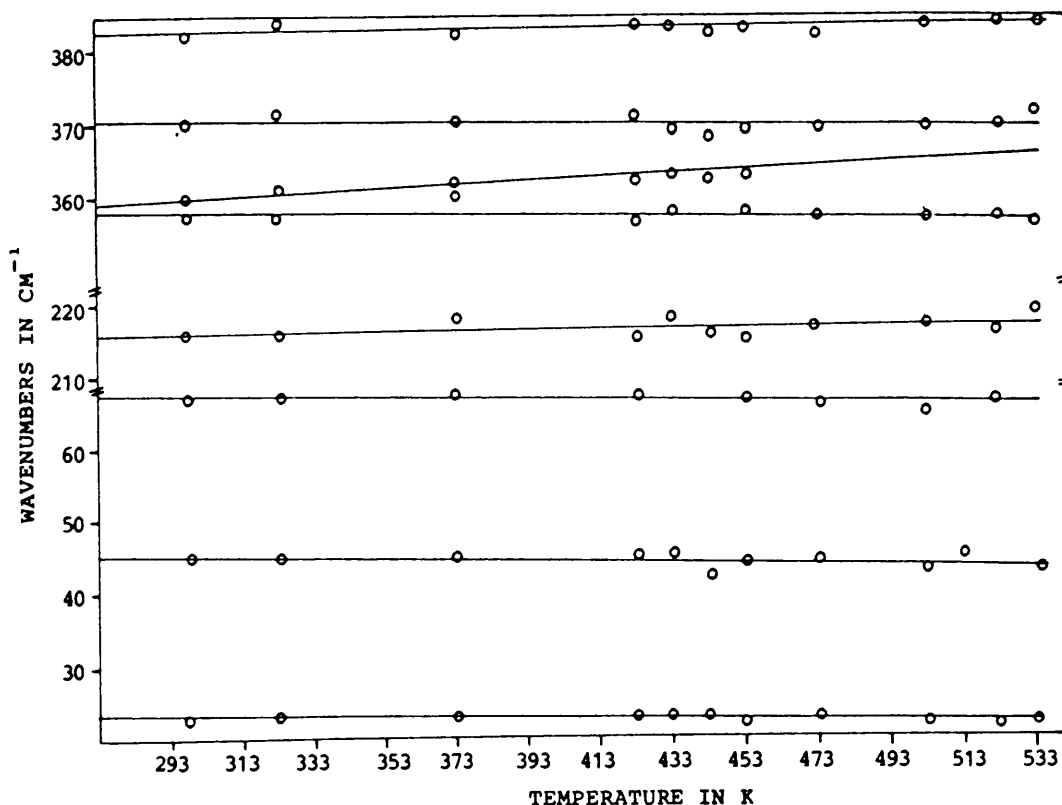
Temp/K	$\nu/\text{cm}^{-1}$									
298	43,6	28,4	94,4	224,6	948,5	902,8	578,1	383,6	366,7	362
323	46,3	28,4	94,4	223,1	945,9	903,6	573,5	383,9	365,3	-
373	45,3	30,1	94,4	224,8	944,2	901,9	575,2	380,5	365,3	361,9
423	45,3	30,1	94,4	226,5	944,2	901,9	570,1	382,2	365,3	360,2
433	47,1	30,1	95,3	226,8	942,3	903,3	576,1	381,1	365	362
443	47	30,1	96,1	224,6	943,4	901,1	576,4	380,2	-	361,6
453	47	-	96,1	-	943,4	901,1	573	-	-	359,9
463	47,1	28,4	-	223,2	943,2	902,6	573,9	-	365	362,2
473	-	31	96	223	-	901	-	-	-	-

**Table (VI.4)** Assignment of  $\text{Cr}_2\text{O}_7^{2-}$  Raman modes with a comparison of  $dv/dT$  values for  $(\text{NH}_4)_2\text{Cr}_2\text{O}_7$  and  $\text{K}_2\text{Cr}_2\text{O}_7$ .

Assignment for $(\text{NH}_4)_2\text{Cr}_2\text{O}_7$ [35]	$(\text{NH}_4)_2\text{Cr}_2\text{O}_7$		Monoclinic $\text{K}_2\text{Cr}_2\text{O}_7$		$\text{K}_2\text{Cr}_2\text{O}_7$ $dv/dT$	Triclinic $\text{K}_2\text{Cr}_2\text{O}_7$		Assignment for $\text{K}_2\text{Cr}_2\text{O}_7$ [64]	
	298 K Raman	$dv/dT$	533 K Raman	From [63]		298 K Raman	From [63]		
CrO <sub>3</sub> stretch	950	-	953	955	-0,030	967	963	CrO <sub>3</sub> asym. stretch	
	949	-0,032	938	931	-0,026	960	958		
					-0,043	952	950		
	919	-	916	918	-0,020	944	942		
	912	-	912(sh)		-0,015	928	927		
Cr-O-Cr stretch	903	-0,010	902	907	-0,026	921	920	CrO <sub>3</sub> sym. in-phase stretch	
	878	-		879		908	905		
	720	-		736			878		CrO <sub>3</sub> sym. out-of-phase stretch
CrO <sub>3</sub> bend	578	-0,025		571	-0,046	568	566	Cr-O-Cr bridge stretch	
	391	-		390	-0,032	557	555		
	385	-	383	385	-	387	388		CrO <sub>3</sub> sym. bend
	384	-0,023			=0	382	383		and
	375	-		377	=0	370	371		CrO <sub>3</sub> scissor deform.
O-CrO <sub>3</sub> bend	373	-	371	368	+0,034	360	362	CrO <sub>3</sub> rocking	
	362	=0	356	357	=0	357	358		
	236(sh)	-							
	230(sh)	-		230	-	231	232		
	228	+0,008							
Cr-O-Cr bend	198	-			-	198		Cr-O-Cr bend	
	160	-							
	225	=0	227	228	+0,013	216	215		
Transl.	105	-		106				lattice modes	
	98	-		100	-	79	79		
	94	=0		89	=0	67	68		
Rot.	61	-	43	64	=0	45	46		
	44	+0,021	38		-	39	38		
	28	+0,015	22		=0	23			

sh = shoulder

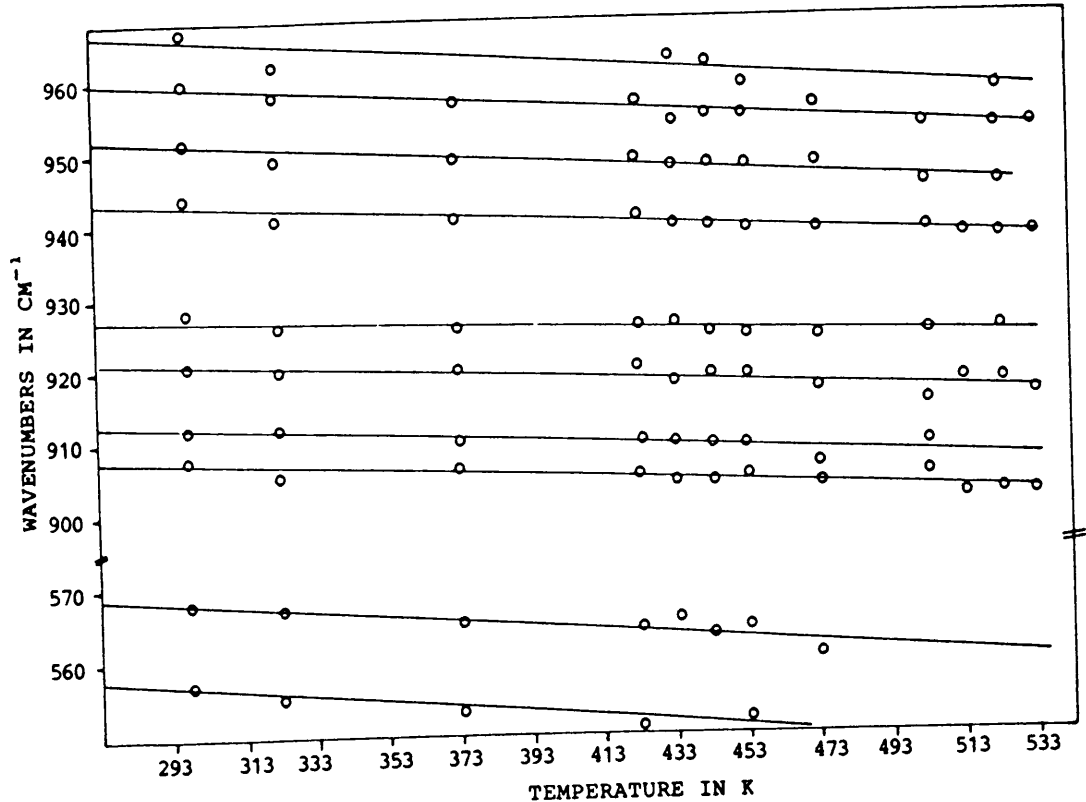
**Fig. (VI.9(a))** Temperature dependence of the Raman bands (20-400  $\text{cm}^{-1}$ ) of  $\text{K}_2\text{Cr}_2\text{O}_7$



Higher temperatures lead to a weakening in Cr-O terminal and Cr-O bridging bonds, especially in  $\text{K}_2\text{Cr}_2\text{O}_7$  as can be seen from all the  $\text{K}_2\text{Cr}_2\text{O}_7$  bands from 557 to 967  $\text{cm}^{-1}$  in Fig. (VI.9(b)) and the  $(\text{NH}_4)_2\text{Cr}_2\text{O}_7$  bands at 578, 903 and 949  $\text{cm}^{-1}$  in Fig. (VI.10). The Cr-O-Cr bending mode of  $\text{K}_2\text{Cr}_2\text{O}_7$  at 216  $\text{cm}^{-1}$  is slightly affected by temperature, shifting towards higher  $\nu$ -values, while this mode in  $(\text{NH}_4)_2\text{Cr}_2\text{O}_7$  at 225  $\text{cm}^{-1}$  remains almost unaffected.  $\text{CrO}_3$  symmetrical bending and deformation modes of  $\text{K}_2\text{Cr}_2\text{O}_7$  at 382, 370 and 357  $\text{cm}^{-1}$  are

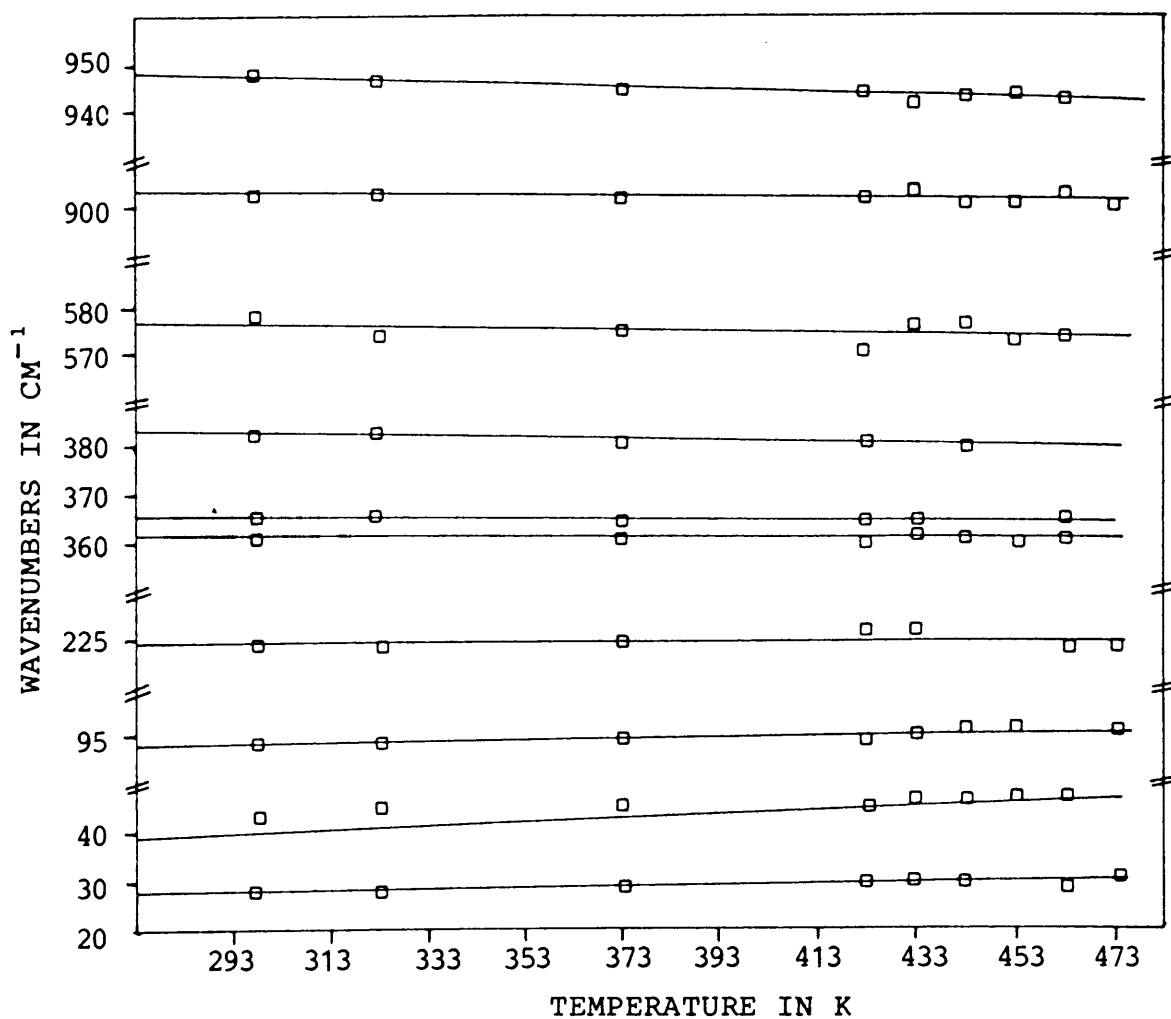


**Fig. (VI.9(b))** Temperature dependence of the Raman bands (550-1000  $\text{cm}^{-1}$ ) of  $\text{K}_2\text{Cr}_2\text{O}_7$



almost unaffected by temperature while the one at  $360 \text{ cm}^{-1}$  actually shifts towards higher  $\nu$ -values. The  $\text{CrO}_3$  bending mode of  $(\text{NH}_4)_2\text{Cr}_2\text{O}_7$  at  $384 \text{ cm}^{-1}$  shows a tendency to shift to lower  $\nu$ -values with an increase in temperature. Consequently the changes that occur upon heating  $\text{K}_2\text{Cr}_2\text{O}_7$  seem to involve considerable changes in the Cr-O-Cr and O-Cr-O angles. This is in contrast to the slight changes in the  $(\text{NH}_4)_2\text{Cr}_2\text{O}_7$  crystal.

**Fig. (VI.10)** Temperature dependence of some of the Raman bands of  $(\text{NH}_4)_2\text{Cr}_2\text{O}_7$ .



#### 4.4 Conclusions

The phase transition in  $\text{K}_2\text{Cr}_2\text{O}_7$  from triclinic to monoclinic structure occurs at  $513 \pm 5$  K. Changes would have to take place in one or both sets of nonequivalent  $\text{Cr}_2\text{O}_7^{2-}$  ions in the triclinic structure as all  $\text{Cr}_2\text{O}_7^{2-}$  ions in the monoclinic crystal structure occupy equivalent positions [62]. The nonequivalent  $\text{Cr}_2\text{O}_7^{2-}$  ions shown in Fig. (VI.6) have some dif-

ferent Cr-O<sub>B</sub>-Cr, O<sub>B</sub>-Cr-O<sub>term</sub> and O<sub>term</sub>-Cr-O<sub>term</sub> angles, as is shown in Table (VI.5) and it is probably changes in these

**Table (VI.5)** Angles (in degrees) in triclinic K<sub>2</sub>Cr<sub>2</sub>O<sub>7</sub> [61]  
Numbering of atoms as in Fig. (VI.6).

Dichromate (1)		Dichromate (2)	
Cr <sub>1</sub> -O <sub>B1</sub> -Cr <sub>2</sub>	124,0	127,6	Cr <sub>3</sub> -O <sub>B3</sub> -Cr <sub>4</sub>
O <sub>B1</sub> -Cr <sub>1</sub> -O <sub>11</sub>	106,1	106,6	O <sub>B3</sub> -Cr <sub>3</sub> -O <sub>31</sub>
O <sub>12</sub>	109,4	109,7	O <sub>32</sub>
O <sub>13</sub>	110,8	110,1	O <sub>33</sub>
O <sub>11</sub> -Cr <sub>1</sub> -O <sub>12</sub>	109,5	109,8	O <sub>31</sub> -Cr <sub>3</sub> -O <sub>32</sub>
O <sub>13</sub>	111,7	110,6	O <sub>33</sub>
O <sub>12</sub> -Cr <sub>1</sub> -O <sub>13</sub>	109,2	110,1	O <sub>32</sub> -Cr <sub>3</sub> -O <sub>33</sub>
O <sub>B1</sub> -Cr <sub>2</sub> -O <sub>21</sub>	109,6	109,7	O <sub>B3</sub> -Cr <sub>4</sub> -O <sub>41</sub>
O <sub>22</sub>	108,5	111,2	O <sub>42</sub>
O <sub>23</sub>	109,5	108,4	O <sub>43</sub>
O <sub>21</sub> -Cr <sub>2</sub> -O <sub>22</sub>	110,2	109,7	O <sub>41</sub> -Cr <sub>4</sub> -O <sub>42</sub>
O <sub>23</sub>	110,6	109,9	O <sub>43</sub>
O <sub>22</sub> -Cr <sub>2</sub> -O <sub>23</sub>	108,4	107,9	O <sub>42</sub> -Cr <sub>4</sub> -O <sub>43</sub>

angles that are reflected in the thermal behaviour of the Raman-active modes of K<sub>2</sub>Cr<sub>2</sub>O<sub>7</sub> at 216, 360, 557 and 568 cm<sup>-1</sup>.

The splitting of internal Cr<sub>2</sub>O<sub>7</sub><sup>2-</sup> modes in the Raman spectra below transition temperature is not present in the high temperature phase because Cr<sub>2</sub>O<sub>7</sub><sup>2-</sup> ions occupy equivalent sites. Up to 473 K the Raman modes of (NH<sub>4</sub>)<sub>2</sub>Cr<sub>2</sub>O<sub>7</sub> seem almost unaffected.

Force constants  $k$  and  $k_{\text{mom}}$  of these two salts were calculated using  $\nu_{\text{S}}(\text{Cr-O}_{\text{bridge}})$  and  $\nu_{\text{as}}(\text{Cr-O}_{\text{bridge}})$  modes from Raman and IR spectra. The results are shown in Table (VI.6).

**Table (VI.6)** Comparison between  $k$  and  $k_{\text{mom}}$  for  $\text{K}_2\text{Cr}_2\text{O}_7$  and  $(\text{NH}_4)_2\text{Cr}_2\text{O}_7$

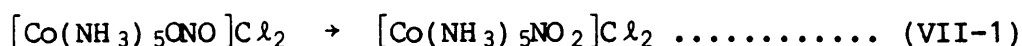
	$\nu_{\text{S}}$ ( $\text{cm}^{-1}$ )	$\nu_{\text{as}}$ ( $\text{cm}^{-1}$ )	$k$	$k_{\text{mom}}$
$\text{K}_2\text{Cr}_2\text{O}_7$	557 (R)	761 (IR)	3,228	0,075
$(\text{NH}_4)_2\text{Cr}_2\text{O}_7$	578 (R)	724 (IR)	3,205	0,351

The value of  $k_{\text{mom}}$  for  $(\text{NH}_4)_2\text{Cr}_2\text{O}_7$  are almost five times the value for  $\text{K}_2\text{Cr}_2\text{O}_7$ . This could be the result of hydrogen bonding in the ammonium salt which is known to follow Waddington's criteria [17] indicating strong hydrogen bonding [11].

The report by Wing *et. al.* [59] that a  $\text{M}_2\text{O}$ -bridge angle is larger than  $115^\circ$  and that  $\nu_{\text{as}}$  is separated from  $\nu_{\text{S}}$  by at least  $215 \text{ cm}^{-1}$  in such a case is confirmed by the separation of  $\nu_{\text{as}}/\nu_{\text{S}}$  ( $\text{Cr-O-Cr}$ ) ( $792/565 \text{ cm}^{-1}$ ) of  $227 \text{ cm}^{-1}$ . The  $\text{Cr-O-Cr}$  bridge angles in the two non-equivalent  $\text{Cr}_2\text{O}_7^{2-}$  ions are  $124$  and  $128^\circ$  [61].

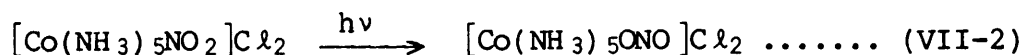
CHAPTER VIITHE PHOTOCHEMICAL CONVERSION OF  $[\text{Co}(\text{NH}_3)_5\text{NO}_2]\text{Cl}_2$  TO  $[\text{Co}(\text{NH}_3)_5\text{ONO}]\text{Cl}_2$ 1. INTRODUCTION

The two complexes, nitro- and nitrito-pentamminecobalt(III)-chloride are structural isomers and have yellow and red colours respectively. Structural isomerism occurs when a ligand is capable of bonding through different types of donor atoms. The metal to ligand bonding is through the nitrogen and one of the oxygen atoms of  $\text{NO}_2^-$  in the respective complexes. Both of the complexes can be prepared [66, 67] but the nitrito complex is transformed to the thermodynamically more stable nitro complex both in solution and in the solid state [68]:



This conversion has been extensively reported in the literature [66,69-73]. Adell [66] measured the rate of isomerization in the reaction photometrically and found it to be a first order reaction. Infrared methods have also been used to study the reaction [71,73].

The nitrito complex can also be obtained from the nitro complex through photoisomerization [68]:



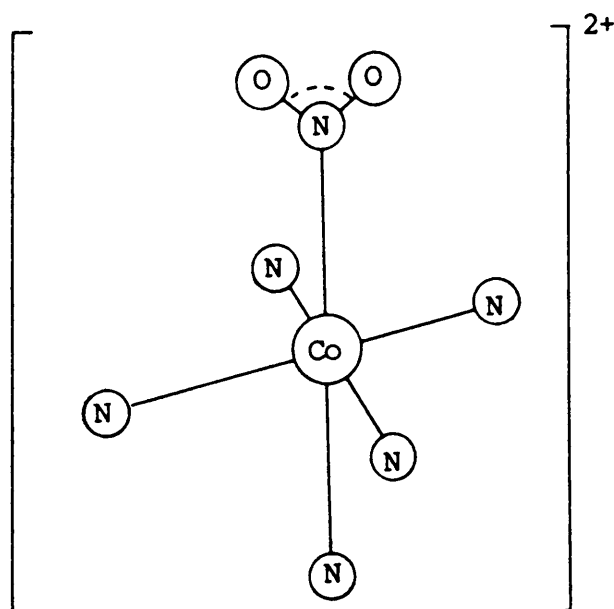
In the present study this reaction is studied in more detail with particular emphasis on the rate of the reaction and the structural properties of the compound so formed.

## 2. CRYSTAL STRUCTURES

### 2.1 $[\text{Co}(\text{NH}_3)_5\text{NO}_2]\text{Cl}_2$

Nitro-pentamminecobalt(III)chloride has a monoclinic crystal structure and belongs to space group  $C2/c$  with  $z = 4$ . The unit cell dimensions are  $a = 10,327 \text{ \AA}$ ;  $b = 8,661 \text{ \AA}$ ;  $c = 10,729 \text{ \AA}$ ;  $\beta = 95,04^\circ$  and  $V = 950,0 \text{ \AA}^3$  [74]. The geometrical arrangement of the ligands in the complex ion is octahedral [74]. The  $[\text{Co}(\text{NH}_3)_5\text{NO}_2]^{2+}$  ion is shown in Fig. (VII.1).

**Fig. (VII.1)** The  $[\text{Co}(\text{NH}_3)_5\text{NO}_2]^{2+}$  ion [74]

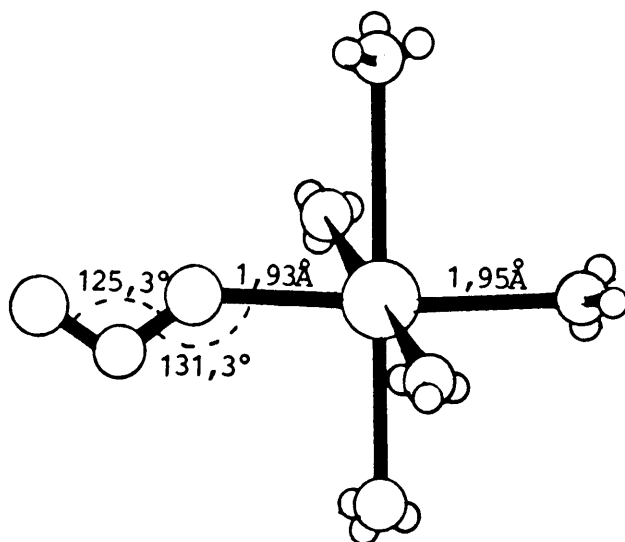


The Co-, one N(NH<sub>3</sub>)- and the N(NO<sub>2</sub>)-atoms all occupy 4e-sites of C<sub>2</sub>-symmetry, while the remaining NH<sub>3</sub>- and the Cl-atoms are situated on 8f-sites. The Co-N(NH<sub>3</sub>) distances are between 1,95 and 1,97 Å with the Co-N(NO<sub>2</sub>) and N-O distances at 1,91 and 1,23 Å. The Co-N-O angle is 119,6°.

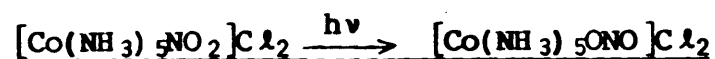
## 2.2 $[\text{Co}(\text{NH}_3)_5\text{ONO}]\text{Cl}_2$

Nitro-pentamminecobalt(III)chloride has an orthorombic crystal structure and belongs to space group  $P2_1nb$  with  $z = 4$ . The unit cell parameters are  $a = 10,349 \text{ \AA}$ ;  $b = 13,228 \text{ \AA}$ ;  $c = 6,864 \text{ \AA}$  and  $V = 939,5 \text{ \AA}^3$  [68]. The structure consists of  $[\text{Co}(\text{NH}_3)_5\text{ONO}]^{2+}$  and  $\text{Cl}^-$  ions which are held together by electrostatic forces and a network of hydrogen bonds. The symmetry of the  $\text{CoN}_5\text{O}$  group in the complex is close to octahedral [68]. The  $[\text{Co}(\text{NH}_3)_5\text{ONO}]^{2+}$  cation is shown in Fig. (VII.2).

Fig. (VII.2) The  $[\text{Co}(\text{NH}_3)_5\text{ONO}]^{2+}$  cation [68]



## 3. AN INFRARED KINETIC STUDY OF THE REACTION



### 3.1 Introduction

The nitrito to nitro isomerization of  $[\text{Co}(\text{NH}_3)_5\text{ONO}]\text{Cl}_2$  (Reaction (VII.1)) was investigated by Grenthe and Nordin [68] by

means of crystallographic methods. They concluded that the nitro complex obtained is an unstable intermediate which slowly converts to a stable product with the same formula as the intermediate but a different crystal structure (Intermediate space group:  $P2_1nb$ ; final product space group:  $C2/c$  [68]. The structure of the final product agrees with that of freshly prepared  $[Co(NH_3)_5NO_2]Cl_2$  [68].)

The nitro to nitrito photoisomerization (Reaction (VII.2)) was reported to produce a  $[Co(NH_3)_5ONO]Cl_2$  complex with a different structure than that of the freshly prepared nitrito complex through an intramolecular process that probably occurs via a seven coordinate transition state [68].

Infrared methods have also been one of the important tools in studying the rate of isomerization of the nitrito to the nitro complex [71,73]. The above findings urged this infrared study on the rate of the nitro to nitrito photoisomerization (Reaction (VII.2)) which has not been reported before. The infrared spectra recorded down to  $50\text{ cm}^{-1}$  will be used to investigate the effect of the reported differences in the structures on the various infrared spectra.

### 3.2 Experimental

$[Co(NH_3)_5NO_2]Cl_2$  and  $[Co(NH_3)_5ONO]Cl_2$  were synthesized according to methods given by Johnson and Pashman [75]. The latter was also prepared photochemically by irradiating the nitro complex with ultraviolet light (350 nm). The infrared spectra were recorded on the Bruker IFS 113 V described in



(VIII.3). A KBr disc containing the nitro complex was irradiated with ultraviolet light and removed from the light for short periods to record the spectra.

### 3.3 Co-NH<sub>3</sub> and Co-NO<sub>2</sub> vibrational modes

The following six normal vibrations are expected for a M-NH<sub>3</sub> molecule with C<sub>3v</sub>-symmetry [46]:

Stretching vibrations:  $\nu_S(\text{N-H})$ ,  $\nu_{\text{as}}(\text{N-H})$ ,  $\nu(\text{M-N})$

Deformation modes :  $\delta_S(\text{NH}_3)$ ,  $\delta_{\text{as}}(\text{NH}_3)$

Rocking mode :  $\rho_R(\text{NH}_3)$

These vibrations are shown in Fig. (VII.3) with assignments in the [Co(NH<sub>3</sub>)<sub>5</sub>NO<sub>2</sub>]Cl<sub>2</sub> complex.

The normal modes of vibration for a planar XYZ<sub>2</sub> molecule (Co-NO<sub>2</sub>) are shown in Fig. (VII.4) with assignments in the [Co(NH<sub>3</sub>)<sub>6</sub>NO<sub>2</sub>]Cl<sub>2</sub> complex.

**Fig. (VII.4)** The Normal vibrations in Co-NO<sub>2</sub>

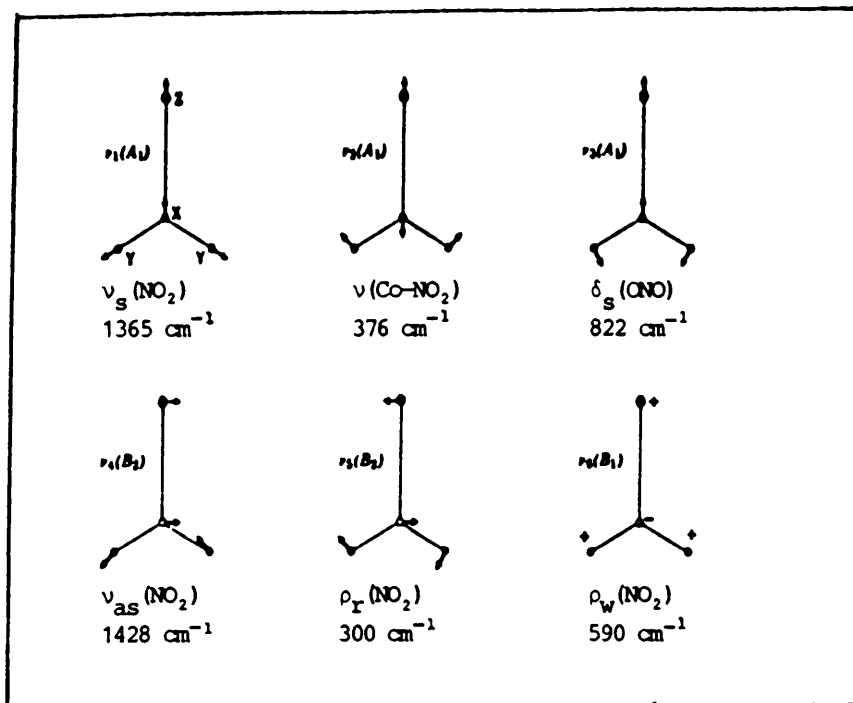
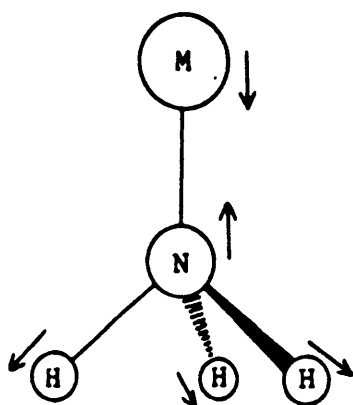
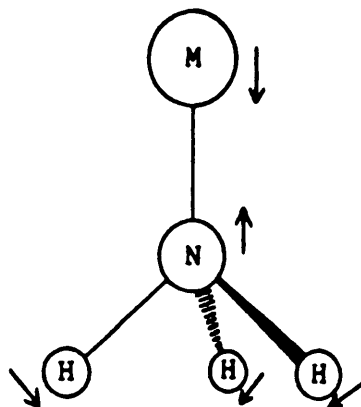


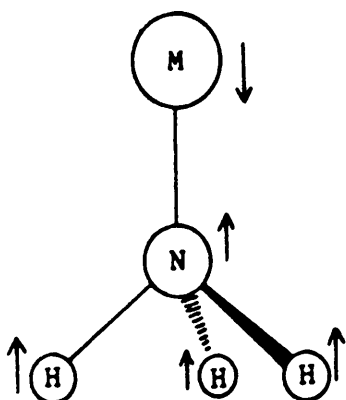
**Fig. (VII.3)** The normal vibrations in Co-NH<sub>3</sub> [46]



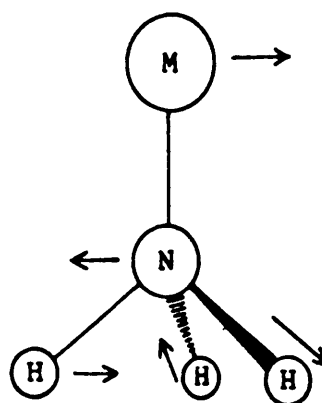
$\nu_1 (A_1)$   
 $\nu_S(N-H)$   
 3190  $\text{cm}^{-1}$



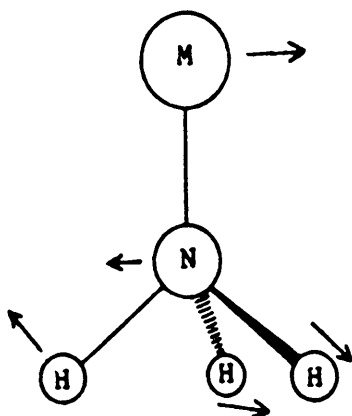
$\nu_2 (A_1)$   
 $\delta_S(NH_3)$



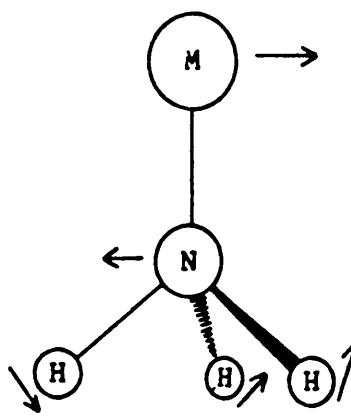
$\nu_3 (A_1)$   
 $\nu(\text{Co-NH}_3)$   
 510/490/485  $\text{cm}^{-1}$



$\nu_4 (E)$   
 $\nu_{as}(N-H)$   
 3270  $\text{cm}^{-1}$



$\nu_5 (E)$   
 $\nu_{as}(NH_3)$   
 1575/1615  $\text{cm}^{-1}$



$\nu_6 (E)$   
 $\rho_r(NH_3)$   
 845  $\text{cm}^{-1}$

### 3.4 The Infrared Spectra

The mid-IR spectra of  $[\text{Co}(\text{NH}_3)_5\text{NO}_2]\text{Cl}$  and freshly and photochemically prepared  $[\text{Co}(\text{NH}_3)_5\text{ONO}]\text{Cl}_2$  at room-temperature, as well as far-IR spectra of each at room-temperature and 83 K are shown in Fig. (VII.5) to Fig. (VII.9). These results are summarized in Table (VII.1).

If the photoreaction (reaction (VII-2)) is considered, it is obvious that the infrared spectrum of the photochemically prepared sample of  $[\text{Co}(\text{NH}_3)_5\text{ONO}]\text{Cl}_2$  is very similar to that of the freshly prepared sample, as can be seen in Fig. (VII.6). However, on closer investigation these results reveal the following:

- i) It is very difficult and even impossible to prepare  $[\text{Co}(\text{NH}_3)_5\text{ONO}]\text{Cl}_2$  photochemically in an absolute pure state without traces of  $\text{NO}_2^-$ -impurities. This is evident from the presence of extremely weak infrared peaks due to  $\text{NO}_2^-$ -groups even after irradiating the samples for several weeks.
- ii)  $\nu_{\text{as}}(\text{N}=\text{O})$  in photochemically prepared  $[\text{Co}(\text{NH}_3)_5\text{ONO}]\text{Cl}_2$  is a strong, sharp band at  $1460\text{ cm}^{-1}$  while it is split into two peaks at  $1460$  and  $1454\text{ cm}^{-1}$  in freshly prepared samples. The N and O atoms all lie in general positions in the crystals of  $[\text{Co}(\text{NH}_3)_5\text{ONO}]\text{Cl}_2$  under  $\text{C}_{2v}^9$ -symmetry [68] and the N=O and N-O stretching modes can each split into  $A_1^{\text{IR/R}} + A_2^{\text{O}} + B_1^{\text{IR/R}} + B_2^{\text{IR/R}}$  components. It is unlikely that all of the

**Fig. (VII.5)** Mid-IR spectrum of  $[\text{Co}(\text{NH}_3)_5\text{NO}_2]\text{Cl}_2$

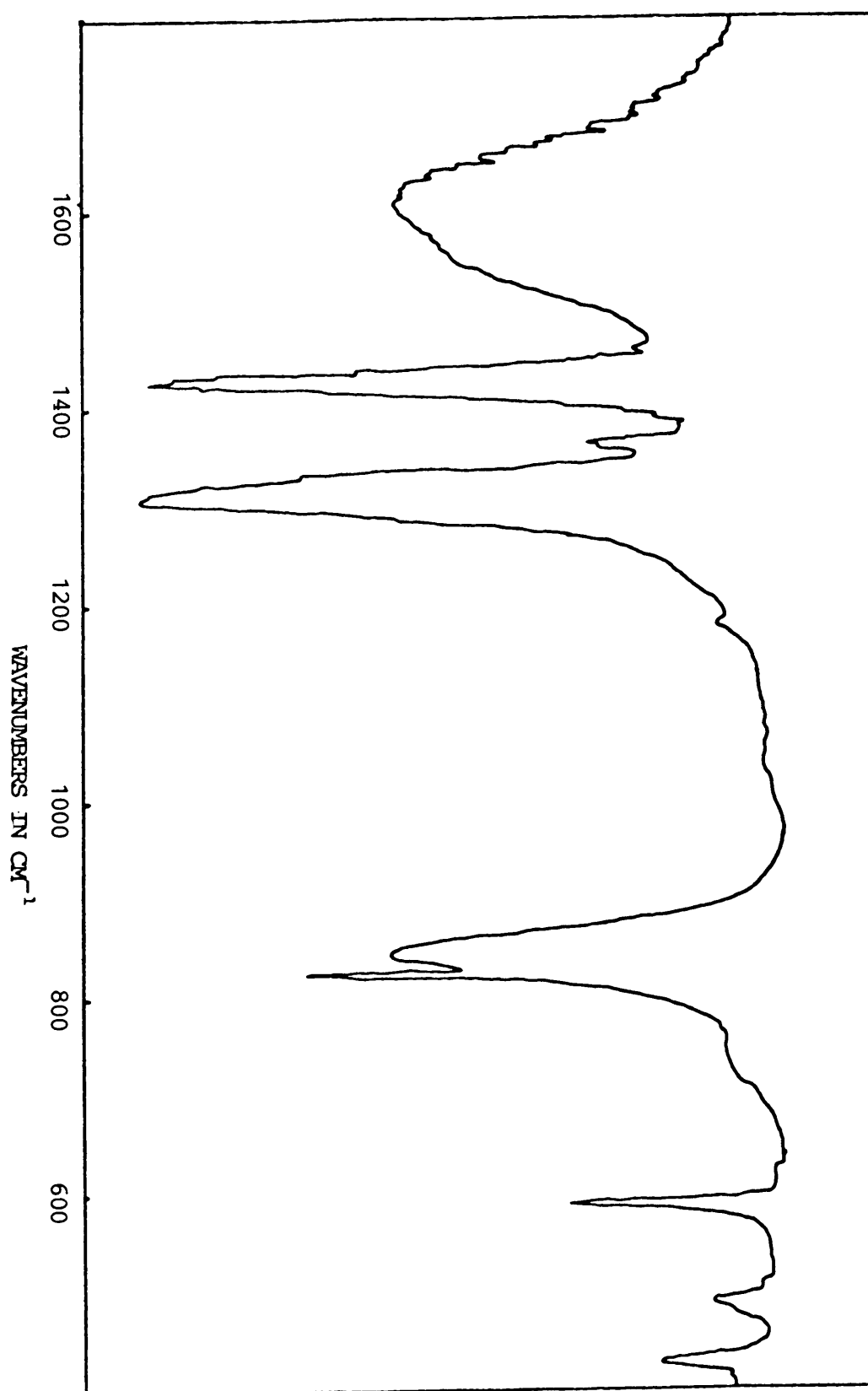


**Fig. (VII.6)** Mid-IR spectra of  $[\text{Co}(\text{NH}_3)_5\text{ONO}]\text{Cl}_2$   
(a) freshly and (b) photochemically prepared

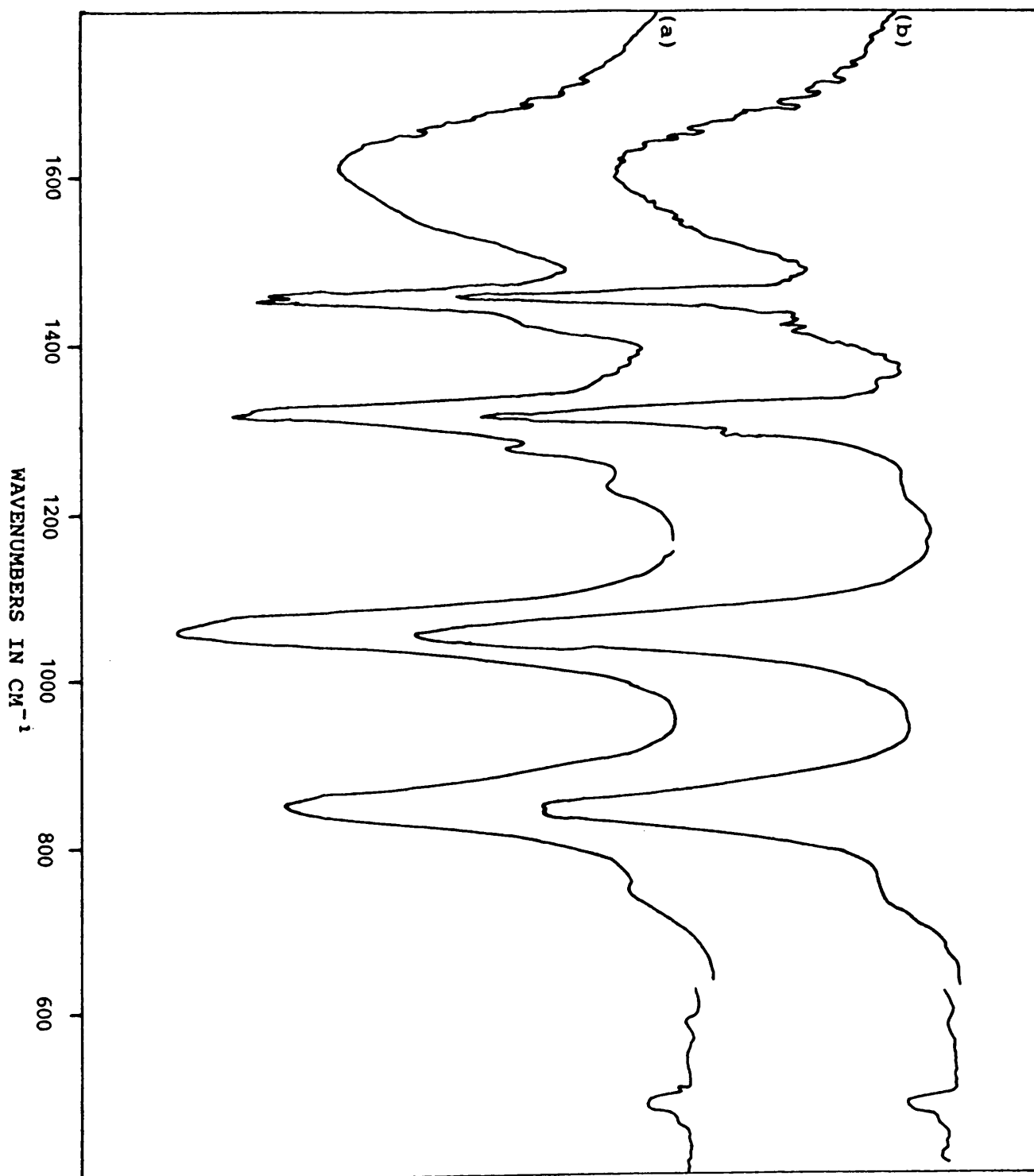


**Fig. (VII.7)** Far-IR spectra of  $[\text{Co}(\text{NH}_3)_5\text{NO}_2]\text{Cl}_2$  at (a) room-temperature and (b) 83 K

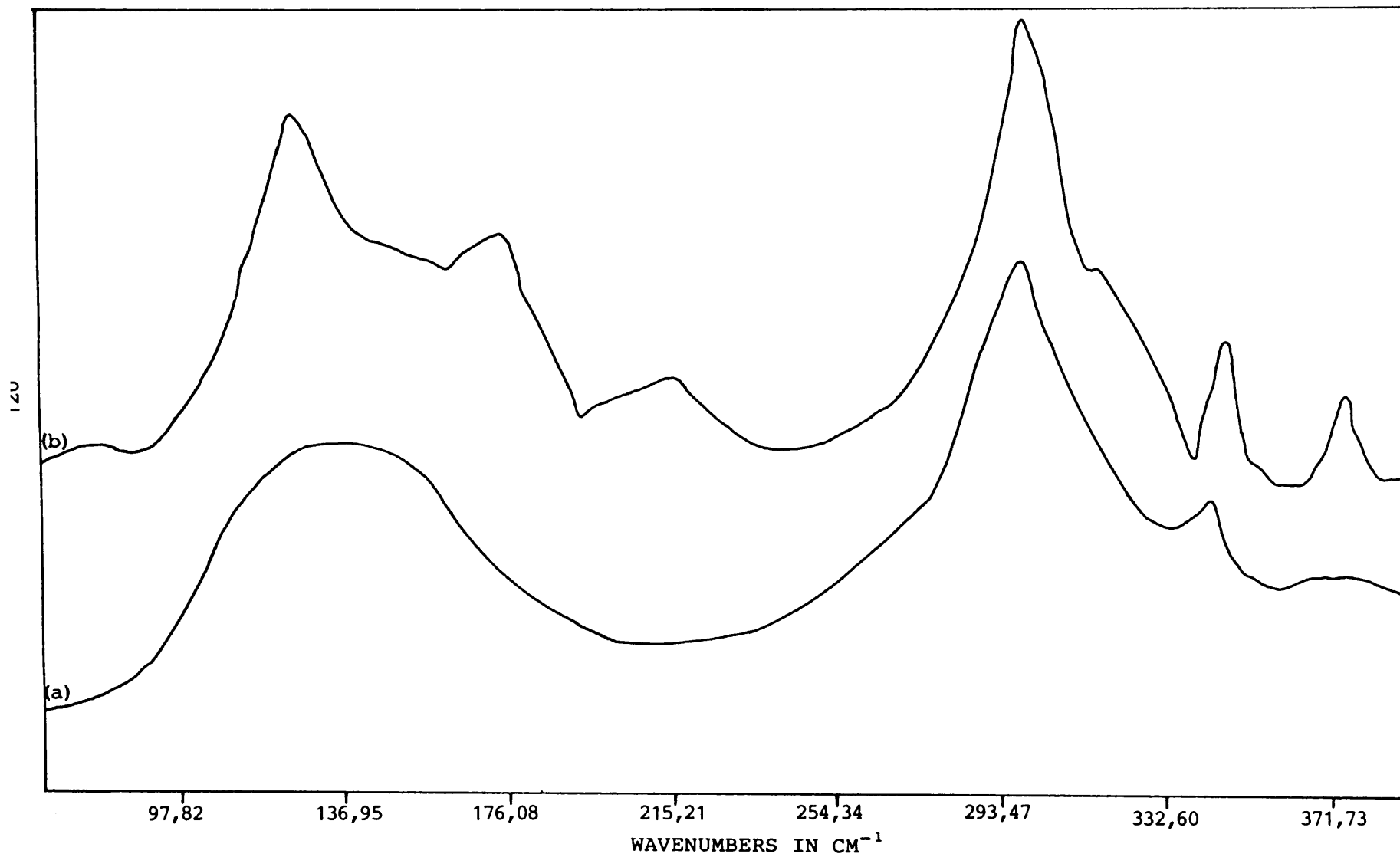


**Fig. (VII.8)** Far-IR spectra of freshly prepared  $[\text{Co}(\text{NH}_3)_5\text{ONO}]\text{Cl}_2$  at (a) room-temperature and (b) 83 K

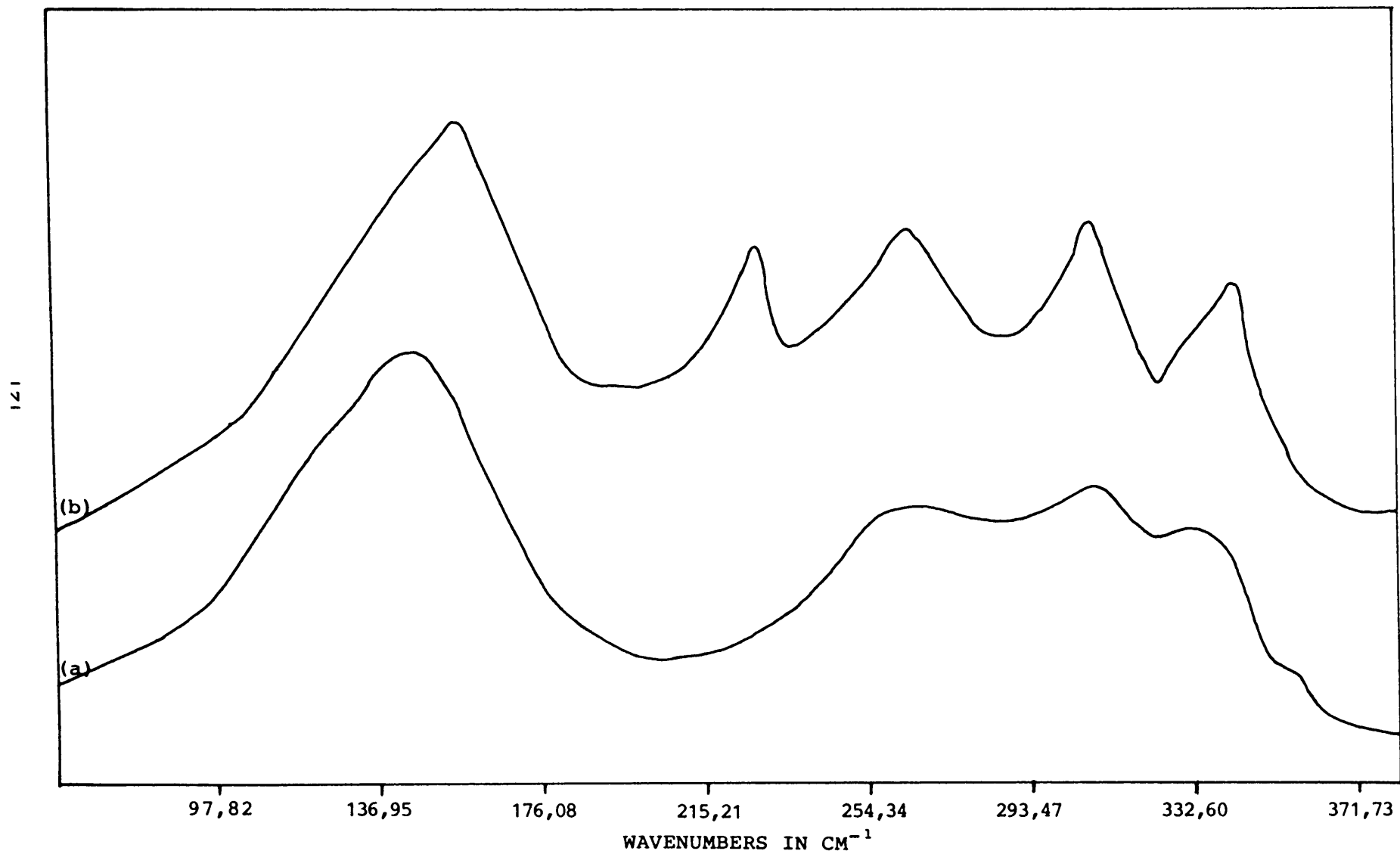


**Fig. (VII.9)** Far-IR spectra of photochemically prepared  $[\text{Co}(\text{NH}_3)_5\text{ONO}]\text{Cl}_2$  at (a) room-temperature and (b) 83 K

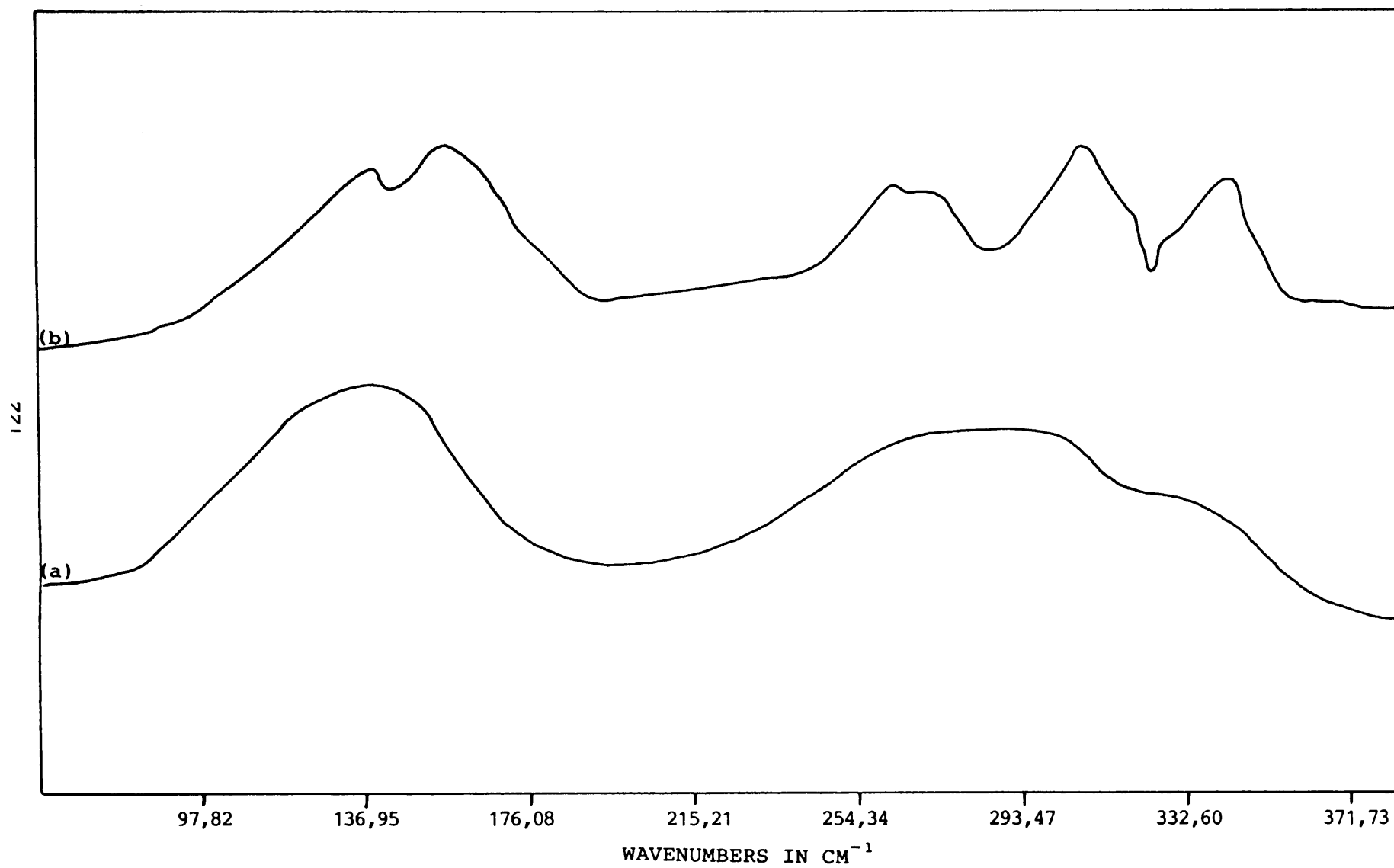




**Table (VII.I)** The Infrared Bands in  $[\text{Co}(\text{NH}_3)_5\text{NO}_2]\text{Cl}_2$  and in freshly and photochemically prepared  $[\text{Co}(\text{NH}_3)_5\text{ONO}]\text{Cl}_2$

$[\text{Co}(\text{NH}_3)_5\text{NO}_2]\text{Cl}_2$		$[\text{Co}(\text{NH}_3)_5\text{ONO}]\text{Cl}_2$		
$\text{cm}^{-1}$	Assignment	Freshly prepared		Photochemically prepared
		$\text{cm}^{-1}$	Assignment	$\text{cm}^{-1}$
3270	$\nu_{\text{as}}(\text{N-H})$	3260 s.	$\nu(\text{NH}_3)$	3270 s.
3190 sh.	$\nu_{\text{s}}(\text{N-H})$	3180 sh.		3190 sh.
1615 s.	$\delta_{\text{as}}(\text{NH}_3)$	1620 s.	$\delta(\text{NH}_3)$	1610 s.
1575 sh.	$\delta_{\text{as}}(\text{NH}_3)$	1460 vs.	$\nu_{\text{as}}(\text{N=O})$	1460 vs.
1428 vs.	$\nu_{\text{as}}(\text{NO}_2)$	1454 vs.		
1365 w.	$\nu_{\text{s}}(\text{NO}_2)$			
1330 sh.		1320 sh.		
1310 s.	$\delta_{\text{s}}(\text{NH}_3)$	1315 s.	$\delta(\text{NH}_3)$	1315 s.
1285 sh.		1270 sh.		1292 sh.
		1225 sh.		1225 sh.
1180 w.	2 x 590	-	-	
-		1055 vs.	$\nu_{\text{s}}(\text{N-O})$	1055 vs.
845 s.	$\rho_{\text{r}}(\text{NH}_3)$	850 s.	$\rho_{\text{r}}(\text{NH}_3)$	[ 853 s. 843 s.
822	$\delta_{\text{s}}(\text{ONO})$	-	-	
730 sh.	-	740 sh.	-	735 sh.
590 s.	$\delta_{\text{w}}(\text{NO}_2)$	-	-	
510 sh.]				
490 m.	$\nu(\text{Co-NH}_3)$	488 m.	$\nu(\text{Co-NH}_3)$	488 m.
485 m.]				
428 s.	-	-	-	
376 m.	$\nu(\text{Co-NO}_2)$	-	-	
347 m.	$\nu(\text{Co-NH}_3)$	339 m.	$\nu(\text{Co-NH}_3)$	341 m.
317 sh.	$\delta(\text{N-Co-N})$	307 w.	$\delta(\text{N-Co-N})$	308 w.
300 s.	$\rho_{\text{r}}(\text{NO}_2)$	-	-	
-	-	260 w.	$\nu(\text{Co-O})$	274 w.
-	-	228 w.		
177 m.]	Lattice	-	Lattice	[ 158
125 s.]	modes	157	mode	[ 139

vs. = very strong, s = strong, m = medium, w = weak, sh = shoulder

factor group components will be resolved in the infrared spectra but it can at least be said that a splitting of bands is possible. However, the same applies to the photochemically prepared nitrito complex and it is not clear at this stage why a splitting should only be observed in one of the modifications.

- iii) The  $\delta_S(\text{NH}_3)$ -mode is of  $A_1$ -symmetry for the 'free' molecule of the  $C_{3V}$ -symmetry and can theoretically split into four factor group components under  $C_{2V}^9$ . There are, however, five different  $\text{NH}_3$  groups with N-H bond lengths varying between 0,65 and 1,23 Å [68] and it can be expected that different infrared components of this mode will be resolved. From Fig. (VII.6) it is evident that at least four components of  $\delta_S(\text{NH}_3)$  can be detected at 1320(sh), 1315, 1270 and 1225  $\text{cm}^{-1}$  in the freshly prepared nitrito complex. The same number of components is observed in the photochemically prepared sample and they differ only in the sense that the broad shoulder at 1225  $\text{cm}^{-1}$  is much weaker in the latter and the component at 1270  $\text{cm}^{-1}$  has shifted to 1292  $\text{cm}^{-1}$ . This band is very characteristic of photochemically prepared  $[\text{Co}(\text{NH}_3)_5\text{ONO}]\text{Cl}_2$  and can be used for identification purposes.

$\rho_r(\text{NH}_3)$  which occurs at 850  $\text{cm}^{-1}$  in freshly prepared  $[\text{Co}(\text{NH}_3)_5\text{ONO}]\text{Cl}_2$  is split into two components at 853 and 843  $\text{cm}^{-1}$  in the photochemically prepared complex and is once again characteristic of this compound.

$\rho_r(\text{NH}_3)$  is of E-symmetry and will split into 2A in the  $C_1$ -site group symmetry that the  $\text{NH}_3$ -groups occupy in the crystal lattice. Five different  $\text{NH}_3$ -groups in the crystal can cause extensive splitting of this band.

The remaining  $\text{NH}_3$ -vibrational modes are broad and reveal no splitting of bands so that very little can be concluded from this as far as the structures of the different complexes are concerned.

- iv) The far-IR spectra of the nitro complex and the nitrito complex prepared in the two different ways are shown in Fig. (VII.7-9). The far-IR spectrum of the former has already been reported [76] and an assignment of the bands has been made by the aid of a normal coordinate analysis. The tentative assignment of bands in Table (VII.1) has partially been based on these results for  $[\text{Co}(\text{NH}_3)_5\text{NO}_2]\text{Cl}_2$  and by comparing these results with those obtained on the two  $[\text{Co}(\text{NH}_3)_5\text{ONO}]\text{Cl}_2$  compounds.

The far-IR spectrum of the freshly prepared nitrito complex reveals sharper and better-defined absorption peaks than those observed in the photochemically prepared sample. This most probably serves as an indication that the sample prepared by chemical methods has a more ordered structure than the one obtained by photochemical methods. There are also some differences with regard to the number of bands and the frequencies of

some of these bands. It is evident from Fig. (VII.8) and (VII.9) that the lattice mode observed at  $157\text{ cm}^{-1}$  is split into two components at  $158$  and  $139\text{ cm}^{-1}$  in the photochemically prepared  $[\text{Co}(\text{NH}_3)_5\text{ONO}]\text{Cl}_2$ . A rather prominent absorption peak at  $228\text{ cm}^{-1}$  in freshly prepared  $[\text{Co}(\text{NH}_3)_5\text{ONO}]\text{Cl}_2$  at  $83\text{ K}$  is also absent in the spectrum of the photochemically prepared sample. The band assigned to a Co-ONO stretching mode at  $260\text{ cm}^{-1}$  in freshly prepared samples shifted upwards to  $274\text{ cm}^{-1}$  in the photochemically prepared crystals. The far-IR spectra of the intermediate product  $[\text{Co}(\text{NH}_3)(\text{ONO})_{\frac{1}{2}}(\text{NO}_2)_{\frac{1}{2}}]\text{Cl}_2$  were featureless and very little, if anything could be concluded from these spectra. This is indicative of disorder existing in these crystals during the isomerization process.

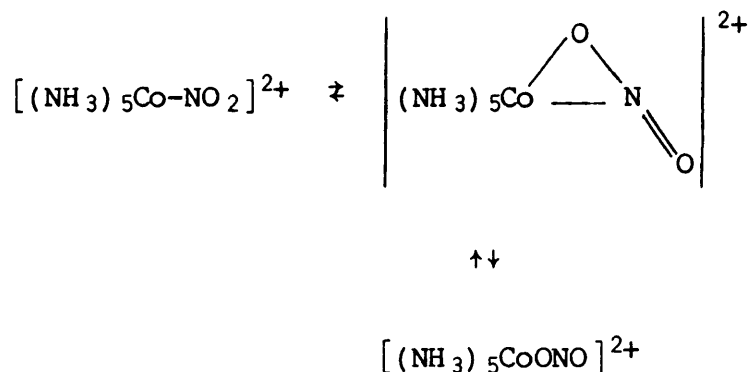
The frequency shifts in the lattice modes which occur between the nitro and nitrito complexes indicate that there are distinct differences in the electrostatic forces and hydrogen bonds holding the cations and anions together in these complexes.

- v) Samples of  $[\text{Co}(\text{NH}_3)_5\text{NO}_2]\text{Cl}_2$  which were left standing for long periods after preparation, as well as samples obtained from the nitrito complex show a very weak absorption peak at  $1040\text{ cm}^{-1}$  with a weak and broad shoulder at  $1055\text{ cm}^{-1}$ . These are indications of the presence of ONO-impurities in the lattice of  $[\text{Co}(\text{NH}_3)_5\text{NO}_2]\text{Cl}_2$ . In other samples the absorption

maximum is at  $\sim 1055 \text{ cm}^{-1}$  with a weak shoulder at  $1040 \text{ cm}^{-1}$ , showing that there are two orientations possible for the  $\text{ONO}^-$ -ion in the lattice of  $[\text{Co}(\text{NH}_3)_5\text{NO}_2]\text{Cl}_2$ . The occupation of these orientations is statistically controlled and can vary in different samples under different conditions. As soon as the sample is irradiated and partial isomerization of  $\text{NO}_2^-$  to  $\text{ONO}^-$  has occurred, a single absorption peak is obtained. Results that have been obtained with a sample that exhibited weak absorption peaks at  $1055$  and  $1040 \text{ cm}^{-1}$  and which has been irradiated, are shown in Fig. (VII.11). It is clear that the absorption peak at  $1040 \text{ cm}^{-1}$  gradually shifts upwards until an equilibrium value at  $1055 \text{ cm}^{-1}$  is obtained. This points to a gradual strengthening of the N-O bond during the isomerization process.

A splitting of the  $\nu_{\text{S}}(\text{N-O})$  band can definitely not be ascribed to any factor group splittings since the concentration of the  $\text{ONO}^-$ -impurities in  $[\text{Co}(\text{NH}_3)_5\text{NO}_2]\text{Cl}_2$  is initially very low. In addition to these components of  $\nu(\text{N-O})$ , a broad, weak and very diffuse absorption maximum at  $\sim 1110 \text{ cm}^{-1}$  can also be discerned in this frequency range in the spectra of  $[\text{Co}(\text{NH}_3)_5\text{NO}_2]\text{Cl}_2$  containing  $\text{ONO}^-$ -impurities. This feature disappears at higher concentrations of the nitrito group and suggests that more orientations of the  $\text{ONO}^-$ -groups might be possible in the early stages of the isomerization process. It was suggested by Johnson and Pashman [75]

that a bidentate metastable transient occurs in the solid state photolysis of  $[\text{Co}(\text{NH}_3)_4\text{NO}_2]\text{Cl}_2$  at liquid nitrogen temperatures:



The formation of such an intermediate will of course have a profound effect on the N-O stretching modes in particular and the broad band at  $1110 \text{ cm}^{-1}$  could possibly indicate the existence of such a transient. This also explains the disappearance of the band during later stages of the photochemical isomerization process.

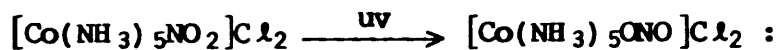
The two orientations of the  $\text{ONO}^-$ -ion in the lattice of  $[\text{Co}(\text{NH}_3)_5\text{NO}_2]\text{Cl}_2$  are not in agreement with the space group of  $\text{C}_2/\text{c}$  for this compound. Once the symmetry of the  $[\text{Co}(\text{NH}_3)_5\text{ONO}]^{2+}$  is lowered from  $\text{C}_s$  of  $[\text{Co}(\text{NH}_3)_5\text{NO}_2]^{2+}$  to  $\text{C}_1$  for the  $[\text{Co}(\text{NH}_3)_5\text{ONO}]^{2+}$ -ions, they should occupy the equivalent sites  $\text{C}_1$  of  $\text{C}_2/\text{c}$ . On the other hand, the  $\text{C}_2$ -symmetry of the  $[\text{Co}(\text{NH}_3)_5\text{NO}_2]^{2+}$  is incompatible with the  $\text{C}_2$ -symmetry that one of the  $\text{NH}_3$ -groups must occupy in the crystal and can only be obtained if there is considerable disorder in the

hydrogen atoms of this  $\text{NH}_3$ -group and/or if this ligand has a great deal of reorientational freedom in the crystal. If the symmetry of the  $[\text{Co}(\text{NH}_3)_5\text{NO}_2]$ -crystal is equal to  $C_C(C_S^4)$  with  $z=4$  then there must be two different sets of cations of  $C_1$ -symmetry (the only positions available under  $C_C$ -symmetry are  $C_1(2)$ ). This can then explain the existence of the two  $\text{ONO}^-$ -orientations in the mixed crystal of  $\text{ONO}^-$  in  $[\text{Co}(\text{NH}_3)_5\text{NO}_2]\text{Cl}_2$ . However, two different sets of cations in the nitrito complex must also be reflected in the infrared bands of the nitrito groups, and as can be seen in Fig. (VII.5) and Table (VII.1) this has not been observed. The question of the structure of this compound, therefore remains largely unresolved.

### 3.5 Rates of isomerization

The kinetic results obtained when the intensities of the  $\nu_{\text{as}}(\text{N}=\text{O})$  band at  $1454 \text{ cm}^{-1}$  and the  $\nu_{\text{s}}(\text{N}-\text{O})$  band at  $1055 \text{ cm}^{-1}$  were recorded at regular intervals between the irradiation of  $[\text{Co}(\text{NH}_3)_5\text{NO}_2]\text{Cl}_2$  with ultraviolet light are shown in Tables (VII.2) and (VII.3). The graph of the fraction of the nitrito present at time  $t$ ,  $\chi_p$ , against time is shown in Fig. (VII.10) for the appearance of the (N=O) band with the graphical representation of  $\ln(1/(1-\chi_p))$  against time in Fig. (VII.11). The straight line obtained in the latter enables the reaction to be classified as a first-order reaction of the form  $1-\chi_p = e^{-kt}$  or  $\chi_r = e^{-kt}$ . This can be interpreted as a special case of the Erofe'ev equation

## Kinetic data on the conversion

**Table (VII.2)** Appearance of the  $\nu_{\text{as}}(\text{N}=\text{O})$  band at  $1460 \text{ cm}^{-1}$ 

no.	t [s]	$\chi_p$	$\ln \left[ \frac{1}{1-\chi_p} \right]$
1	0	0,087	0,091
2	358	0,242	0,277
3	659	0,345	0,423
4	1079	0,445	0,589
5	1560	0,526	0,747
6	2340	0,614	0,952
7	3238	0,692	1,178
8	3719	0,729	1,306
9	4440	0,773	1,483
10	5459	0,822	1,726
11	6359	0,857	1,945
12	7019	0,883	2,146
13	8398	0,903	2,333
14	9419	0,935	2,733
15	10259	0,947	2,937
16	11159	0,958	3,170

**Table (VII.3)** Appearance of the  $\nu_{\text{s}}(\text{N}=\text{O})$  band at  $1055 \text{ cm}^{-1}$ 

no.	t [s]	$\chi_p$	$\ln \left[ \frac{1}{1-\chi_p} \right]$
1	0	0,116	0,123
2	313	0,386	0,488
3	626	0,474	0,642
4	1096	0,582	0,872
5	1566	0,655	1,064
6	2349	0,757	1,415
7	3289	0,810	1,661
8	3758	0,834	1,796
9	3915	0,881	2,129
10	5481	0,907	2,375
11	6420	0,927	2,617
12	7047	0,945	2,900
13	9396	0,989	4,510
14	10336	0,992	4,828
15	11119	0,998	6,215



**Fig. (VII.10)** Fraction nitrito present at time  $t$  for the reaction  $[\text{Co}(\text{NH}_3)_5\text{NO}_2]\text{Cl}_2 \xrightarrow{h\nu} [\text{Co}(\text{NH}_3)_5\text{ONO}]\text{Cl}_2$

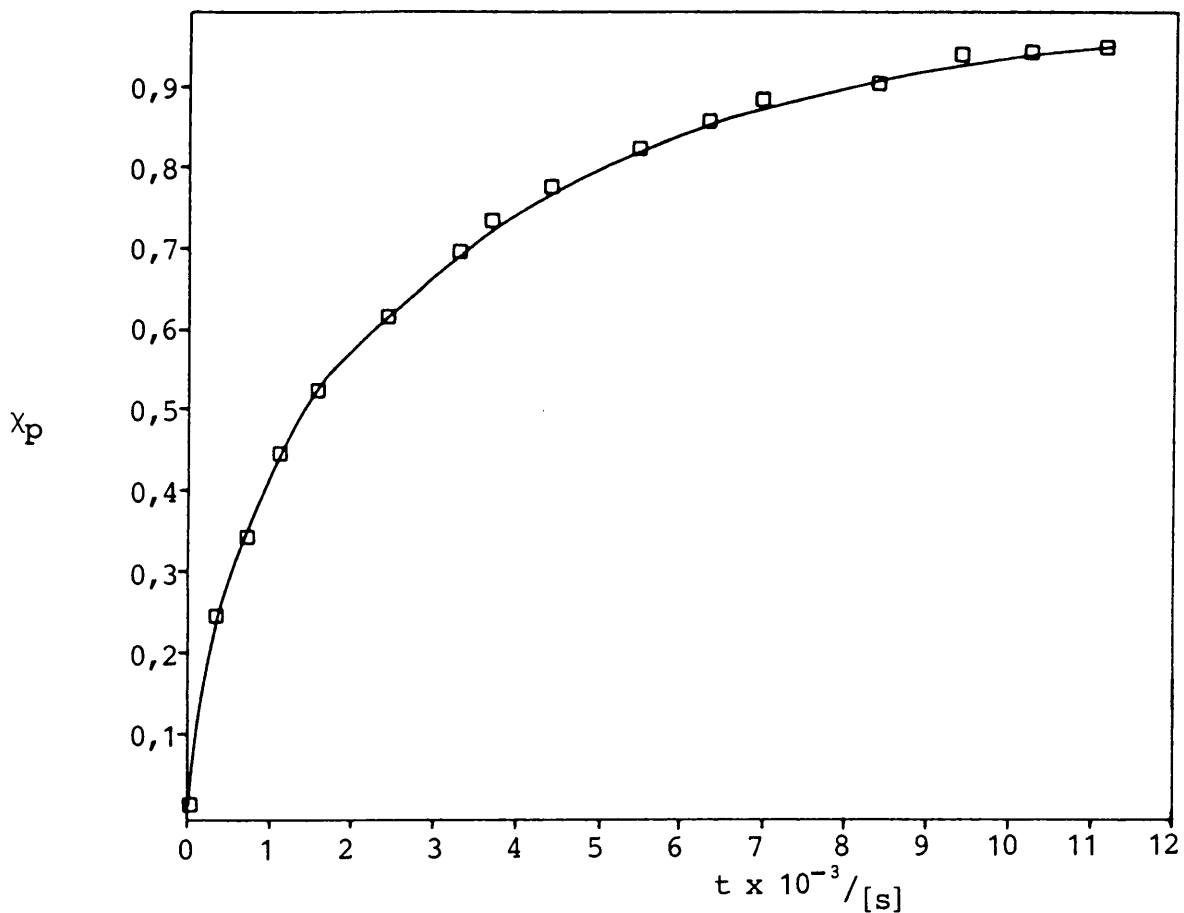
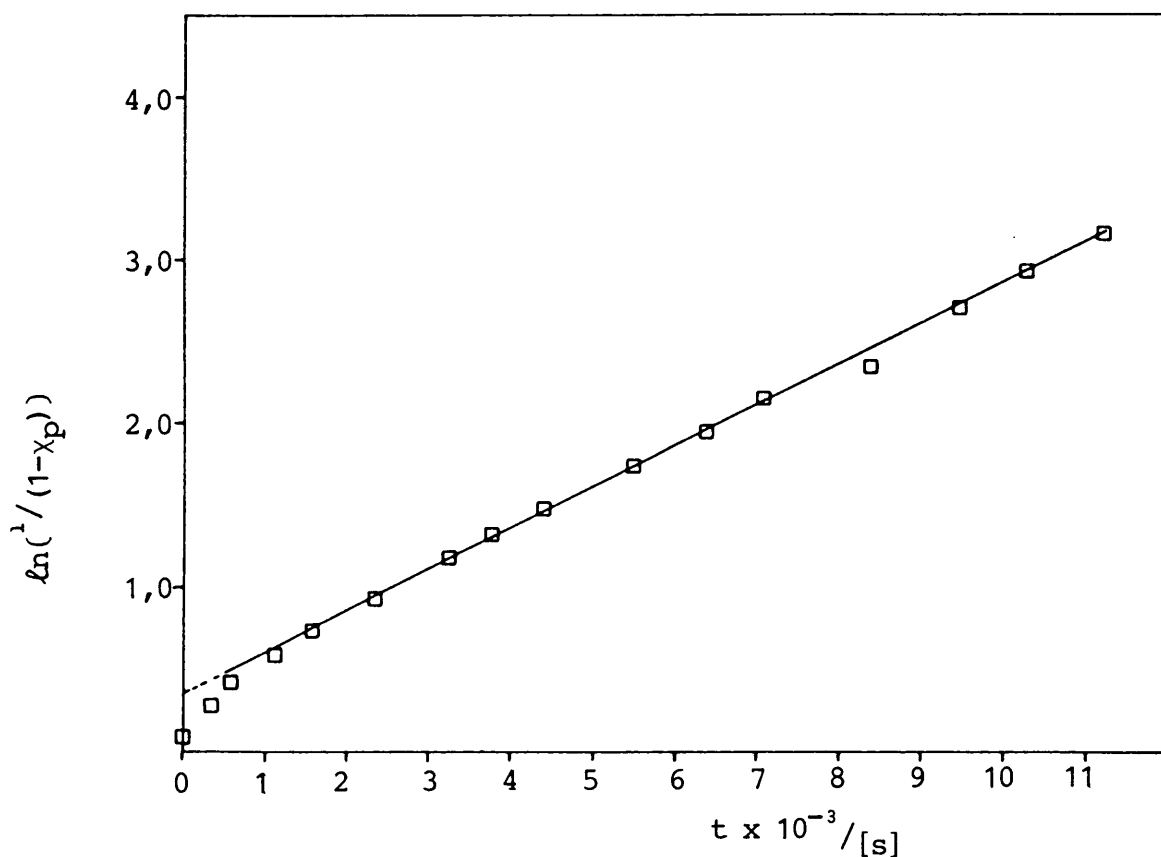
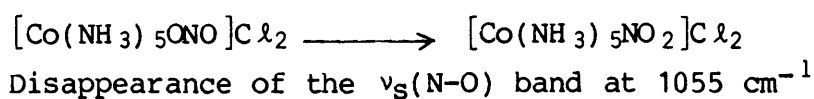


**Fig. (VII.11)** Obedience of kinetic data to the first order reaction  $1 - X_p = e^{-kt}$



$[(1-\chi_p) = \exp(-kt)^n]$  with  $n = 1$ . The rate constant  $k$ , was calculated from the results shown in Fig. (VII.11) as  $2,57 \pm 0,005 \times 10^{-4} \text{ s}^{-1}$ . After the completion of the nitrito formation the well-known nitrito  $\rightarrow$  nitro isomerization was studied by recording the disappearing  $\nu_s(\text{N-O})$  band at  $1055 \text{ cm}^{-1}$  to compare the rates of isomerization of freshly and photochemically prepared  $[\text{Co}(\text{NH}_3)_5\text{ONO}]\text{Cl}_2$ . The results are summarized in Table (VII.4). The rate constant was

**Table (VII.4)** Kinetic data on the conversion



no.	t [hour]	$\chi_r$	$\ln[1/\chi_r]$
1	0,991	0,995	$4,785 \times 10^{-3}$
2	1,981	0,952	0,049
3	3	0,934	0,068
4	4	0,945	0,057
5	22,5	0,897	0,109
6	23,51	0,864	0,146
7	46,48	0,761	0,273
8	48,50	0,749	0,289
9	71,51	0,686	0,377
10	143,48	0,597	0,516
11	166,50	0,415	0,879
12	189,01	0,351	1,047
13	284,99	0,246	1,402
14	332,99	0,212	1,551
15	381	0,110	2,207

calculated from the results for a first order reaction, and is equal to  $1,43 \pm 0,002 \times 10^{-6} \text{ s}^{-1}$ . This compares well with the value obtained by Adell [69] who studied the

reaction both with freshly and photochemically prepared  $[\text{Co}(\text{NH}_3)_5\text{ONO}]\text{Cl}_2$  [73]. There is a significant difference in the rates of the photochemical nitro  $\rightarrow$  nitrito isomerization ( $t_{1/2} = 49$  minutes) and the spontaneous nitrito  $\rightarrow$  nitro isomerization ( $t_{1/2} \approx 6$  days).

## CHAPTER VIII

### EXPERIMENTAL DETAIL

#### 1. INTRODUCTION

Some of the techniques used are described in this chapter with information on instruments and accessories: the Raman spectrometer with its high temperature cell and the Fourier-transform infrared (FT-IR) and UV-spectrometers with its different diffuse reflection cells.

#### 2. RAMAN SPECTROMETER AND OVEN

All Raman measurements were made on a Z-24 Dilor Raman Spectrometer, using a He-Ne laser (632,8 nm) to excite the spectra. A high temperature cell obtained from Dilor, Lille, France was used to heat the samples in a glass tube, 3 mm in diameter. The heating head and sample holder are shown in Fig. (VIII.1).

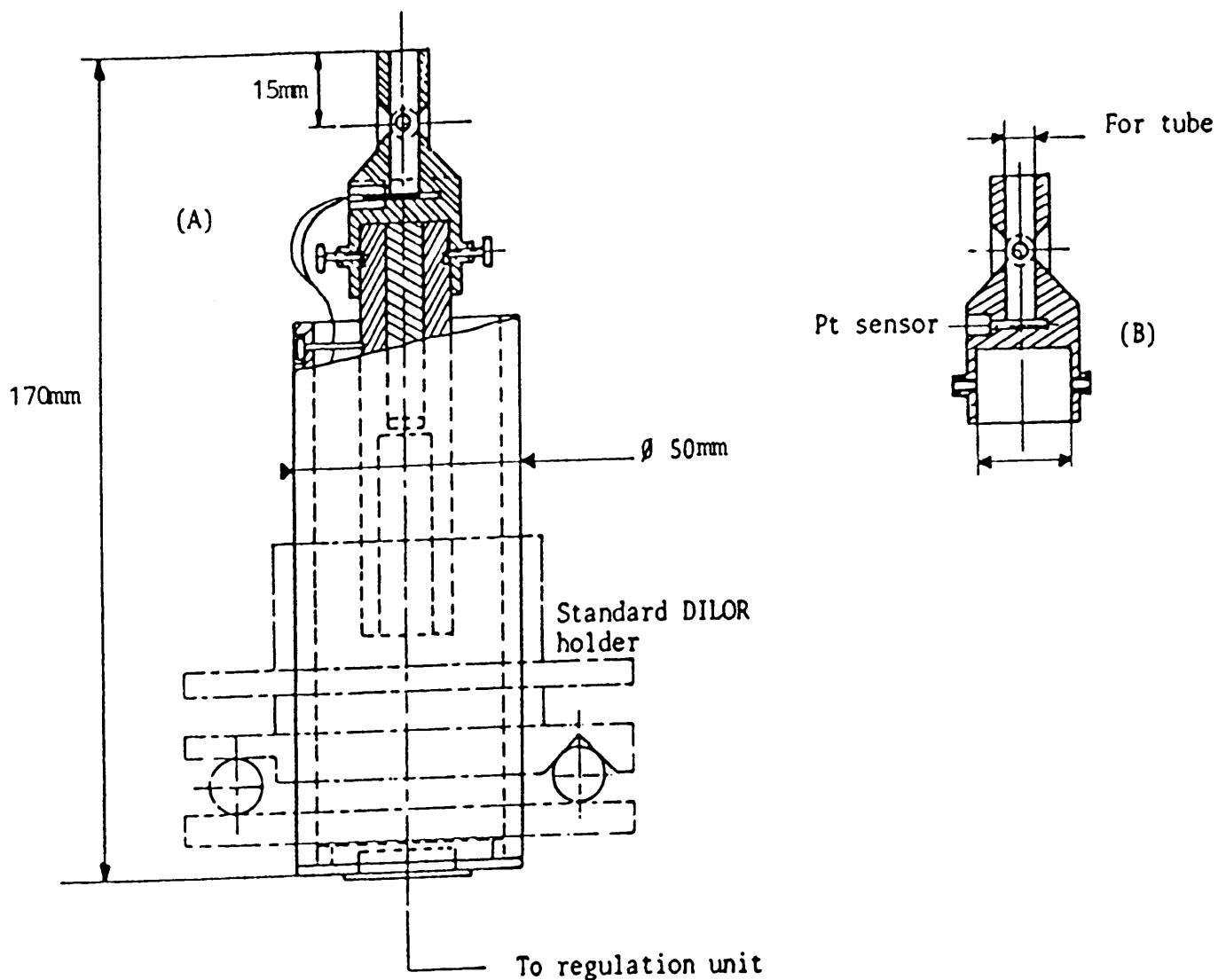
The utilization range is from room-temperature to 673 K with all temperatures being correct within 5 K. Heating time from room- to maximum temperature is 20 minutes [77].

#### 3. FT-IR SPECTROSCOPY

##### 3.1 Introduction

Fourier-transform infrared (FT-IR) spectroscopy allows all

**Fig. (VIII.1)** The cell used for high temperature Raman measurements including the  
 (A) heating head and the  
 (B) sample holder for the tube [77]

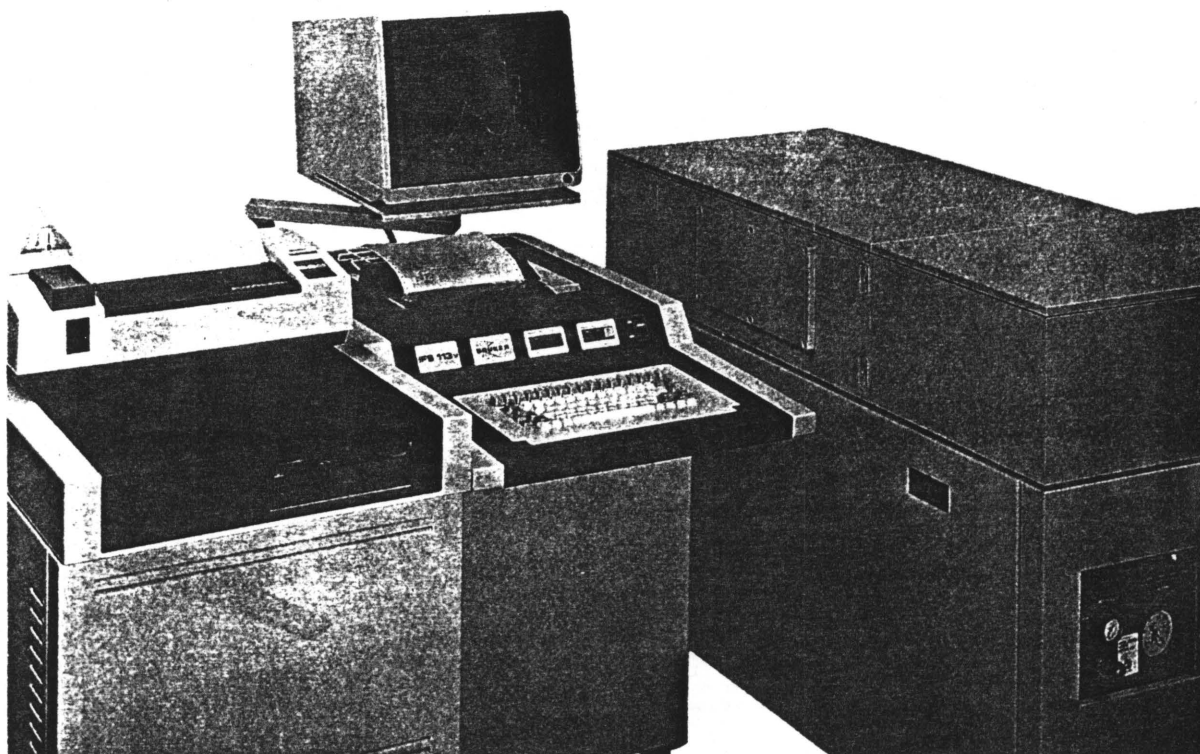


frequencies in a broad region of infrared energy to be measured simultaneously and a mathematical operation, Fourier transformation, is used to convert the measurement (known as an interferogram) into a spectrum of the compound [78].

### 3.2 FT-IR spectrometer

FT-IR spectra were recorded using the Bruker IFS 113 V vacuum spectrometer shown in Fig. (VIII.2). The optical system

Fig. (VIII.2) The Bruker IFS 113 V spectrometer (FT-IR)



features modular construction of the vacuum cabinets with the infrared radiation focussed on the beamsplitter with an effective diameter of 10 mm. Beamsplitters can be exchanged under vacuum conditions. The sample compartment allows the use of common and specifically designed sampling attachments such as diffuse reflectance equipment. Changes in the optical components allow coverage of the mid, far and near IR spectral ranges.

### 3.3 Sample form

KBr and polyethylene (PE) windows were used respectively in the regions 4000-500 and 500-20  $\text{cm}^{-1}$ . Sample pellets were obtained by mixing 1 mg of sample with 100 mg KBr or 30 mg PE.

### 3.4 IR Diffuse reflection spectroscopy

This has been used in many fields as an adjunct to more well known spectroscopic methods, often when conventional techniques fail. The spectra are complex and strongly dependent upon the conditions under which they are obtained [79]. The infrared diffuse reflection spectrum of  $(\text{NH}_4)_2\text{CrO}_4$  [III.3.3.2] was recorded after Diffuse Reflectance Attachments (DRA) were fitted into the sampling compartment of the FT-IR spectrometer. This 'Praying Mantis' DRA model is shown in Fig. (VIII.3) with a ray diagram in Fig. (VIII.4).

Fig. (VIII.3) The 'Praying Mantis' DRA model downward looking [79]

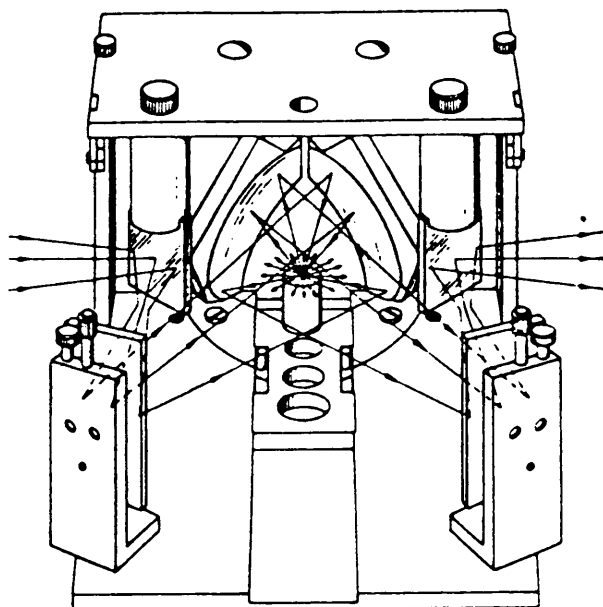
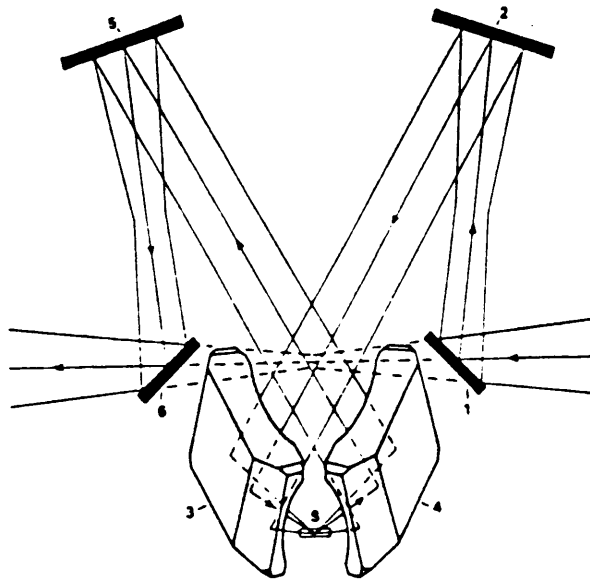


**Fig. (VIII.4)** A Ray diagram of the 'Praying Mantis' Diffuse Reflectance Attachment. The sample is placed in position S. Numbers 3 and 4 are the ellipsoidal mirrors [79].



The design incorporates two  $90^\circ$  ellipsoidal mirrors, one focussing the incident beam on the sample while the second collects the radiation diffusely reflected by the sample [79].

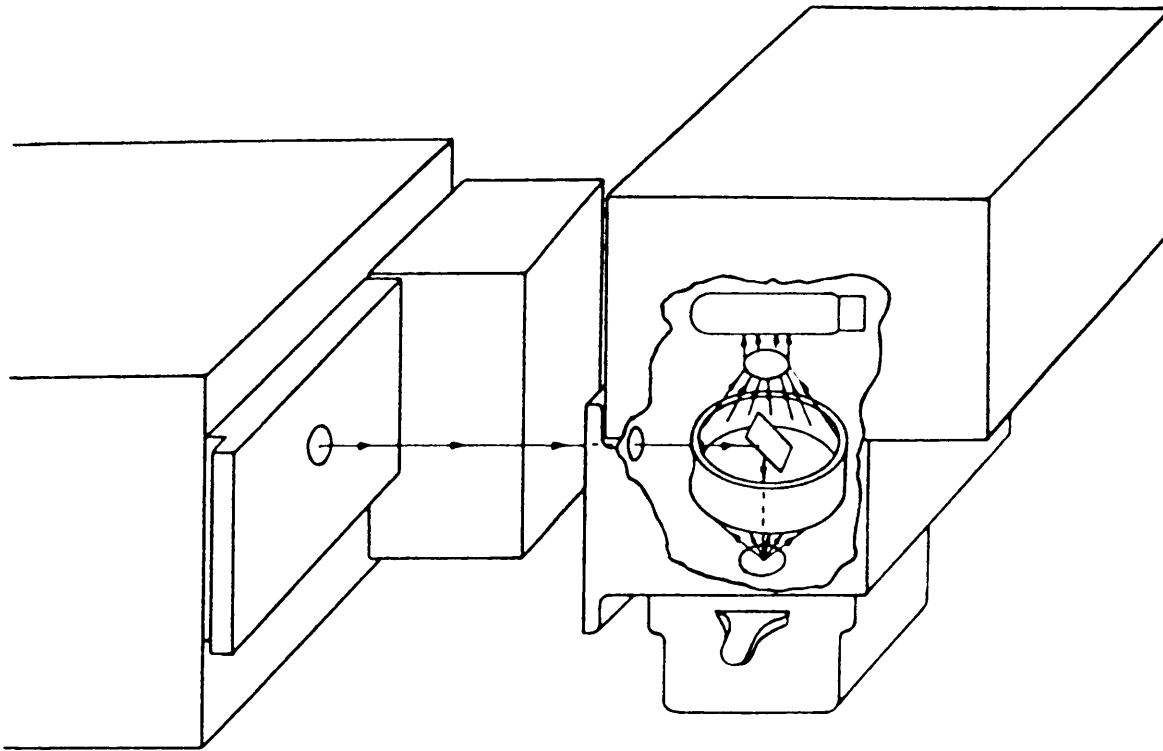
#### 4. ELECTRONIC DIFFUSE REFLECTANCE SPECTRA

These spectra were recorded using a Beckman DU-2 spectrophotometer with a tungsten ( $26\ 667 - 15\ 385\ \text{cm}^{-1}$ ) and hydrogen ( $36\ 364 - 25\ 000\ \text{cm}^{-1}$ ) lamp. The optical diagram for the attachment that replaces the standard cell compartment is shown in Fig. (VIII.5).

The radiation beam is directed from the monochromator into the reflectance compartment. A plane mirror in the center of the



Fig. (VIII.5) Optical diagram for the reflectance attachment in the DU-2 spectrophotometer [80]



compartment reflects the beam unto the sample or reference positioned in the sample drawer below the compartment. The diffuse rays reflected upwards at angles between  $35$  and  $55^\circ$  are focussed by an ellipsoidal mirror onto a quartz diffusing screen at the top of the compartment. A phototube mounted above the diffusing screen detects the amount of energy that falls upon the screen [80].



**TABLE (A1)**

**Kinetic data for the decomposition of ammoniumchromate to ammoniumdichromate at 343 K.**

Microcrystals

$I_0 = 1038$

Nr	t[s]	ln t	I	$I/I_0 = \chi_{\text{CrO}_4^{2-}}$	$\ln[\ln(1/\chi_{\text{CrO}_4^{2-}})]$	$1-(\chi_{\text{CrO}_4^{2-}})^{1/2}$	$1-(\chi_{\text{CrO}_4^{2-}})^{1/3}$
1	45	3,807	984	0,948	-2,929	0,026	0,018
2	90	4,500	898	0,865	-1,932	0,070	0,047
3	135	4,905	712	0,686	-0,976	0,172	0,118
4	180	5,193	600	0,578	-0,601	0,240	0,167
5	225	5,416	606	0,584	-0,620	0,236	0,164
6	270	5,598	590	0,568	-0,571	0,246	0,172
7	315	5,753	595	0,573	-0,586	0,243	0,169
8	360	5,886	601	0,579	-0,604	0,239	0,167
9	405	6,004	572	0,551	-0,518	0,258	0,180
10	450	6,109	601	0,579	-0,604	0,239	0,167
11	495	6,205	587	0,566	-0,562	0,248	0,173
12	540	6,292	597	0,575	-0,592	0,242	0,168
13	600	6,397	600	0,578	-0,601	0,240	0,167

**TABLE (A2)**

**Kinetic data for the decomposition of ammoniumchromate to ammoniumdichromate at 348 K.**

Microcrystals

$I_0 = 933$

Nr	t[s]	Int	I	$I/I_0 = x\text{CrO}_4^{2-}$	$\ln[\ln(1/x\text{CrO}_4^{2-})]$	$1-(x\text{CrO}_4^{2-})^{1/2}$	$1-(x\text{CrO}_4^{2-})^{1/3}$
1	49	3,807	894	0,958	-3,154	0,021	0,014
2	90	4,500	648	0,695	-1,009	0,167	0,114
3	135	4,905	558	0,598	-0,665	0,227	0,157
4	180	5,193	551	0,591	-0,641	0,232	0,161
5	225	5,416	541	0,580	-0,607	0,239	0,166
6	270	5,598	504	0,540	-0,485	0,265	0,186
7	315	5,753	485	0,520	-0,424	0,279	0,196
8	360	5,886	483	0,518	-0,418	0,280	0,197
9	405	6,004	499	0,535	-0,469	0,269	0,188
10	450	6,109	472	0,506	-0,384	0,289	0,203
11	495	6,205	451	0,483	-0,319	0,305	0,215
12	540	6,292	463	0,496	-0,356	0,296	0,208

**TABLE (A3)**

Kinetic data for the decomposition of ammoniumchromate to ammoniumdichromate at 358 K.

Microcrystals

 $I_0 = 1306$ 

Nr	t[s]	lnI	I	$I/I_0 = \chi_{\text{CrO}_4^{2-}}$	$\ln[\ln(1/\chi_{\text{CrO}_4^{2-}})]$	$1-(\chi_{\text{CrO}_4^{2-}})^{1/2}$	$1-(\chi_{\text{CrO}_4^{2-}})^{1/3}$
1	45	3,807	1113	0,852	-1,833	0,077	0,052
2	90	4,500	864	0,662	-0,884	0,187	0,129
3	135	4,905	697	0,534	-0,465	0,269	0,189
4	180	5,193	604	0,462	-0,260	0,320	0,227
5	225	5,416	438	0,335	0,088	0,421	0,305
6	270	5,598	318	0,243	0,345	0,507	0,376
7	315	5,753	214	0,164	0,593	0,595	0,453
8	360	5,886	177	0,136	0,692	0,632	0,486
9	405	6,004	168	0,129	0,718	0,641	0,495
10	450	6,109	154	0,118	0,760	0,657	0,510
11	495	6,205	164	0,126	0,730	0,646	0,499
12	540	6,292	161	0,123	0,739	0,649	0,502
13	600	6,397	145	0,111	0,788	0,667	0,519

**TABLE (A4)**

Kinetic data for the decomposition of ammoniumchromate to ammoniumdichromate at 363 K.

Microcrystals

$I_0 = 1082$

Nr	t[s]	ln t	I	$I/I_0 = \chi_{\text{CrO}_4^{2-}}$	$\ln[\ln(1/\chi_{\text{CrO}_4^{2-}})]$	$1-(\chi_{\text{CrO}_4^{2-}})^{1/2}$	$1-(\chi_{\text{CrO}_4^{2-}})^{1/3}$
1	45	3,807	706	0,652	-0,851	0,192	0,133
2	90	4,500	571	0,528	-0,448	0,274	0,192
3	135	4,905	556	0,514	-0,407	0,283	0,199
4	180	5,193	368	0,340	0,076	0,417	0,302
5	225	5,416	257	0,238	0,363	0,513	0,381
6	270	5,598	170	0,157	0,616	0,604	0,460
7	315	5,753	138	0,128	0,722	0,643	0,497
8	360	5,886	137	0,127	0,726	0,644	0,498
9	405	6,004	123	0,114	0,777	0,663	0,516
10	450	6,109	136	0,126	0,729	0,645	0,499
11	495	6,205	152	0,140	0,674	0,625	0,480
12	540	6,292	129	0,119	0,755	0,655	0,508

**TABLE (A5)**

Kinetic data for the decomposition of ammoniumchromate to ammoniumdichromate at 343 K.

Powder

 $I_0 = 707$ 

Nr	t[s]	Int	I	$I/I_0 = \chi_{\text{CrO}_4^{2-}}$	$\ln[\ln(1/\chi_{\text{CrO}_4^{2-}})]$	$1-(\chi_{\text{CrO}_4^{2-}})^{1/2}$	$1-(\chi_{\text{CrO}_4^{2-}})^{1/3}$
1	45	3,807	704	0,996	-5,460	0,002	0,001
2	90	4,500	682	0,965	-3,324	0,018	0,012
3	135	4,905	661	0,935	-2,699	0,033	0,022
4	180	5,193	631	0,893	-2,174	0,055	0,037
5	225	5,416	628	0,888	-2,133	0,058	0,039
6	270	5,598	605	0,856	-1,859	0,075	0,051
7	315	5,753	590	0,835	-1,710	0,086	0,059
8	360	5,886	597	0,844	-1,777	0,081	0,055
9	405	6,004	564	0,798	-1,487	0,107	0,073
10	450	6,109	582	0,823	-1,637	0,093	0,063
11	495	6,205	542	0,767	-1,325	0,124	0,085
12	540	6,292	552	0,781	-1,396	0,116	0,079
13	600	6,397	564	0,798	-1,487	0,107	0,073

**TABLE (A6)**

Kinetic data for the decomposition of ammoniumchromate to ammoniumdichromate at 348 K.

Powder

$$I_0 = 704$$

Nr	t[s]	Int	I	$I/I_0 = \chi_{\text{CrO}_4^{2-}}$	$\ln[\ln(1/\chi_{\text{CrO}_4^{2-}})]$	$1-(\chi_{\text{CrO}_4^{2-}})^{1/2}$	$1-(\chi_{\text{CrO}_4^{2-}})^{1/3}$
1	45	3,807	684	0,972	-3,547	0,014	0,010
2	90	4,500	624	0,886	-2,115	0,059	0,039
3	135	4,905	501	0,712	-1,078	0,156	0,107
4	180	5,193	402	0,571	-0,579	0,244	0,170
5	225	5,416	373	0,530	-0,454	0,272	0,191
6	270	5,598	335	0,476	-0,298	0,310	0,219
7	315	5,753	298	0,423	-0,151	0,349	0,249
8	360	5,886	311	0,442	-0,202	0,335	0,238
9	405	6,004	296	0,420	-0,143	0,352	0,251
10	450	6,109	277	0,393	-0,070	0,373	0,267
11	495	6,205	270	0,384	-0,043	0,381	0,273
12	540	6,292	276	0,392	-0,066	0,374	0,268
13	600	6,397	262	0,372	-0,012	0,390	0,281



**TABLE (A7)**

Kinetic data for the decomposition of ammoniumchromate to ammoniumdichromate at 353 K.

Powder

 $I_0 = 550$ 

Nr	t[s]	Int	I	$I/I_0 = \chi_{\text{CrO}_4^{2-}}$	$\ln[\ln(1/\chi_{\text{CrO}_4^{2-}})]$	$1-(\chi_{\text{CrO}_4^{2-}})^{1/2}$	$1-(\chi_{\text{CrO}_4^{2-}})^{1/3}$
1	45	3,807	506	0,920	-2,484	0,041	0,027
2	90	4,500	370	0,673	-0,925	0,180	0,124
3	135	4,905	274	0,498	-0,361	0,294	0,207
4	180	5,193	231	0,420	-0,142	0,352	0,251
5	225	5,416	192	0,349	0,051	0,409	0,296
6	270	5,598	190	0,345	0,061	0,412	0,298
7	315	5,753	201	0,365	0,007	0,395	0,285
8	360	5,886	182	0,331	0,101	0,425	0,308
9	405	6,004	179	0,325	0,116	0,430	0,312
10	450	6,109	189	0,344	0,066	0,414	0,300
11	495	6,205	175	0,318	0,136	0,436	0,317
12	540	6,292	174	0,316	0,141	0,438	0,319

**TABLE (A8)**

**Kinetic data for the decomposition of ammoniumchromate to ammoniumdichromate at 358 K.**

Powder

$$I_0 = 520$$

Nr	t[s]	ln t	I	$I/I_0 = \chi_{\text{CrO}_4^{2-}}$	$\ln[\ln(1/\chi_{\text{CrO}_4^{2-}})]$	$1-(\chi_{\text{CrO}_4^{2-}})^{1/2}$	$1-(\chi_{\text{CrO}_4^{2-}})^{1/3}$
1	45	3,807	476	0,915	-2,426	0,043	0,029
2	90	4,500	383	0,737	-1,185	0,142	0,097
3	135	4,905	256	0,492	-0,344	0,298	0,210
4	180	5,193	197	0,379	-0,030	0,384	0,276
5	225	5,416	154	0,296	0,196	0,456	0,333
6	270	5,598	132	0,254	0,316	0,496	0,367
7	315	5,753	137	0,263	0,288	0,487	0,359
8	360	5,886	134	0,258	0,305	0,492	0,364
9	405	6,004	135	0,260	0,299	0,490	0,362
10	450	6,109	147	0,283	0,234	0,468	0,344
11	495	6,205	135	0,260	0,299	0,490	0,362
12	540	6,292	143	0,275	0,255	0,476	0,350
13	600	6,397	137	0,263	0,288	0,487	0,359

**TABLE (A9)** Values of the order of the reaction (n) and the rate constant (k) for the decomposition reaction of microcrystalline and powdered  $(\text{NH}_4)_2\text{CrO}_4$ .

	Temperature	$\ln[\ln(1/\chi_{\text{CrO}_4^{2-}}) v_s \cdot \ln t]$	$1 - (\chi_{\text{CrO}_4^{2-}})^{1/2}$		$1 - (\chi_{\text{CrO}_4^{2-}})^{1/3}$	
	K	n	$k[\text{s}^{-1}]$	$r^*$	$k[\text{s}^{-1}]$	$r^*$
Microcrystals	343	-	$4.84 \cdot 10^{-4}$	0.814	$3.53 \cdot 10^{-4}$	0.819
	348	-	$2.69 \cdot 10^{-4}$	0.924	$2.04 \cdot 10^{-4}$	0.923
	358	1.09	$1.76 \cdot 10^{-3}$	0.995	$1.36 \cdot 10^{-3}$	0.994
	363	1.03	$1.98 \cdot 10^{-3}$	0.979	$1.60 \cdot 10^{-3}$	0.979
Powder	343	0.88	$8.35 \cdot 10^{-5}$	0.972	$1.73 \cdot 10^{-4}$	0.970
	348	1.10	$1.09 \cdot 10^{-3}$	0.966	$7.93 \cdot 10^{-4}$	0.968
	353	0.81	$1.28 \cdot 10^{-3}$	1.000	$9.89 \cdot 10^{-4}$	1.000
	358	1.06	$1.77 \cdot 10^{-3}$	0.999	$1.37 \cdot 10^{-3}$	0.999

\*r = correlation coefficient

**TABLE (A10)** A comparison of the values of  $\log A$ , where  $A$  is the frequency factor and  $E$ , the activation energy for the decomposition of  $(\text{NH}_4)_2\text{CrO}_4$ .

From  $\ln k$  against  $1/T$  plots

Microcrystals			Powder		
	$1-(\chi_{\text{CrO}_4^{2-}})^{1/2}$	$1-(\chi_{\text{CrO}_4^{2-}})^{1/3}$		$1-(\chi_{\text{CrO}_4^{2-}})^{1/2}$	$1-(\chi_{\text{CrO}_4^{2-}})^{1/3}$
<u>This work</u>			<u>This work</u>		
$\log (A/\text{s}^{-1})$	$11.29 \pm 1.45$	$11.8 \pm 1.4$	$\log (A/\text{s}^{-1})$	$4.49 \pm 0.1$	$5.4 \pm 0.04$
$E/\text{kJ}\cdot\text{mol}^{-1}$	$97 \pm 12$	$101 \pm 12$	$E/\text{kJ}\cdot\text{mol}^{-1}$	$49 \pm 0.9$	$56 \pm 0.4$
<u>Galwey [6]</u>			<u>Galwey [6]</u>		
$\log (A/\text{s}^{-1})$	10.3	-	$\log (A/\text{s}^{-1})$	6.7	-
$E/\text{kJ}\cdot\text{mol}^{-1}$	$97 \pm 5$	-	$E/\text{kJ}\cdot\text{mol}^{-1}$	$70 \pm 5$	-

$A[\text{s}^{-1}]$  = frequency factor

$E[\text{kJ}\cdot\text{mol}^{-1}]$  = activation energy

LITERATURE

1. W.G. Fateley, F.R. Dollish, N.T. McDevitt and F.F. Bentley, *Infrared and Raman Selection Rules for Molecular and Lattice Vibrations: The Correlation Method*, Wiley-Interscience, New York (1972).
2. D.M. Adams and D.C. Newton, *Tables for Factor Group and Point Group Analysis*, Beckmann-RIIIC Ltd. Croydon (England) (1970).
3. R.E. Newham and Y.M. de Haan, *Zeitschrift für Kristallographie* Bd. 117, S235 (1962).
4. J.S. Stephens and D.W.J. Cruickshank, *Acta Cryst.*, B26, 222 (1970).
5. A. Byström and K. Wilhelmi, *Acta Chim. Scand.*, 5, 1003 (1951).
6. C.J. Keattch and D. Dollimore, *An Introduction to Thermogravimetry*, Second edition, Heyden, New York (1975).
7. S.J. Gregg and R.I. Razouk, *J. Chem. Soc.*, 536 (1949).
8. W.D. Spencer and B. Topley, *J. Chem. Soc.*, 2633 (1929).
9. J.S. Stephens and D.W.J. Cruickshank, *Acta Cryst.*, B26, 437 (1970).
10. B.M. Gatehouse and P. Leverett, *J. Chem. Soc. (A)*, 1857 (1969).

11. J.A. Campbell, *Spectrochim. Acta*, 21, 1333 (1965).
12. O. Muller, W.B. White and R. Roy, *Spectrochim. Acta*, 25A, 1419 (1969).
13. T. Dupuis and M.L. Hackspill, *C.R. Acad. Sci.* T246II, 3332 (1958).
14. G. Michel and R. Machiroux, *J. Raman Spectroscopy*, 14, 22 (1983).
15. H. Stammreich, D. Bassi and O. Sala, *Spectrochim. Acta*, 12, 403 (1958).
16. D.M. Adams and M.M. Hargreave, *Chem. Soc. Dalton Trans.*, 1426 (1973).
17. T. Waddington, *J. Chem. Soc.*, 4340 (1958).
18. Ill-Huyn Park, *Bull. Chem. Soc. Japan*, 45, 2749 (1972).
19. Ill-Huyn Park, *Bull. Chem. Soc. Japan*, 45, 2753 (1972).
20. S. Rajam and A.K. Galwey, *J. Chem. Soc. Faraday Trans. 1*, 79, 2553 (1982).
21. A.B.P. Lever, *Studies in physical and theoretical chemistry 33 - Inorganic and Electronic Spectroscopy (second edition)*, Elsevier Science Publishers B.V. (1984).

22. M. Avrami, J. Chem. Phys., 7, 1103 (1939).
23. M. Avrami, J. Chem. Phys., 8, 212 (1940).
24. M. Avrami, J. Chem. Phys., 9, 177 (1941).
25. B.V. Erofe'ev, Dokl. Akad. Nauk SSSR, 52, 511 (1964).
26. E. Mampel, Z. Phys. Chem., A187, 43 (1940).
27. F.M. Turner (Ed.), The condensed chemical dictionary, second edition, The chemical catalog company (1930).
28. A. Byström and K. Wilhelmi, Acta Chim. Scand., 5, 1003 (1951).
29. F.A. Miller and C.H. Watkins, Analytical Chemistry, 24(8), 1253 (1952).
30. H. Stammreich, D. Bassi, O. Sala and H. Siebert, Spectrochim. Acta, 13, 192 (1958).
31. Luu Dang Vinh, J. Reynaud and R. Lafont, C.R. Acad. Sci., 263B, 192 (1966).
32. M.S. Mathur, C.A. Frenzel and E.B. Bradley, Journal of Molecular Structure, 2, 429 (1968).
33. Luu Dang Vinh, C. Clement and R. Lafont, C.R. Acad. Sci., 264B, 1822 (1967).

34. A.M. Heyns, "Die temperatuurafhanklikheid van die infrarooi-spektra van Kristallyne vastestowwe" (1968).
35. Luu Dang Vinh and P. Hillaire, C.R. Acad. Sci. Ser. B, 270(7), 496 (1970).
36. A. Harris and M. Bertolucci, Symmetry and Spectroscopy, Plenum Press (1969).
37. B. Mahieu, D.J. Apers and C.P. Capron, J. Inorg. Nucl. Chem., 33, 2857 (1971).
38. J. Simpson, D. Taylor and B.M.W. Anderson, J. Chem. Soc., 2375 (1958).
39. Schmitz Du Mont, Z. Electrochem., 60, 866 (1956).
40. C. Bailar, Chemistry of the Coordination Compounds, Reinhold N.Y. (1956).
41. R. Fischbeck and H. Spingler, Z. Anorg. Chem., 241, 209 (1939).
42. A.K. Galwey, L. Pöppl and S. Rajam, J. Chem. Soc. Faraday Trans. 1, 79, 2143 (1983).
43. M.I. Zaki and R.B. Fahim, J. Therm. Anal., 31, 825 (1986).
44. N.N. Greenwood and E. Earnshaw, Chemistry of the elements, Pergamon Press Ltd. (1984).



45. D.M. Adams, *Metal-Ligand and Related Vibrations*, Edward Arnold Publishers Ltd. London (1967).
46. K. Nakamoto, *Infrared Spectra of Inorganic and Coordination Compounds*, John Wiley and Sons, New York (1963).
47. L. Fève, R. Fontaine, J. Arsène, M. Leglet and R. Caillat, *C.R. Acad. Sci. Paris*, 301, Series II no. 10 (1985).
48. R. Mattes, *Z. Anorg. Chem.*, 382, 163 (1971).
49. A. Byström and K. Wilhelmi, *Acta Chim. Scand.*, 4, 1131 (1950).
50. C. Duval, C. Wadier and J. Lecompte, *C.R. Acad. Sci.*, 257, 3766 (1963).
51. C.G. Baraclough, J. Lewis and R.S. Nyholm, *J. Chem. Soc.*, 3552 (1959).
52. N.T. McDevitt and W.I. Baun, *Spectrochim. Acta*, 20, 799 (1964).
53. H.F. Franzen, *Physical Chemistry of Inorganic Crystalline Solids*, Springer-Verlag Berlin Heidelberg (1986).
54. L. Pauling and S.B. Hendricks, *J. Am. Chem. Soc.*, 47, 781 (1925).
55. E.G. Brame, J.L. Margrave and W.V. Meloche, *J. Inorg. Nucl. Chem.*, 5, 48 (1957).

56. M.A. Khilla, Z.M. Hanaf and A.K. Mohammed, *Thermochim. Acta*, 54, 319 (1982).
57. D.A. Brown, D. Cunningham and W.K. Glass, *Spectrochim. Acta*, 24A, 965 (1968).
58. S.D. Ross, *Inorganic Infrared and Raman Spectra*, McGraw-Hill Book Company (United Kingdom) (1972).
59. R.M. Wing and K.P. Callahan, *Inorg. Chem.*, 8, 871 (1969).
60. R. Mattes, *Z. Naturforsch.*, 24b, 772 (1969).
61. J.K. Brandon and I.D. Brown, *Canadian Journal of Chemistry*, 46, 933 (1968).
62. L.A. Zhukova, Z.G. Pinsker, *Soviet Phys. Cryst.*, 9, 31 (1964).
63. J.S. Bates, L.M. Toth, A.S. Quist and G.E. Boyd, *Spectrochim. Acta*, 29A, 1585 (1973).
64. R.L. Carter and C.L. Bricker, *Spectrochim. Acta*, 29A, 253 (1973).
65. R.C. Weast (Ed.), *Handbook of Chemistry and Physics*, CRC Press, 53rd edition (1972-73).
66. B. Adell, *Z. Anorg. Chem.*, 252, 272 (1944).
67. B. Adell, *Z. Anorg. Allg. Chem.*, 271, 49 (1952).

68. I. Grenthe and E. Nordin, *Inorg. Chem.*, 18, 1869 (1979).
69. B. Adell, *Z. Anorg. Allg. Chem.*, 279, 219 (1955).
70. R.G. Pearson, P.M. Henry, J.G. Bergmann and F. Basolo, *J. Am. Chem. Soc.*, 76, 5920 (1954).
71. I.R. Beattie and D.P.N. Satchell, *Trans. Faraday Soc.*, 52, 1590 (1956).
72. W.W. Wendlandt and J.H. Woodlock, *J. Inorg. Nucl. Chem.*, 27, 259 (1965).
73. W.H. Hohman, *J. Chem. Educ.*, 51, 553 (1974).
74. O. Börtin, *Acta Chim. Scand.*, 22, 2890 (1968).
75. D.A. Johnson and K.A. Pashman, *Inorg. Nucl. Chem. Lett.* 11, 23 (1975).
76. I. Nakagawa and T. Shimanouchi, *Spectrochim. Acta*, 23A, 2099 (1967).
77. *Multichannel Spectroscopy Attachments Manual*, Dillor, Lille, France.
78. *IFS User's Manual*, Bruker Analytische Meßtechnik GmbH (1986).

79. Optical spectroscopy: Sampling techniques manual, Harrick Scientific Corporation, N.Y. (1987).
  
80. Model BU-2 UV spectrophotometer instruction manual, Beckman instruments, Inc. U.S.A. (1964).